Quantum control of light and matter fields in the nonlinear regime

vorgelegt von
Nicolas Ludwig Naumann, M. Sc.
geboren in Büren

von der Fakultät II – Mathematik und Naturwissenschaften
der Technischen Universität Berlin
zur Erlangung des akademischen Grades
Doktor der Naturwissenschaften
– Dr. rer. nat. –

genehmigte Dissertation

Promotionsausschuss:
Vorsitzender: Prof. Dr. Michael Lehmann
1. Gutachter: Prof. Dr. Andreas Knorr
2. Gutachter: Priv.-Doz. Dr. Uwe Bandelow

Tag der wissenschaftlichen Aussprache: 29.11.2017

Berlin, 2017

Abstract

In this thesis three different approaches to control the quantum statistics in nanoscopic devices are investigated. In the first part of the thesis, mechanical oscillations in solid state devices are manipulated by an external laser to show bistabilities, coherent amplification, and enhanced damping. The dynamics is controlled by the frequency of the external laser. This study is performed in a semiclassical approximation, where expectation values of operators are factorized. These effects are used to show the similarities and differences between optomechanical systems and phonon cavities. In the regime of coherent amplification of phonons the theoretical description is extended to a fully quantum mechanical model. This reveals additional resonances due to collective processes that can be addressed via the frequency of the external laser.

In the second part, a quantum light source is considered for manipulation of the emission statistics of a second quantum optical system serving as target. A Jaynes-Cummings system is used as a source that may be tuned from nonclassical to thermal emission via the pump strength. The target consists of a cavity with two emitters. The nature of the imprinted statistics is studied by higher order correlation functions. The resulting statistics deviates strongly from thermal, coherent or antibunched statistics.

The third part considers coherent self feedback with time-delay, which is motivated by classical Pyragas control. The finite time delay is used as control parameter. The matrix product state evolution in the picture of the quantum stochastic Schrödinger equation is employed as a systematic way of dealing with quantum self-feedback. In this thesis, the approach is extended to include higher order terms in the time evolution operator. This is done systematically so that arbitrary order can be included enabling faster numerical evaluation. This extension of the matrix product state evolution method allows to investigate efficiently the emission statistics of a single mode cavity containing two emitters. It is shown that feedback can enhance antibunching in the light field while also counter-intuitively increasing the number of emitted photons at the same time. Expressing the time evolution operator as a sum of sparse matrices allows to include time dependent Hamiltonians in an efficient manner. Considering the pulsed excitation of a two level emitter, it is demonstrated that emission statistics may be tuned via feedback. This allows to switch between single photon emission and enhanced two photon emission.

Zusammenfassung

Diese Arbeit behandelt drei Methoden der Kontrolle von Quantenstatistik von nanoskaligen Strukturen. Im ersten Teil der Arbeit werden mechanische Oszillatoren in Festkörpern durch externe Laser gesteuert um Bistabilitäten, kohärente Verstärkung der Oszillationen und vergrößerte Dämpfung zu erreichen. Dies wird innerhalb einer semiklassichen Näherung durchgeführt, wobei Erwartungswerte von Operatoren faktorisiert werden. Diese Effekte zeigen Analogien zwischen optomechanischen Systemen und halbleiterbasierten akustischen Kavitäten auf. Im Regime kohärenter Phononenverstärkung wird die theoretische Beschreibung auf ein voll quantenmechanisches Modell erweitert. Hier zeigen sich zusätzliche Prozesse die durch eine Verstimmung des Lasers adressiert werden können.

Im zweiten Teil wird der Einfluss von nichtklassischem Licht, das von einem System emittiert wird, auf die Emissionsstatistik eines zweiten quantenoptischen Systems untersucht. Ein Jaynes-Cummings-Modell dient als Lichtquelle für nichtklassisches Licht. Das beschienene Quantensystem besteht aus einer Kavität mit zwei Emittern. Die Lichtquelle wird anhand von Korrelationsfunktionen höherer Ordnung charakterisiert. Dies zeigt, dass die resultierende Lichtstatistik stark von thermischer und kohärenter Statistik abweicht und kein Antibunching aufweist.

Im dritten Teil wird kohärente, zeitverzögerte Rückkopplung, die durch klassische Pyragas-Kontrolle motiviert ist, im Quantenlimit untersucht. Die endliche Zeitverzögerung dient als Kontrollparameter. Hier wird die Methode auf Basis von Matrixprodutzuständen verwendet, die von der stochastischen Schrödingergleichung ausgeht. In dieser Arbeit wird diese Methode systematisch auf Evolutionsoperatoren in höherer Ordnung erweitert, was die numerische Simulation beschleunigt. Mit dieser Methode wird die Quantenstatistik in einem System mit Kavitätsmode und zwei Emittern untersucht. Hier können nichtklassische Signaturen verstärkt werden. Insbesondere wird in unintuitiver Weise das Antibunching zusammen mit der Lichtintensität erhöht. Wenn der Zeitentwicklungsoperator durch dünn besetzte Matrizen ausgedrückt werden kann, kann auch die Zeitevolution durch zeitabhängige Hamiltonoperatoren effizient durchgeführt werden. Hier wird ein gepulst getriebenes Zweiniveausystem simuliert, wobei sich zeigt, dass bei konstruktiver Interferenz eine höhere Emissionswahrscheinlichkeit für zwei Photonen erreicht werden kann.

Contents

1. Introduction

1.1. Motivation

The advent of the laser opened new possibilities in all fields of physics being an indispensable tool not only for fundamental research but also for technical applications. These achievements are possible due to the high level of control over the output characteristics of lasers. Wide ranges of frequencies and intensities are accessible as well as emission of short pulses [EE10].

In particular semiconductor lasers are of interest as they allow for industrial manufacturing. However, they are also interesting from a fundamental point of view since nonlinear dynamics govern their behavior in the classical regime so that bifurcations [EGK96] and chaos [Oht06] are observed. When the laser is subject to feedback new dynamics may be imprinted onto the system to create, e.g., multistabilites [LK80]. However, time-delayed feedback was also proposed to stabilize the dynamics of dynamical systems [Pyr92]. This allows to stabilize chaotic behavior [SH96].

The laser is the embodiment of two important concepts underlying this thesis. First, lasers light exhibits characteristic properties. From a quantum optical perspective the photons emitted from lasers are uncorrelated [MW95]. Second, lasers are important tools for controlling quantum systems optically [SZ08]. However, in this thesis each of this aspects will be considered with a certain modification. While optical lasers are very advanced, recently the interest in a mechanical analog of the optical laser has been growing, which could bring the advantages of the lasers for devices with very low frequency [Khu10]. In the context of coherent generation of mechanical oscillations optomechanical systems are of interest, where a mechanical mode is coupled to the light field via the radiation pressure force [AKM14]. As a previous study that has lead to this thesis it was shown theoretically that also the dynamics in optomechanical systems can be stabilized via time-delayed optical feedback [Nau+14].

As for the optical laser, realizing a phonon laser by implementing it as a semicondutor nanostructure would increase its technological relevance. Thus, next to other realizations of phonon lasers [Gru+10; Bea+10; Vah+07; Men+10] semiconductor quantum dots were proposed as active material to induce laser action [Kab+12], which is based on recent progress in phonon cavities [Lac+04; Roz+09; LKFJ15]. In this thesis analogies between the optomechanical and the semiconductor approach are investigated [Nau+16]. This reveals that the semiconductor case approaches the optomechanical system for the case of many emitters. Furthermore, coherent phonon generation is also possible by multi-phonon processes. This triggered the fully quantum mechanical study of the quantum dot phonon laser in the multi-emitter case [Dro+17]. The fully quantum mechanical model shows that there are even more processes that enable the creation of phonon with coherent statistics.

The quantum mechanical study also shows that there are regimes which do not show coherent dynamics. The deviation from the coherent dynamics is in particular interesting

in optical systems as non-classical states of light in the form of single photons [Shi07] enable secure exchange of keys for the encryption of communication [Jen+00]. The above studies for control via feedback are all performed using classical, i.e., coherent light fields. This leads to the question if also quantum optical emitters may be controlled and stabilized by their output. For measurement based feedback it has been shown that single photon state may be stabilized [Zho+12]. Quantum coherent time-delayed feedback, where no measurement is performed, is an interesting route as a quantum state is not perturbed by any measurement. However, it is more involved from a theoretical point of view due to its non-Markovian dynamics. As an intermediate study in this thesis a cascaded setup is considered, where a quantum optical system is driven by nonclassical light [Azi+17]. Here, the source also needs to be taken into account fully quantum mechanically. The study reveals that the dissipative channel perturbs lower order correlations creating complex photon statistical output.

This is even more involved for self-feedback as now the source is influenced by the target, as they are one and the same. Starting with theoretical investigations of closed systems [DZ02], recently the stabilization of Rabi-oscillations [Car+13] and the enhancement of entanglement were shown [Hei+14]. However, driven systems with feedback as necessary for realistic emitters and lasers have proven to be challenging. A first method for modeling driven feedback systems was proposed in Ref. [Gri15], which used the notion of feedback as multiple cascaded systems. In this thesis, however, the approach proposed in Ref. [PZ16] will be employed. There, the dynamics of the system subjected to feedback is evaluated by using a matrix product state (MPS) formulation for a stochastic Schrödinger equation. In this thesis the approach is extended to higher order evolution operators, which enables the simulation of more complex systems than before. Thus, a Tavis-Cummings [TC68] system is subjected to feedback, which reveals that the photon statistics may be controlled increasing non-classical signatures in the light field. Creating non-classical states of light with a certain number of photons may be done using cavity quantum electrodynamics [Mun+14]. However, also a two level system can be manipulated to emit two photons with a high probability by pulsed excitation [Fis+17]. Feedback is able to increase this effect generating two photons with a higher probability. This investigation is possible by extending the MPS evolution method to time-dependent Hamiltonians.

These findings show that feedback may also be used in the regime of non-classical light to shape the output of sources in a desired fashion being powerful method to control nanoscale systems optically.

1.2. Structure of this thesis

This thesis is divided into three parts which each address a different method of controlling the output statistics of quantum systems. As the quantum statistics will be the common feature of interest for all parts of the thesis a brief introduction will be given in Chapter 2. Afterwards, in Part I, the control of mechanical oscillations in nanoscopic devices by a light source will be studied. In Chapter 3 optomechanical systems and phonon cavities will be introduced, which are both the realization of a single mechanical mode that couples to the light field. These may be controlled by a pump laser to exhibit certain features such as bistabilities, lasing, and enhanced damping. In Chapter 4 these are studied in

both systems regarding the similarities and differences. Then, in Chapter 5 the phonon cavity is studied fully quantum mechanically in the regime where it exhibits coherent phonon generation for multiple quantum dots as the acoustic analog of the optical laser.

So far the dynamics of the nanostructures was manipulated by using an exteral coherent laser input. This is changed in Part II, where a cascaded optical setup is considered. There the impact of non-classical light on the output statistics of a second optical system is studied and higher order correlations are taken into account.

The last part of this thesis, Part III, features the control of a system by its own output, to which an overview is given in Chapter 7. In order to investigate the impact of time-delayed self-feedback in the quantum limit in Chapter 8 a numerically exact method to model this used throughout the last chapter is the thesis is presented and extended. It is used in Chapter 10 together with an approximate method to investigate the impact on a quantum cavity electrodynamics setup. In Chapter 11 the impact of feedback on a pulsed two level emitter is studied. Final remarks and an outlook conclude the thesis.

2. Quantum statistics of light and matter

An important concept for all parts of this thesis is the statistics of quantized fields. It is used to characterize light fields with respect to their processes of origin. In Part I the phonon field will be considered where the statistics reveal whether coherent phonons are generated by the processes that are investigated. In Parts II and III the creation and stabilization of statistics deviating from this ideal case will be studied. That is on the one hand thermal statistics and on the other hand non-classical statistics as emitted, e.g., by a single photon source. In this part a brief introduction into the quantized description of the statistics is given as it serves as the theoretically connecting concept between the different parts of the thesis.

The statistics of the field are characterized by the correlation functions. The most popular experimental setup in this regard is the Hanbury Brown-Twiss setup [BT56] as it is a rather simple experimental setup and allows to measure the second order correlation function. The setup is shown in Fig. 2.0.1. The system under investigation emits light, which is divided by a beam splitter and fed into two detectors. Detector 1 will start a time that will be stopped when detector 2 registers a photon. In quantized notation this reads [Fox06]

$$G^{(2)}(t_1, t_2) = \langle b_1^\dagger(t_1) b_2^\dagger(t_2) b_2(t_2) b_1(t_1) \rangle, \tag{2.0.1}$$

where b_1 is the field at detector 1 and b_2 is the field at detector 2. With this setup multiphoton events can be measured. In particular no two photon correlation will be measured if only one photon is emitted as a single photon cannot be divided at the beam splitter. In experiment only the cumulative second order correlation may be measured, which corresponds to the integral over t_1 and t_2 in Eq. (2.0.1), when a system prepared in a certain state is considered. Only in Part III the full dynamics of the external modes are taken into account. For most of the thesis a proportionality between the system field and the external field is assumed [Lou00] so that

$$G^{(2)}(t_1, t_2) \propto \langle c^\dagger(t_1) c^\dagger(t_2) c(t_2) c(t_1) \rangle, \tag{2.0.2}$$

where c is the operator of the cavity mode. This dissipates weakly into an external mode so that for most cases the proportionality is true and gives a qualitative picture of the statistics of the light field emitted from a system. Using pulsed excitation, however, scenarios can be constructed, where this proportionality is not true [Fis+17]. This case will be discussed in more detail in chapter 11, where pulsed excitation with additional feedback will be considered. Then it is necessary to directly evaluate the correlation functions from the external bath modes.

In this introduction the focus will be on the case of continuous excitation via an external laser as this is the prototypical case and will also be relevant for most cases in this thesis. When initial conditions or a single pulse are assumed only a finite excitation is present so that over all times is integrated. For the stationary case the two time integrals would

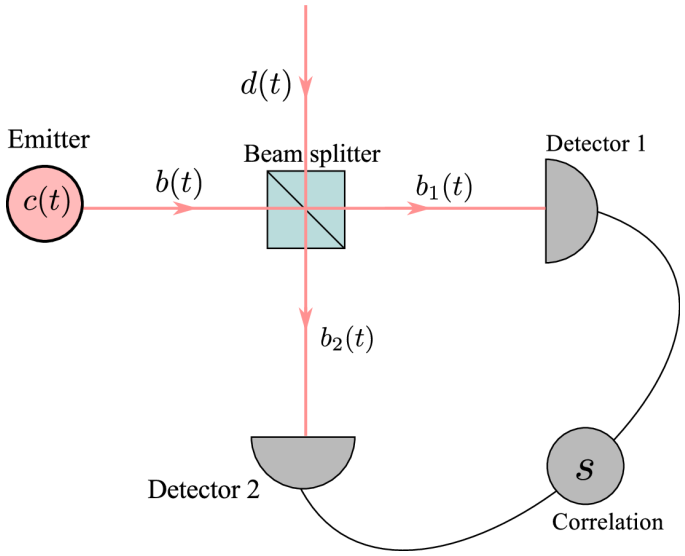

Figure 2.0.1.: With the Hanbury Brown-Twiss setup the second order correlation function is measured. The emitter emits the field $b(t)$ which is split at the beam splitter into the field $b_1(t)$ going to detector 1 and $b_2(t)$ going to detector 2. At the beam splitter also the input field $d(t)$ exists, which is assumed to be a vacuum field throughout this thesis.

diverge as continuous excitation will lead to constant emission of photons. Thus, the normalized second order correlation function in the steady state is considered [GZ04]

$$g^{(2)}(t,s) = \frac{\langle c^\dagger(t)c^\dagger(t+s)c(t+s)c(t)\rangle}{\langle c^\dagger(t)c(t)\rangle^2}. \tag{2.0.3}$$

In the steady state this becomes

$$g^{(2)}(s) = \lim_{t\to\infty} \frac{\langle c^\dagger(t)c^\dagger(t+s)c(t+s)c(t)\rangle}{\langle c^\dagger(t)c(t)\rangle^2}. \tag{2.0.4}$$

The system is taken at a large time t, where no transient dynamics are present anymore and then the correlation between fields with time difference s are considered. As the system is stationary only this offset is relevant. Finally, the usual characterization of the light field can be made. When $g^{(2)}(0) < g^{(2)}(s)$, $s > 0$ then the light field is called antibunched. On the other hand, when $g^{(2)}(0) > g^{(2)}(s)$, $s > 0$ the light field is called bunched [MW95]. As the correlations will vanish for large s, the normalization ensures that $\lim_{s\to\infty} g^{(2)}(s) = 1$. A value of $g^{(2)}(0) = 1$ is valid in case of a coherent light field as a coherent field is always uncorrelated. As the time evolution in s can be involved from a theoretical point of view, the fact that $\lim_{s\to\infty} g^{(2)}(s) = 1$ will be exploited for simplifying the theoretical considerations. When $g^{(2)}(0) < 1$ it is clear that the field is antibunched. Furthermore, the field obeys sub-Poissonian statistics. An example for this is the single photon state. As discussed before no correlations involving more than a single photon may be observed so that $g^{(2)}(0) = 0$. If $g^{(2)}(0) > 1$ bunching is present. For thermal light $g^{(2)}(0) = 2$ is expected [MW95]. These are the categories by which the light field is

usually characterized. In analogy this characterization will also be used for the phonon field in Part I of this thesis. However, the second order correlation function does not fully characterize the light statistics. While it is used as a standard measure also in this thesis, there are cases in which higher order correlations need to be taken into account. While the second order correlation function is not influenced by single photon events it contains not only two photon events but also events involving multiple photons. If two photon events are of interest as in Chapters 6 and 11 of this thesis at least the third order correlation has to be taken into account additionally. This is necessary to distinguish two photon events from three and higher order events.

The stationary higher order correlations in analogy to Eq. (2.0.4) without time difference read

$$g^{(n)}_{\text{stat}} = \lim_{t\to\infty} \frac{\langle c^\dagger(t)^n c(t)^n\rangle}{\langle c^\dagger(t)c(t)\rangle^n}. \tag{2.0.5}$$

For some important cases the correlation functions may be given for all orders. For a coherent state

$$g^{(n)}_{\text{stat,coh}} = 1 \tag{2.0.6}$$

for all n [MW95]. For thermal state this reads [MW95]

$$g^{(n)}_{\text{stat,therm}} = n! \tag{2.0.7}$$

Finally, a Fock state with N photons shows the correlations

$$g^{(n)}_{\text{stat,Fock}} = \frac{N!}{N^n(N-n)!}. \tag{2.0.8}$$

These correlations will be used in Part II of this thesis as reference to gain a clearer picture of the output from systems subject to non-classical light.

This concludes the brief introduction into light statistics. The special cases which were mentioned here will be discussed in more detail throughout the thesis.

Part I.

Optical control of mechanical oscillations

3. Mechanical oscillators

In this and the following chapters, the focus lies on controlling mechanical oscillations via an external laser. Two realizations of microscopic mechanical oscillators will be considered: On the one hand oscillators specifically designed to exploit the radiation pressure force in order to achieve a coupling to the radiation field [AKM14] and on the other hand phonons, which are the quantization of lattice oscillations in solid state materials. In particular this thesis considers the phonon coupled to the conduction band in semiconductor quantum dots (QDs).

Achieving a coupling between mechanical and optical degrees of freedom may open new aspects in fields such as optical information processing [CD10; CA11], sensors [Kra+12], or quantum information processing [AKM14].

The feedback control of the optomechancial system was considered in Ref. [Nau+14]. As the optomechanical interaction becomes only relevant at high pump strengths, a semiclassical theory may be applied. This study also connects this part of the thesis to Part. III.

In Chapter 4, the analogy between optomechanics and the electron phonon interaction will be motivated theoretically focusing on bistable behavior, lasing and enhanced damping as effects connecting these physical realizations of mechanical oscillators. This investigation based on a semiclassical evaluation of the underlying Hamiltonian was published in [Nau+16]. In chapter 5 the focus will be on phonon lasing, i.e. generation of a high number of phonons via external pumping, in the semiconductor system. This work was done in collaboration with Leon Droenner [Dro+17] and is accepted for publication in Phys. Rev. A. It is a fully quantum mechanical study of phonon lasing in the multi-emitter case and gives further insight into multi-particle effects, such as two phonon lasing or collective phonon generation.

In this introductory chapter, the two considered physical systems will be introduced. First, the optomechanical system will be discussed. It consists of a single cavity mode coupled to a single mechanical mode. Afterwards a semiconductor device, in which a single phonon mode is in resonance with a surrounding phonon cavity couples to the conduction band of a quantum dot. These two systems have a single mechanical oscillator mode, which may be addressed by an external optical laser in order to control the dynamics of the mechanical oscillator. While the mechanical mode in the optomechanical system is coupled directly to the light field by the radiation pressure force, in the semiconductor system the interaction is mediated by the quantum dot. These two systems and their Hamiltonians will be introduced in the following.

3.1. Optomechanical oscillator

In optomechanics the interaction between the light field and a mechanical oscillator due to the radiation pressure force is investigated. Here, the optical pincer [Ash70], as well as

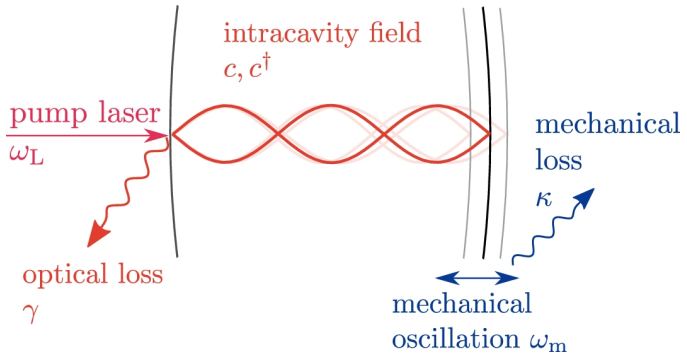

Figure 3.1.1.: Schematic depiction of the optomechanical system, where the optical cavity has one movable mirror. The cavity mode is pumped via an optical laser and thus populated to enable a strong interaction due to the radiation pressure force. This figure is adapted from Ref. [Nau+16].

laser cooling [HS75], is relevant. Cavity optomechanics, where the interaction is amplified by high intensity fields inside an optical cavity were considered early for gravitational wave detectors [Cav80]. Recently, also possible applications for quantum information science and sensors are proposed [AKM14; KV08; ZBM14].

In Fig. 3.1.1 the basic optomechanical system is shown. An optical cavity, where one of the mirrors may oscillate, is pumped by an external laser to introduce a high intensity field into the cavity, which enables a strong interaction with the radiation pressure force. This is only a schematic depiction as there are several different ways of realizing an optomechanical coupling. Starting with the Farby-Perot setup depicted in 3.1.1 [Dor+83] more recent advances use, e.g., microtoroids [Ver+12], nanomembranes [Usa+12], or silicon based monolithic oscillators [Wu+17]. The impact of the radiation pressure force inside the cavity may be derived by considering the forces on the mirrors surface via the Maxwell stress tensor. To derive the Hamiltonian a canonical quantization of the Hamiltonian creating the equations of motion may be conducted [Law95]. When assuming only a single relevant optical mode the Hamiltonian reads [AKM14]

$$H_{\mathrm{OM}} = \hbar\omega_{\mathrm{cav}} c^\dagger c + \hbar\omega_{\mathrm{m}} b^\dagger b - \hbar g c^\dagger c \left(b + b^\dagger\right) + \hbar E_1 \left(c^\dagger e^{-i\omega_{\mathrm{L}} t} + c e^{i\omega_{\mathrm{L}} t}\right). \tag{3.1.1}$$

The first term describes the frequency of the cavity mode ω_{cav} while the second term constitutes the frequency of the mechanically oscillating mirror ω_{m}. These two harmonic oscillators are coupled with the coupling constant g, where an increased intensity in the cavity mode pushes the mirror outward. The last term describes the coherent, optical pump laser pumping the cavity mode in rotating wave approximation. As the cavity mode and the mechanical oscillator are both harmonic oscillators, they obey the commutation relations $[c, c^\dagger] = 1$ and $[b, b^\dagger] = 1$.

3.2. Acoustic cavity

Similar to the optomechanical system where a mechanical mode is coupled to the light field, phonon modes as mechanical oscillations are coupled to electronic transitions. This

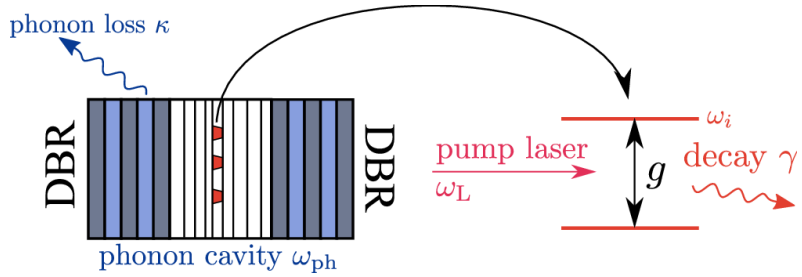

Figure 3.2.1.: Proposed semiconductor quantum optical approach to exploring acoustic phonon dynamics. The phonon cavity consists of materials of alternating acoustic impedance in analogy to an optical distributed Bragg reflectors (DBR)[Tri+02; LKFJ15] and a number of coherently pumped quantum dots (QDs). This figure is adapted from Ref. [Nau+16].

may be derived from the solid state Hamiltonian involving all contributions by the nuclei, the electrons and their electromagnetic coupling. To write the Hamiltonian in second quantized form, first electrons and nuclei are assumed to move independently in the Born-Oppenheimer approximation. This leads to the basis for nuclei and electrons. In the next step the coupling via the coulomb interaction may be introduced again. Thus, the coupling term may be derived with the corresponding coupling strength resulting from the coulomb matrix elements in the respective basis. This procedure is given in solid state textbooks [Mad13].

In recent years acoustic cavities that act in analogy to optical cavities were introduced [Lac+04; Roz+09; BRV12; Fai+13; LK+11; LK+07; LKFJ15]. A single phonon mode is selected by creating a cavity using distributed Bragg reflectors as used in the optical case. A structure of alternating layers with different optical impedances lead to a high reflectance of the phonons.

This leads to the Hamiltonian is in the form as in Refs. [Kab+12; KCK13; AHK99]. However, now multiple emitters are taken into account. Altogether this reads

$$\begin{aligned} H_{\mathrm{SC}} &= \hbar \sum_{i=1}^{N_{\mathrm{QD}}} \omega_{\mathrm{vc},i} \hat{a}^{\dagger}_{\mathrm{c},i} \hat{a}_{\mathrm{c},i} + \hbar \omega_{\mathrm{ph}} b^{\dagger} b \\ &+ \hbar \sum_{i=1}^{N_{\mathrm{QD}}} g_i \hat{a}^{\dagger}_{\mathrm{c},i} \hat{a}_{\mathrm{c},i} \left(b^{\dagger} + b \right) + \hbar \sum_{i=1}^{N_{\mathrm{QD}}} E_i \left(\hat{a}^{\dagger}_{\mathrm{c},i} \hat{a}_{\mathrm{v},i} e^{-i\omega_{\mathrm{L}} t} + \hat{a}^{\dagger}_{\mathrm{v},i} \hat{a}_{\mathrm{c},i} e^{i\omega_{\mathrm{L}} t} \right). \end{aligned} \tag{3.2.1}$$

The first term describes the transition frequency $\omega_{\mathrm{vc},i}$ of the quantum dots, which is written via the electronic creation and annihilation operators. Since the quantum dots represent an electronic system, the operators obey the fermionic anti-commutation relations

$$\{\hat{a}_{\mu,j}, \hat{a}^{\dagger}_{\nu,l}\} = \delta_{\mu,\nu} \delta_{j,l}. \tag{3.2.2}$$

The operator $a_{\mu,j}$ is the annihilation operator for an electron in the band μ in the jth QD. Effectively N_{QD} two level systems are considered, as only conduction and valence band will be taken into account. In a real sample, the transition energies for the QDs may be different. However, in this chapter the idealized case of resonant quantum dots

will be studied. In Chapter 5 the aspect of non-identical QDs will be considered again. The second term describes the energy of the single phonon mode of frequency ω_{ph}, which is selected by the acoustic cavity. This phonon mode is described by a harmonic oscillator and thus the operators obey the bosonic commutation relation $[b, b^\dagger] = 1$. The third term describes the electron phonon coupling with strength g, resulting from the impact of the deformation of the lattice due to the interaction with the electrons [Mad13; Web+08]. As a first approximation, in the following, all quantum dot transitions are assumed to couple with the same strength to the phonon mode. In Chapter 5 the impact of different coupling strengths will be addressed. The last term gives the optical pumping of the quantum dots in rotating wave approximation.

4. Semiconductor analogue of optomechanics

In this chapter the semicondutor system presented in Sec. 3.2 will be shown to exhibit in certain regimes a behavior, which is analogous to the optomechanical system presented in Sec. 3.1. This analogy will be discussed based on the Hamiltonians introduced in the previous chapter.

While phonons often have undesirable effects such as heating of solid state devices [Zha+01], addressing certain phonon assisted resonances can allow to exploit phonon interactions for, e.g., single-photon generation [Eis+11] or self-cooling [Usa+12] of devices.

The possibility of reaching the strong coupling regime with the semicondutor structures presented in Sec. 3.2 may enable mechanically induced transparency [Mah+12] or synchronization effects between mechanical oscillators [WNB15]. The possibility of strong coupling and high phonon frequencies permits a selective excitation of certain transitions. In Fig. 3.1.1 the most basic optomechanical setup was shown: Photons exert a force onto the mirror upon reflection, which in turn changes the length of the cavity leading to the optomechanical coupling.

In contrast, Fig. 3.2.1 shows the semiconductor structure implementing the strong electron phonon interaction. Driving the quantum dot optically with a detuning triggers the creation of acoustic phonons [MZ07; Kab+11b]. Phonon cavities may be fabricated as distributed Bragg reflectors (DBR) confining a single acoustic phonon mode [Tri+02; LKFJ15] in analogy to microlaser structures [ST95]. For optical phonons an effective phonon mode with the same coupling characteristics may be derived [MZ07]. In Chapter 5 the scenario of phonon lasing will be discussed in more detail, when the full quantum mechanical model is considered.

Optomechancis as well as semiconductor laser show a variety of nonlinear dynamical phenomena such as instabilities or bifurcations [Lin+13; Mil+15]. To model quantum optical effects in lasers, typically the Tavis-Cummings model is employed [TC68; Kop+15], where a cavity mode is coupled to a number of two level systems, and effects like superradiance may be observed[Dic54; Ley+15]. From a theoretical point of view a major difference between the electron-photon coupling in the Tavis-Cummings model with rotating wave approximation and the electron-phonon coupling will be discussed later on.

In the present chapter, the focus is on the regime of coherent dynamics. The quantum mechanical treatment in the lasing regime will be presented in Chapter 5.

The optomechanical (OM) and the semiconductor (SC) system, both, are constituted of similar components. In the optomechanical system there is the cavity mode and the mechanical oscillator, while in the semiconductor system there is the resonant optical transition of the semiconductor quantum dot and a distinct phonon frequency. Thus, both systems have a component of a high (optical) frequency (HF) and a low (mechanical) frequency (LF).

For achieving an exploitable coupling due to the radiation pressure force multiple designs exist, e.g., whispering gallery modes in toroids or microscopic membranes [AKM14].

In the following, the analogy between the optomechanical and the semiconductor system will be motivated using bistable behavior, lasing and enhanced damping of oscillations. First, the Hamiltonians for both systems will be introduced and is shown to have a similar form. Investigating these effects will reveal, that the optomechanical system may be understood as the limiting case of the semiconductor system for a large number of quantum dots, and thus as a physical realization of the Holstein-Primakoff approximation [HP40], which states that many weakly excited fermions may act as a boson.

Furthermore, the case of lasing is of particular interest in context of phonon lasers [Kab+12; KCK13]. Here, when increasing the number of emitters, higher order phonon processes may be observed, which will be investigated closer using a description via the full density matrix. Although, already the semiclassical description shows multiphonon effects.

4.1. Optomechanical versus electron-phonon coupling

The two compared systems differ fundamentally by the nature of the high frequency component. In both cases the high frequency component is controlled by the external optical pump laser. In the optomechanical system, the high frequency component consists of the cavity and thus a bosonic mode, while the quantum dots constitute a fermonic system. Both of them couple to a bosonic mode. The focus will lie on the similarities between the system in spite of these differences, but the mentioned distinguishing features will also be discussed.

Both Hamiltonians can be brought formally to the same form by rewriting and shifting the energy scale. This form stresses the formal analogy between the two systems and introduces a common notation, and reads

$$H = \hbar\Omega b^\dagger b + \hbar\omega \hat{\mathbf{p}}^\dagger \hat{\mathbf{p}} + \hbar g \hat{\mathbf{p}}^\dagger \hat{\mathbf{p}} \left(b + b^\dagger\right) + i\hbar \mathbf{E} \left(\hat{\mathbf{p}}^\dagger e^{-i\omega_\mathrm{L} t} - \hat{\mathbf{p}} e^{i\omega_\mathrm{L} t}\right). \tag{4.1.1}$$

The first term describes the harmonic oscillator of frequency Ω representing the low frequency (LF) component of the system. In the optomechanical system this is the mechancial oscillator, while in the semiconductor system it is a phonon mode. The operators $b^\dagger$ and b create and destroy an excitation in the oscillatory mode, respectively.

The second term describes the high frequency (HF) component of frequency ω, which is the optical cavity in the optomechanical system and the optical transition of the quantum dot in the semiconductor system. The operators $\hat{\mathbf{p}}^\dagger$ and $\hat{\mathbf{p}}$ represent the transition operator of the high frequency component. In the optomechanical setup it is $\hat{\mathbf{p}} = c$, which means that the HF component is the bosonic cavity mode. However, in the semiconductor system $\hat{\mathbf{p}}$ is a vector with N_QD elements $\hat{p}_j = \hat{a}^\dagger_{\mathrm{v},j} \hat{a}_{\mathrm{c},j}$. Since the QD is described as a two level system (TLS), the energy can be rewritten in this way. Here, N_QD is the total number of quantum dots inside the phonon cavity.

The third term introduces the coupling of the HF to the LO component, where the number of excitations in the HF component is coupled to the position of the LF mode $q = (b + b^\dagger)/\sqrt{2}$.

The last term describes the external optical pumping of the coherence $\hat{\mathbf{p}}$ with a coherent laser field. In case of the semiconductor system, $\mathbf{E}$ is a vector containing individual pump strengths E_j of all QDs. The external laser is characterized by the frequency ω_L.

In the following all QDs are assumed to be identical. Above, they already have the same transition energy, so that no inhomogeneous broadening is considered. Furthermore, the coupling g is identical and the pump strengths E_j are the same. Now, the fundamental difference between the systems becomes more clear: While the HF component of the optomechanical system obeys a bosonic commutation relation, the HF part of the semiconductor system is fermionic. In the first case an arbitrary number of excitations may be brought to the system, while in the second case only a limited number of excitations may be present. This limit can be increased by increasing the number of quantum dots.

4.1.1. Equations of motion

The equation of motion for an arbitrary operator $\hat{O}$ is derived from the Hamiltonian Eq. (4.1.1) via [Kab+12]

$$\begin{aligned}\frac{d}{dt}\langle\hat{O}\rangle &= \frac{i}{\hbar}\langle[H,\hat{O}]\rangle + \gamma\sum_j \mathrm{Tr}(\hat{O}\mathcal{L}[\hat{p}_j]\rho) + \kappa\mathrm{Tr}(\hat{O}\mathcal{L}[b]\rho)\\ &\quad + \sum_j \frac{\gamma_\mathrm{PD}}{2}\mathrm{Tr}(\hat{O}\mathcal{L}[\hat{p}_j\hat{p}_j^\dagger - \hat{p}_j^\dagger\hat{p}_j]\rho), \qquad (4.1.2)\\ \mathcal{L}[\hat{X}]\rho &= 2\hat{X}\rho\hat{X}^\dagger - \hat{X}^\dagger\hat{X}\rho - \rho\hat{X}^\dagger\hat{X}.\end{aligned}$$

Radiative damping and nonradiative dephasing are taken into account in Lindblad form [Car02]. The incoherent processes occurring in the optomechanical system are the radiative damping of the cavity mode via the rate γ, which is due to scattering onto other mode and imperfect mirrors. The mechanically oscillating mirror is damped with the rate κ because its oscillations are coupled to the substrate. For the semiconductor system the quantum dot transition is damped by 2γ and the phonon is damped by κ. This is again due to coupling to neglected modes. The last term corresponds to the dephasing of the electron coherence, which destroys the polarization of the QD without introducing a decay. For the case of the longitudinal acoustic (LA) phonon mode, pure dephasing is neglected as these processes are assumed to be negligible due to the introduction of the phonon cavity. When considering longitudinal optical (LO) phonons, pure dephasing has to be considered and is due to the coupling to the energetically lower lying acoustic phonon modes [KAK02],

From (4.1.2) a system of equations of motion is derived. To break the hierarchy of equations of motion coherent fields are assumed due to the external coherent pumping. Then, products of operators are factorized into products of expectations values leading to a set of nonlinear equations of motion. In Chapter 5, a full quantum mechanical study will be done for the case of lasing. It is assumed, that all QDs follow the same dynamics, thus reducing the number of equations. This leads to one common equation for all QDs. This assumption will not be made when considering the fully quantum mechanical system.

For the optomechanical system, it results in two equations of motion, while there are three for the semiconductor system. The cavity field can be factorized into a product $\langle c^\dagger c\rangle = \langle c^\dagger\rangle\langle c\rangle$, while the product of the fermionic operators $\langle\sigma_{+,j}\sigma_{-,j}\rangle$ is not factorizable,

since a single QD can only be excited once. The equation of motion for the HF part is transformed into a frame rotating with the pump laser frequency ω_L. The equations then read with the shorthand notations $P_\mp = \langle \hat{p}_1 \rangle e^{i\omega_\mathrm{L} t}$, $B = \langle b \rangle$, and (only for the SC system) $U = \langle \hat{p}_1^\dagger \hat{p}_1 \rangle$

$$\dot{B} = -(i\Omega + \kappa)B - igNU \tag{4.1.3a}$$

$$\dot{P}_\mp = (i\Delta - \gamma - \gamma_\mathrm{PD})\, P_\mp - ig(B + B^*)P_\mp + E_1\,(1 - U \mp U) \tag{4.1.3b}$$

$$\dot{U} = E_1(P_- + P_-^*) - 2\gamma U. \tag{4.1.3c}$$

In (4.1.3b) the minus accounts for the semiconductor system, while the plus is valid for the case of the optomechanical system so that in the OM system the U vanished from the equation. Then, for the OM system, the pump term is independent of the occupation of the HF component, so that Eq. (4.1.3c) is not part of the set of equations, so that $U = P_+^* P_+$ and $N = 1$. For the SC system $N = N_\mathrm{QD}$. This system of coupled first order nonlinear differential equations is solved by a fourth order Runge-Kutta algorithm [Pre+07].

Formally, the equations for the coherences P and B are analogous for the OM and SC case: The HF component (P) oscillates with the detuning $\Delta = \omega_\mathrm{L} - \omega$ and is damped by γ. The HF coherence couples to the LF position ($B + B^*$), which leads to an effective frequency shift. Furthermore, it is pumped by an external laser. Here, the main difference in the equations occurs: In the OM system, the pumping may be arbitrarily strong, while the pumping in the SC system saturates at some point due to the limited number of QDs. The last equation accounts for the fact that there may only be a finite amount of excitations in the SC system.

The above Hamiltonian follows for LA phonons due to the fact, that only one phonon mode is present in the phonon cavity by design. However, in the LO case, multiple phonon modes are present. By employing the Einstein approximation of constant dispersion a collective phonon mode can be introduced [MZ07; Kab+11b]. Then, a Hamiltonian can be derived that leads to the same equations of motion.

For a clearer notation the number of excitations in the HF component are abbreviated as $n_\mathrm{HF} = NU$ in the SC system, where it is the expectation value for the number of excited QDs, and $n_\mathrm{HF} = P^*P$ in the OM system, where it is the expectation value of the photon number inside the cavity. The number of excitations in the LF component is written as $n_\mathrm{LF} = B^*B$. The OM equations may be employed in the SC case, when the QDs are excited very weakly as will become apparent in the following. This is consistent with the Holstein Primakoff approximation [HP40]. However, here the approximate equations for the SC system are indeed the full equations for the OM system. Thus, the OM system is the realization of the SC case in the limit of many QDs.

If possible, we choose the parameters according to experimental data, as for the optomechancial system [Vit+07]. In the semiconductor system, the parameters, which are not directly accessible are estimated according to a microscopic theory [Web+08; MZ07; Mac06] and taken close to previous publications [Kab+12; KCK13]. All parameters are given in Tables 4.2.1 and 4.3.1. The strong coupling regime $g > (\gamma + \kappa)/2$ may be more easily accessible in a semicondutor setup than in optomechanics.

4.2. Bistability

	Optomechanical	Semiconductor (LA)	Semiconductor (LO)
LF frequency	$\Omega = 2\pi \times 10$ MHz	$\Omega = 556.6$ GHz	$\Omega = 55.3$ THz
Detuning	$\Delta = -2.6 \times \Omega$	$\Delta = -\Omega/8$	$\Delta = -\Omega$
Pump rate	$E_1 = 2\pi \times 10$ MHz	$E_1 = 556.6$ GHz	$E_1 = 55.3$ THz
Losses (HF)	$\gamma = 2\pi \times 14$ MHz	$\gamma = 5$ GHz	$\gamma = 5$ GHz
Losses (LF)	$\kappa = 2\pi \times 50$ Hz	$\kappa = 0.5$ GHz	$\kappa = 100$ GHz
Dephasing			$\gamma_{\mathrm{PD}} = 100$ GHz
Coupling strength	$\lvert g\rvert = 952.7$ Hz	$\lvert g\rvert = 197.5$ GHz	$\lvert g\rvert = 5.1$ THz
Number of QDs	–	1	10

Table 4.2.1.: Parameter values used for the bistabilities in Sec. 4.2. The optomechanical parameters are taken from [Vit+07]. The semiconductor parameters for acoustic phonons are taken according to [Kab+12; KCK13]. For the optical phonons, references [Web+08; MZ07] are used for coupling constants and losses, while pure dephasing is taken from [Mac06].

In all of the systems discussed here bistable behavior can be observed. For the optomechanical system this has been studied in detail in Ref. [GBS11]. In order to illustrate the bistability, the equations of motion Eq. (4.1.3) are evaluated in the steady state. Thus, the derivatives can be set to zero because no change over time will occur. Whether a state is stable or not may be evaluated by linearizing the system of equations in the vicinity of the steady state, as done in Ref. [Nau+14] for the optomechanical system in the context of state control. This method is common for analyzing of nonlinear dynamical systems [Str00]. To facilitate this procedure, the equations of motion Eq. (4.1.3) may be written in vector form

$$\dot{\mathbf{x}} = \mathbf{F}(\mathbf{x}(t)), \tag{4.2.1}$$

where $\mathbf{x}$ is a vector containing all variables and their complex conjugate. The vector $\mathbf{F}$ contains the corresponding equations of motion. By writing the equation in this form, the linearized version of the equations may be derived from the Jacobian matrix $\mathbf{J} = \frac{\partial \mathbf{F}}{\partial \mathbf{x}}$:

$$\dot{\mathbf{x}} = \mathbf{J}(\mathbf{x})\big|_{\mathbf{x}=\mathbf{x}_S}\mathbf{x} + \mathcal{O}(\mathbf{x}^2). \tag{4.2.2}$$

Evaluating the steady state values and the stability by considering the maximal Lyapunov exponent, the bistability in the phonon number can be considered. The state is stable if the largest Lyapunov exponent is negative. In the following, excitations of the mechanical oscillator in the optomechanical system are also called phonons for brevity. The bistabilities are shown in Fig. 4.2.1(a) for the optomechanical system and in Figs. 4.2.1(b) and 4.2.1(c) for the semiconductor systems with LA phonons and LO phonons, respectively.

To gain further insight into the occurrence of the bistability, the forces that act on the LF component may be considered. This force incorporates two competing processes: On the one hand the restoring force due to the harmonic potential F_h and on the other hand the force due to the coupling to the HF component F_c. The general forces may be derived

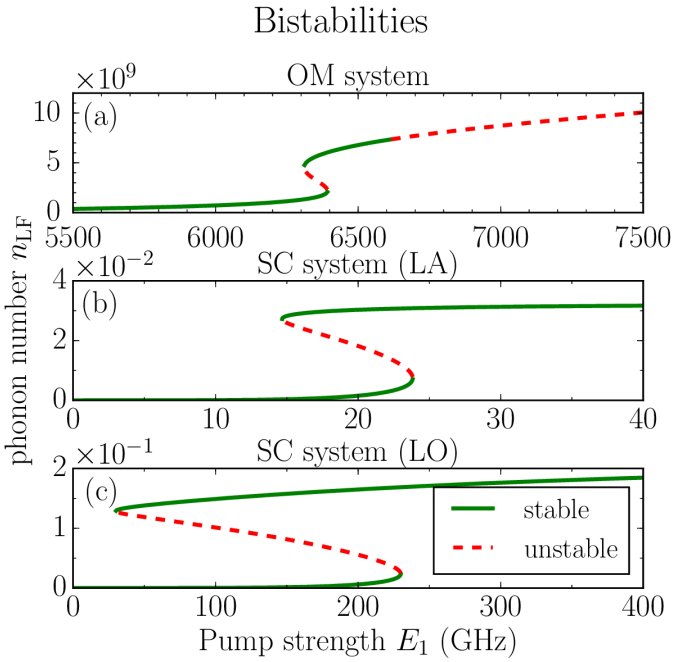

Figure 4.2.1.: Phonon number n_{LF} of the low frequency component for (a) the OM system, (b) the SC system with acoustic phonons, and (c) for the SC system with optical phonons. Due to the different coupling strengths, the bistabilities occurs at very different pump strengths. The parameters are given in Tab. 4.2.1. (This figure was previously published in Ref. [Nau+16]. © 2016 Optical Society of America, used with permission.)

from the equations of motion Eq. (4.1.3) by $F_{\mathrm{tot}} = (\dot{B} - \dot{B}^*)/(\sqrt{2}i)$.. In the steady state there exists an equilibrium of forces, so that $F_{\mathrm{tot}} = F_h + F_c = 0$. The steady state value for the dynamical variables is indicated by the index s. The harmonic force reads for the OM as well as for the SC system

$$F_h = \left(\Omega + \frac{\kappa^2}{\Omega}\right) q_s, \tag{4.2.3}$$

where $q_s = (B_s + B_s^*)/\sqrt{2}$ is the normalized displacement of the LF component. For the optomechanical case it may be understood as the force of the mount of the mechanical mirror which tends to return to the initial position because of the strain in the material. In the semiconductor the harmonic force is due to the displacement of the cores of the material system. In both cases the force is approximated as a harmonic force, which is valid for small displacements. The nonlinear effects occur due to optomechanical and electron phonon coupling. The radiation pressure force in the OM system is given by

$$F_{\mathrm{c,OM}} = \frac{g}{\sqrt{2}} \frac{2E_1^2}{\left(\Delta - \sqrt{2} g q_s\right)^2 + \gamma^2}. \tag{4.2.4}$$

In the case of the coupling of the phonon mode to the electronic excitation this force

reads

$$F_{\mathrm{c,SC}} = \frac{Ng}{\sqrt{2}} \frac{1}{1 + \frac{\gamma}{\gamma+\gamma_{\mathrm{PD}}} \frac{\left(\Delta - \sqrt{2} g q_s\right)^2 + (\gamma+\gamma_{\mathrm{PD}})^2}{2E_1^2}}. \tag{4.2.5}$$

Since, in both cases, the maximum of these forces lies at a value $\Delta < 0$ for the detuning, the maximum may only be observed in this regime. This is the case as only in this regime the steady state equations have three solutions.

In all cases a bistability can be found. The different stability behavior of the OM system is discussed in Ref. [Nau+14]. For the semicondutor system the phonon number saturates at some point for large pump strengths, while the phonon number in the OM system is not limited. This difference occurs, since the nonlinear coupling force F_c depends on the number of excitations in the HF component. For the OM system it may be increased arbitrarily, so that always a configuration with three solutions may be found. However, they may be unstable if the pump is too high (or even outside the linear regime). For the SC system there are not necessarily three solutions as the maximum coupling force in this case is $\frac{Ng}{\sqrt{2}}$, so that either the coupling strength or the number of QDs has to be large enough. Simply increasing the pump strength may not be advantageous. This difference is due to the different statistics of the HF component.

When increasing the number of quantum dots, the maximum number of excitations becomes large, so that it may be neglected for the regime of weak pumping. This behavior is shown in Fig. 4.2.2(a), where the semiconductor system approaches the optomechanical one with the same parameters. The same is true for the OM parameters, while here the number of QDs needed to reach the same behavior is much higher, since a much higher pumping strength is needed to observe the bistability. This behavior can be also shown from an analytical consideration by investigating the equations $F_h + F_c = 0$ which are valid in the steady state. When using $q_s = -\frac{\sqrt{2} g \Omega U_{\mathrm{tot}}}{\Omega^2 + \kappa^2}$, which follows from Eq. (4.1.3a), a cubic equation emerges that has up to three solutions in the bistable regime. For the OM system it reads

$$\left[\left(\Delta + \frac{2g^2 \Omega U_{\mathrm{tot}}}{\Omega^2 + \kappa^2}\right)^2 + (\gamma + \gamma_{\mathrm{PD}})^2\right] U_{\mathrm{tot}} = E_1^2., \tag{4.2.6}$$

while it is

$$\left[\left(\Delta + \frac{2g^2 \Omega U_{\mathrm{tot}}}{\Omega^2 + \kappa^2}\right)^2 + (\gamma + \gamma_{\mathrm{PD}})^2\right] U_{\mathrm{tot}} = N E_1^2 \left(1 - \frac{\gamma_{\mathrm{PD}}}{\gamma}\right)\left(1 - 2\frac{U_{\mathrm{tot}}}{N}\right) \tag{4.2.7}$$

in the SC system. When neglecting pure dephasing and assuming that $\frac{U_{\mathrm{tot}}}{N} \ll 1$, also the SC case tends to $U_{\mathrm{tot}} \approx P^* P$. This is what is illustrated in Fig. 4.2.2. For both parameters, the ratio $N_{\mathrm{QD}}/n_{\mathrm{LF}} \approx 10^3$ gives an estimate for the number of quantum dots needed for the approximation to be valid.

With this, also the high number of phonons in the OM bistability can be explained. Here, the coupling strength g is much smaller than in the SC case, so that a much higher pump is needed in order to observe nonlinear effects. For a SC system with a similar coupling strength, no bistability could be observed, so that the bosonic statistics of the cavity mode allow to observe nonlinear effects even for small coupling strengths. When considering pure dephasing as in the case of LO phonons, this behavior is not valid anymore.

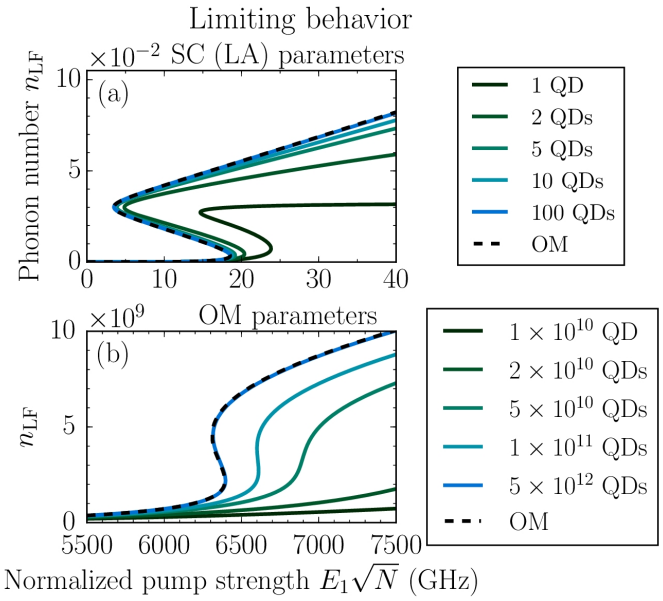

Figure 4.2.2.: The behavior of the stationary states of the LF component n_{LF} for (a) the SC system parameters for LA phonons and (b) the OM parameters (cf. Tab 4.2.1). When increasing the number of QDs for the SC equations, the behavior given by the OM equations is approached. (This figure was previously published in Ref. [Nau+16]. © 2016 Optical Society of America, used with permission.)

In this section the bistability was considered, which is a stationary property. For increasing numbers of quantum dots the behavior of the semiconductor system approaches the one the the optomechancial system as the limit in the number of excitations is lifted to a certain degree. In the next section the dynamical properties of lasing and enhanced damping will be studied.

4.3. Lasing

In this section mechanical lasing, also called phonon lasing, which is studied in the optomechanical [MHG06; LKM08; AKM14] and the semiconductor system [Kab+12; KCK13], will be studied. In this section the above semiclassical model will be considered in order to get an overview of this effect. In Chapter 5, a full quamtum mechanical model will be used to get a closer look at certain interesting effects, such as the two phonon laser process. With the semiclassical model, however, it is possible to study the general behavior of the systems for a vast parameter range. Some of the parameters used throughout this and the following section deviate from the ones used in the previous section [cf. Tab. 4.3.1].

The fundamental process underlying the phonon laser is the anti-Stokes process: The pump laser has to be blue detuned from the optical (high frequency) resonance of the system. With the definitions used here, the detuning is positive $\Delta > 0$ and in the order of a single phonon frequency for the commonly exploited process. When exciting the QD optically, the excess in energy is transformed due to the electron phonon interaction into

	Optomechanical	Semiconductor	Semiconductor (LO)
LF frequency	$\Omega = 2\pi \times 10$ MHz	$\Omega = 556.6$ GHz	$\Omega = 55.3$ THz
Pump rate	$E_1 = 60$ GHz	$E_1 = 80$ GHz	$E_1 = 9.01$ THz
	[cf. Fig. 4.3.1(a)]	[cf. Fig. 4.3.1(b)]	[cf. Fig. 4.3.1(c)]
Detuning	$\Delta \approx \pm\Omega$	$\Delta \approx \pm\Omega$	$\Delta \approx \pm\Omega$
Coupling strength	$E_1 = 2\pi \times 10$ MHz	$E_1 = 556.6$ GHz	$E_1 = 55.3$ THz
Losses (HF)	$\gamma = 2\pi \times 2$ MHz	$\gamma = 5$ GHz	$\gamma = 5$ GHz
Losses (LF)	$\kappa = 2\pi \times 50$ Hz	$\kappa = 0.5$ GHz	$\kappa = 50$ GHz
			$\gamma_{\mathrm{PD}} = 100$ GHz
Coupling strength	$\lvert g\rvert = 205$ Hz	$\lvert g\rvert = 197.5$ GHz	$\lvert g\rvert = 5.1$ THz
Number of QDs	–	1 [cf. Fig. 4.3.1(b)]	10 [cf. Fig. 4.3.1(c)]

Table 4.3.1.: Parameter values for lasing and enhanced damping, as used throughout Secs. 4.3 and 4.4. For the OM system, this time the parameters according to Ref. [Gen+08] is used, for showing the features of the investigated processes more clearly. For the semiconductor systems the parameters are used as in Tab. 4.2.1 from Refs. [Kab+12; KCK13] and [Web+08; MZ07; Mac06] with adjusted detunings and pumping strengths. The positive sign in the detuning is used in case of lasing, while the negative sign is used for enhanced damping. Furthermore, the number of quantum dots used in the figures, where it is not explicitly states, is given.

mechanical oscillations [cf. Fig. 4.3.1, Left]. Here, a quantum mechanical picture reveals a major difference between the OM and the SC system. While the upper and lower levels in the OM system are two adjacent photon number states in the cavity, for the QD these are the upper and the lower level of the (fermionic) two level system. This means that the cavity mode is excited from the state with n phonon to the one with $n+1$ phonons. Thus, a decay back to the n phonon level is not necessary. The QD, in contrast, only may create a second phonon after the electronic excitation decayed. For realistic quantum dots, the level structure is of course more complex than a two level system. However there is not an infinite number of levels allowing the phonon creating process. Thus, the main limiting factor for the phonon number [Kab+12] is not present in the OM system. As phonon lasing is considered in the semiclassical model, the lasing occurs as a parametric instability. The steady state predicted by the equations becomes instable in the regime of lasing [cf. Sec. 4.2]. Instead, a periodic orbit governs the systems dynamics in this regime. The quantum mechanical model will behave differently, as will be shown in Sec. 5. The time dynamics of the semiclassical model are shown in Fig. 4.3.1, where also the oscillations are shown in the inset. For the OM system and the SC system with LA phonons, the amplitude of the oscillations is small in comparison to the number of phonons, for the LO phonons. However, the decay is very large, so that it is the dominating time scale of the dynamics, which leads to the large orscillations.

In Figs. 4.3.2 the time averaged phonon number in the steady state is shown as a function of the detuning and the pump strength. For the SC systems, also the cases with multiple QDs are shown.

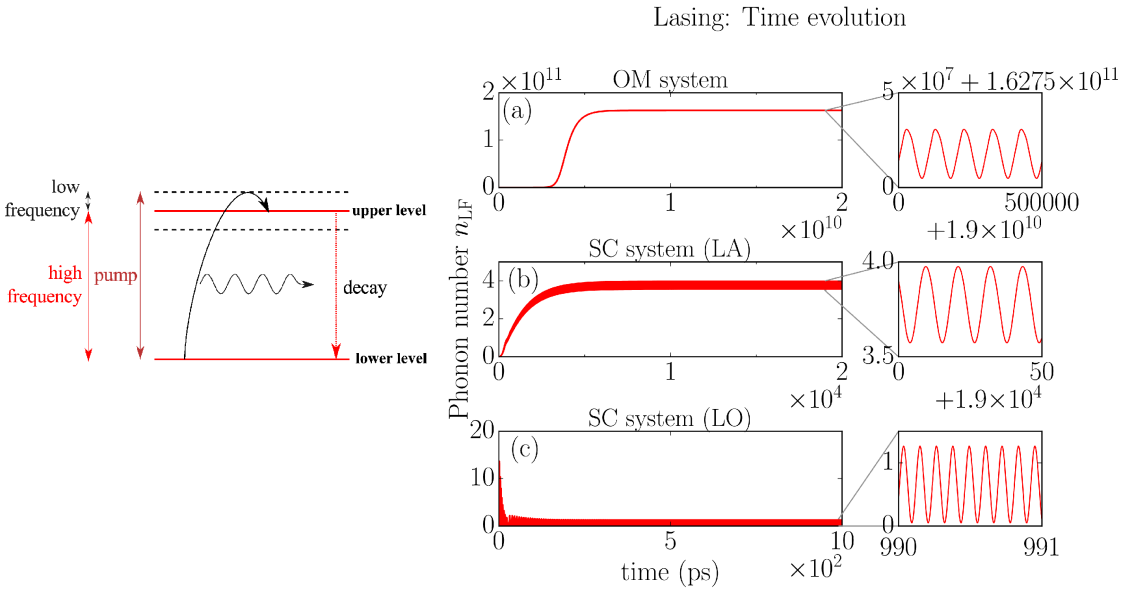

Figure 4.3.1.: Left: Schematic depiction of the process enabling phonon lasing. The system is pumped with a frequency that is roughly the sum of low and high frequency. Then each time the system is excited an excitation in the low frequency mode is created. When the high frequency mode is decayed back to the ground state the process can occur again. Right:The time evolution of the phonon number for (a) the OM (Parameters: cf. Tab. 4.3.1), (b) the SC system with LA phonons (Parameters cf. Tab. 4.3.1 and $\Delta = 0.973 \times \Omega$, $E_1 = 80$ GHz), and for (c) the SC system with LO phonons (Parameters cf. Tab. 4.3.1 and $\Delta = 0.845 \times \Omega$, $E_1 = 9.01$ THz). (These figures were previously published in Ref. [Nau+16]. © 2016 Optical Society of America, used with permission.)

In case of the OM system, in the regime of low pump strength, the maximum phonon number is indeed observed at the detuning corresponding to the single phonon process [cf. Figs. 4.3.2(a)]. When the pump power increases also higher order phonon processes become accessible and allows for higher phonon numbers, as then in a single cycle multiple phonons may be created. Then the maximum phonon number is observed at higher detunings. In contrast to the SC case, the resonances are broad, so that individual processes may not be distinguished. Multi phonon processes will be discussed in more detail in Sec. 5. In case of the SC system with LA phonons, the resonances are more sharp, so that the single phonon process can be clearly distinguished from the two phonon process, which becomes efficient for 5 QDs at high pump strengths [cf. Fig. 4.3.2(c)]. For even more QDs [cf. Fig. 4.3.2(d)] the regimes of the processes mix, as the lasing regime becomes larger, when increasing the number of QDs. Also the mean number of phonons is increased proportional to the number of QDs. Furthermore, the number of phonons, that are created is higher when the second order process is available. Again, this will be investigated in more detail using a full quantum mechancial model in Sec. 5. For the SC systems one can clearly observe the shift of the lasing resonance to lower detuning when increasing the pump strength [cf. Fig. 4.3.2(b)]. This shift can be evaluated approximately by considering the second order process depicted in Fig. 4.3.1, Left. The derivation for multiple QDs is shown in the App. A.1, which follows Ref. [Kab+12; KCK13]. The detuning, at which the resonance will be

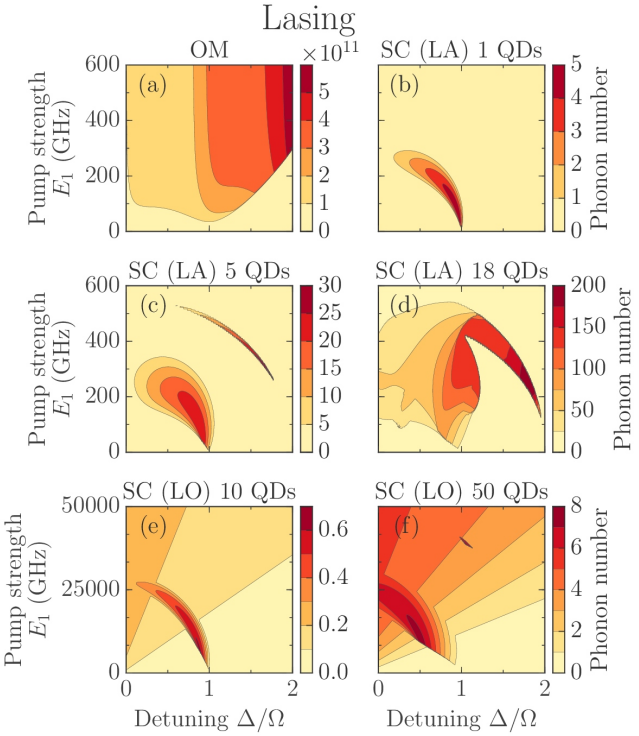

Figure 4.3.2.: The time averaged phonon number in the steady state is shown as a function of the detuning and the pump strength for (a) the OM system (Parameters cf. Tab. 4.3.1), the SC (LA) system (Parameters cf. Tab. 4.3.1) with (b) 1, (c) 5, and (d) 18 QDs, and the SC (LO) system (Parameters cf. Tab. 4.3.1) with (e) 10 and (f) 50 QDs. (This figure was previously published in Ref. [Nau+16]. © 2016 Optical Society of America, used with permission.)

observed is approximately $\Delta_{\text{eff}} = -\Delta - 2\frac{E_1^2}{\Delta} - n_{\text{HF}}\frac{g^2}{\Omega}$. Here, self quenching (second term) and the polaron shift (third term) alter the unperturbed resonance. For multiple QDs [cf. Figs. 4.3.2(c),(d)] the polaron shift increases with the excitation of the QDs. As the QD excitation saturates, the shift is roughly proportional to the number of QDs. This is shown in Fig. 4.3.3 for the case of 3 QDs. The effective resonance with $n_{\text{HF}} \approx 3$ is plotted (blue, dashed). For low pump strengths the maximum of the phonon number is estimated well. When increasing the pump strength the effective resonance overestimated the shift. This is attributed to missing higher order terms in the effective Hamiltonian which become relevant for high E_1.

For the OM system also an effective resonance can be obtained, which reads $\Delta_{\text{eff}} = -\Delta - \frac{g^2}{\Omega} n_{\text{HF}}$. In this case, there is no direct self quenching with the laser power as the cavity mode is bosonic. However, there is a dispersive shift proportional to the excitation of the cavity mode, which indirectly also leads to a shift with the pump power. Due to the broad resonances and because g^2/Ω is very small due to the small coupling strength, the shift is not visible in Fig. 4.3.2(a).

The effective shift is strictly only valid for the single phonon resonance, however the two phonon resonance seems to obey a similar shift [cf. Fig. 4.3.2(c)], while a quantification is

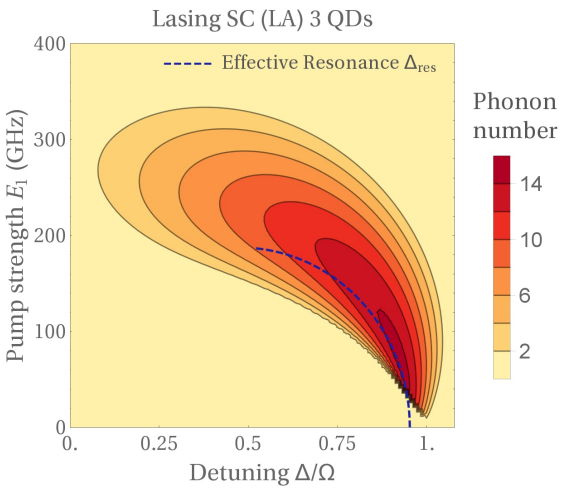

Figure 4.3.3.: Comparison between the numerically evaluated phonon number and the resonance predicted by the effective Hamiltonian Eq. (A.1.4). The blue dashed line corresponds to the resonance condition $\Delta_{\text{res}}^2 + (-\Omega + 3\frac{g^2}{\Omega})\Delta_{\text{res}} + 2E_1^2 = 0$. For low pump strengths the maximum of the phonon number is estimated well.

difficult due to the third order processes that have to be considered.

For the SC system with LO phonons, the qualitative behavior is similar as for LA phonons. However, the phonon number is much smaller due to the high phonon losses and the additional pure dephasing.

4.4. Enhancement of phonon damping

As complementary effect to lasing, the last effect, that will be considered here is the enhanced damping of the LF component (mechanical mode) caused by the interaction with the HF component (cavity mode/TLS). This effect is closely related to back-action cooling of the optomechanical mirror [WR+07; Mar+07; Gen+08; Hab+12]. In the following the computation is simplified as no noise input will be considered. This is done in order to keep the semiclassical description, which still allows to consider the change of the damping rate [cf. [AKM14; Gen+08]].

This will be done by evaluating the largest Lyapunov exponent governing the dynamics of the coupled system by computing it for the linearized equations as done for the stability analysis, cf. Sec. 4.2 and Ref. [Nau+14].

The enhancement of the damping rate for all systems is illustrated in Fig. 4.4.1, where the largest Lyapunov exponent $\kappa_{\text{eff,L}}$ is given as a function of the detuning Δ and the pump strength E_1. In this section different parameters with smaller coupling strengths are used [cf. Tab. 4.3.1]. With larger pumping strengths as in Sec. 4.2 the OM system becomes instable for pump rates large enough to observe a significant enhancement of the damping rate. For the SC system this problem does not occur as the saturation of the excitation of the quantum dots also leads to a limited enhancement of the damping rate, which occurs before the system may become unstable.

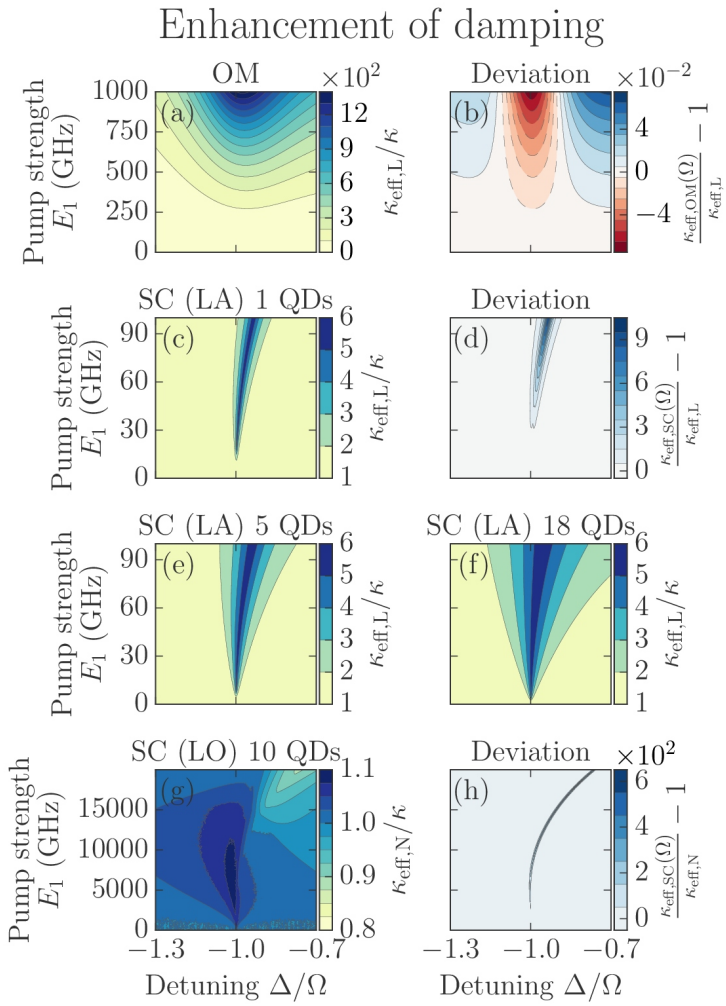

Figure 4.4.1.: Here, the effective damping rate for the OM and the SC with LA and LO phonons is depicted. (a) In case of the OM system, the damping is increased strongly up to 1400 times. (b) For this case, the formula (4.4.1) [cf. Ref. [Gen+08]] agrees well with the numerical evaluation. (c,e,f) By increasing the numbers of quantum dots in the SC system with LA phonons, the damping can be enhanced in a broader parameter range, while there is a maximum enhancement of about six times the inherent rate. (d) The analytical formula [cf. Eq. (4.4.2)] for the SC system falsely predicts a higher damping rate than observed numerically as it is only valid in the range of weak QD excitation. This is also the case for LO phonons (g), where the analytical formula also fails (h). (This figure was previously published in Ref. [Nau+16]. © 2016 Optical Society of America, used with permission.)

In Fig. [cf. Fig. 4.4.2] the process relevant for enhanced damping is depicted: Pumping the HF component to create a HF excitation leads to the absorption of a phonon. As for the case of lasing, this process is limited by the decay of the HF component and the number of times the HF component may be excited. Thus, in Fig. 4.4.1(a) a high enhancement

of the damping may be observed by 1400 times. For the SC system with LA phonons, depicted in Fig. 4.4.1(c), an enhanced damping by the factor of six may be observed. The maximal enhancement may not be increased by considering multiple quantum dots, cf. Fig. 4.4.1(e,f), but the range of paramters, where the damping is enhanced is indeed becoming larger. In the case of lasing the QDs were excited significantly. However, in the case of damping, the QDs are only excited very weakly and the phonon number is very small. This means that in this regime the Holstein-Primakoff approximation holds. Due to this fact, the relevant process does not become more efficient after a certain point, as no further phonons may be absorbed.

For the OM system and the SC system with LA phonons, the effective damping rate of the LF component may be computed as shown in Sec. 4.2 by considering the largest Lyapunov exponent, as the LF excitations have the longest lifetime. In case of LO phonons, however, the damping rate of the QD excitation is smaller than the one of the LO phonons, cf. Tab. 4.3.1. Thus, the largest Lyapunov exponent will be related to the QD system. In this case, the effective damping rate $\kappa_{\mathrm{eff,N}}$ of the LF component is determined by fitting an exponential enveloping function to the time evolution of the LF component position. This is shown in Fig. 4.4.1(g) for 10 QDs. The enhancement is very small as the decay rate itself is already very high. This renders the additional contribution due to the interaction rather insignificant.

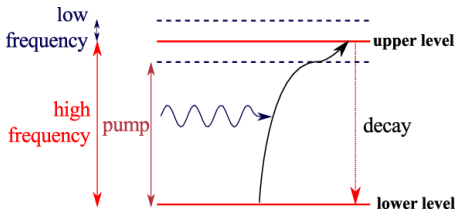

Figure 4.4.2.: Scheme of the mechanism leading to enhanced damping. The high frequency component is pumped with a frequency that is smaller than the high frequency. As this difference equals the low frequency each time the HF component is excited an excitation in the LF component is destroyed. This can be repeated after a decay of the HF component. (This figure was previously published in Ref. [Nau+16]. © 2016 Optical Society of America, used with permission.)

In the regime of small coupling strengths and pump rates, an analytical formula for the effective damping can be derived by assuming the dynamics of a harmonic oscillator in the vicinity of the steady state [Gen+08]: $\dot{B}_{\mathrm{eff}} = -\left(i\Omega_{\mathrm{eff}} + \kappa_{\mathrm{eff}}\right) B$. In addition to the effective damping rate an effective frequency due to the interaction Ω_{eff} can be evaluated. This which will be approximated by Ω in the following. In general also in vicinity of the steady state more complex dynamics may be possible.

The formula is derived as the linear response to some external force acting on the LF component in Eq. (4.1.3). After linearization, the equations may be Fourier transformed and a susceptibility may be defined, which is compared to the susceptibility of the harmonic oscillator. The details of this computation are shown in App. A.2.

In the case of the optomechanical system, the effective damping reads [Gen+08]

$$\kappa_{\mathrm{eff,OM}}\left(\bar{\omega}\right) = \kappa - \frac{4g^2 C_s^* C_s \Omega \gamma \tilde{\Delta}}{\left[\gamma^2 + \left(\bar{\omega} + \tilde{\Delta}\right)^2\right]\left[\gamma^2 + \left(\bar{\omega} - \tilde{\Delta}\right)^2\right]}. \tag{4.4.1}$$

This is valid if $C^*C \gg 1$. For the SC system, the resulting equation reads

$$\kappa_{\mathrm{eff,SC}}(\bar{\omega}) = \kappa - \frac{2Ng^2E_1\Omega}{\bar{\omega}^2+4\gamma^2} \frac{\left[\Re P_s\tilde{\Delta} - \Im P_s(\gamma-\gamma_{\mathrm{PD}})\right]\left(\gamma_r^2-\tilde{\Delta}^2-\omega_R^2\right) + 2\left[2\Re P_s\tilde{\Delta}\gamma + \Im P_s\left(2\gamma\tilde{\gamma}+\bar{\omega}^2\right)\right]\gamma_r\sqrt{1+\frac{\mathcal{D}}{2}}\sqrt{1-\frac{4E_1^2}{\bar{\omega}^2+4\gamma^2}}}{\left[\gamma_r^2+\left(\omega_R+\tilde{\Delta}\right)^2\right]\left[\gamma_r^2+\left(\omega_R-\tilde{\Delta}\right)^2\right]+2\mathcal{D}\gamma_r^2\omega_R^2}, \tag{4.4.2}$$

where $\Re(c)$ indicates the real part and $\Im(c)$ indicates the imaginary part of a complex number c. The short hand notation $\tilde{\Delta} = \Delta + \frac{Ng^2\Omega U_s}{\Omega^2+\kappa^2}$ is used in both equations. This effective detuning includes the dispersive shift for the stationary state.

While the equation in the SC system is more complicated the two equations share a common structure: For weak excitation, $\omega_R \approx \omega$, $\gamma_r \approx \tilde{\gamma}$, and $\mathcal{D} \approx 0$. As discussed before, the main shortcoming of the approximative formula is its reliance on a harmonic oscillator, which fails at some point for all systems. However, the failure is much more drastic for the SC system as the coupling strength is much larger. The comparison of the numerically evaluated effective damping with the analytical formula is shown in Figs. 4.4.1(b,d,h) for the OM system, the SC system with LA phonons and the SC system with LO phonons. For the OM system the deviation is small and is only in the range of a few percent even for high pump strengths. For the SC system with LA phonons, the effect is overestimated by about an order of magnitude. For the LO phonons it is overestimated by two orders of magnitude. Due to the large coupling strength for the phonons, the dynamics are not well approximated by a harmonic oscillator.

4.5. Conclusion

In this chapter of the thesis, the analogies between effects observable in optomechanical and semiconductor systems were studied. Two simple theories in semiclassical approximation were derived, where one component with a high frequency and one component with a low frequency were involved. Essential is the coupling between both parts. In the case of the optomechanical system, the high frequency component is a cavity while the low frequency component is the mechanically oscillating mirror. For the semiconductor system, the high frequency component is the excitonic QD transition and the low frequency component is either an acoustic phonon mode selected by an acoustic cavity or a collective mode of optical phonons.

In this simple model some principal features may be observed: While a bistability, lasing and enhanced damping is in principle present in all systems, the quantum dot can not be excited arbitrarily high, even when higher excited states are considered. The cavity mode on the other hand may sustain an arbitrary number of excitations. This difference leads to limited possibilities for a bistability and limited lasing in case of the semicondutor system. However, by increasing the number of considered quantum dots, this limitation may be lifted.

Another difference are the parameter regimes: While the coupling strength of the optomechanical system is very small in comparison to the cavity damping rate, the coupling

strength of the semiconductor system is within a strong coupling regime. This enables to observe nonlinear effects such as the bistability at low pump strengths. Furthermore, in the case of lasing it allows to observe the resonances of processes involving certain numbers of phonons. In the OM system these processes are not distinguishable, as the resonances are smeared out. For the SC system this aspect is considered in more detail in the next chapter, where a fully quantum mechanical description of phonon lasing in the few emitter regime is employed to investigate collective processes.

5. Collective effects in multi-emitter phonon lasing

After considering analogies between optoemechanical oscillators and semiconductor phonons, this section will focus on the lasing in the semiconductor system. Phonon lasing borrows its name from an analogy between sound and light waves. The optical laser amplifies the light field by stimulated emission. This concept is transferred to sound waves, which are quantized as phonons. To achieve this, several physical systems are candidates to build a phonon lasing device e.g. trapped ions [Vah+07; Men+10], coupled microtoriods [Gru+10], nitrogen-vacancy centers [Kep+13], electromagnetic resonators [Mah+13], and different semiconductor heterostructures [Cam+01; Bea+10; Kab+12]. In contrast to the previous section, the focus lies in particular on realizing the phonon amplification via stimulated emission using quantum dots embedded in acoustic cavities. The controlled fabrication of these cavities with a high quality factors has become more refined in recent years [Tri+02; LK+07; Roz+09; SRT11; LK+11; Fai+13; LKFJ15].

In Ref. [Nau+16], as presented in the previous section, effects in phonon lasers due to many emitters are studied using a semiclassical approximation and the assumption of identically behaving emitters. This simplifies the investigation for high numbers of emitters. However, it does not allow conclusions regarding the quantum statistics properties of the phonons. For the following work published in Ref. [Dro+17], these assumptions will be dropped to consider the correlations involved in the lasing with several emitters, as it has been done for single emitter phonon lasing [Kab+12]. Furthermore, additional resonances are observed which stem from processes where not all quantum dots behave in an identical manner. At the end of the chapter the impact of unequal coupling strengths and resonance frequencies will be briefly considered.

In the prototypical Tavis-Cummings model [TC68], which describes the interaction of the light field with multiple emitters, effects such as superradiance may be observed [Ley+15]. With these collective effects in mind, two phonon resonances and processes involving multiple QDs are of particular interest.

In this chapter, the new resonances appearing for multiple quantum dots are discussed. The underlying processes are considered by employing a quantum mechanical perspective. There may be several processes leading to single and two phonon emission. These are discussed and illustrated by using a higher electron phonon coupling than in Ref. [Kab+12] for the numerical study of the phonon laser Hamiltonian. The quantum mechanical framework allows to evaluate the statistics of the phonons, which is found to be coherent at all resonances. This permits to create a higher number of coherent phonons at the same pump strength using multi-phonon processes.

5.1. Fully quantized solution

In Chapter 4, a semiclassical approximation was used in order to simplify the system of equations that is needed to be solved. By furthermore assuming that all emitters follow the same dynamics it was possible to reduce the problem to a system of three nonlinear first order differential equations. When studying collective processes in the following the assumption of identical emitters is also made but scrutinized later on. In order to simulate the fully quantum mechanical system dynamics the full evolution of the density matrix is considered. Here the focus will be on the few emitter regime of up to three emitters as. As already described in the last chapter, losses in the emitter occupation and of phonons are included by the Lindblad terms $\sum_i \mathcal{L}[p_i]\rho$ and $\mathcal{L}[b]\rho$, respectively. Here, pure dephasing is neglected as this is beyond the scope of this thesis. However, a future question may be the stability of the effects discussed here against pure dephasing. However, as discussed before, the pure dephasing is assumed to be small for acoustic phonons that are considered in this chapter. Thus the system dynamics is given by the equation for the density matrix [BP02]

$$\dot{\rho} = -\frac{i}{\hbar}[H,\rho] + \gamma \sum_{i=1} \mathcal{L}^{N_{\mathrm{QD}}}[p_i]\rho + \kappa \mathcal{L}[b]\rho. \tag{5.1.1}$$

For the numerical evaluation this equation is expanded in the set of basis states spanned by $|i_1,...,i_{N_{\mathrm{QD}}},i_{\mathrm{ph}}\rangle$. Here, i_{ph} indexes the phonon number states from 0 to N_{ph}, where N_{ph} is the maximal number of phonons taken into account. This has to be chosen large enough so that the observables of interest do not change with increasing N_{ph}. The indices $i_1,...,i_{N_{\mathrm{QD}}}$ state whether the emitters are in the exited (e) or in the ground state (g). Writing Eq. (5.1.1) in this basis leads to a set of $N_{\mathrm{eq}} = \left(2^{N_{\mathrm{QD}}} N_{\mathrm{ph}}\right)^2$ coupled first order linear differential equations. These are again solved by a fourth order Runge-Kutta algorithm. After shortly introducing the theoretical approach now, a short overview of some processes allowed by the Hamiltonian Eq. (3.2.1) is given in order to allow the interpretation of the numerical results.

5.2. Processes leading to the creation of phonons

In this section, the processes that allow to create phonons are discussed in more detail and from a different perspective than in Sec. 4.3. This will help to explain the numerical results in the following section. Investigating the Hamiltonian Eq. (3.2.1) allows for a zeroth order estimation in the coupling strength of the energies involved. The relevant energies for $H_0 = \hbar\omega_{\mathrm{vc}}\sigma_+\sigma_- + \hbar\omega_{\mathrm{ph}}b^\dagger b$ in the case of two quantum dots are $E_{n_1,n_2,n_{\mathrm{ph}}}/\hbar = n_1\omega_1 + n_2\omega_2 + n_{\mathrm{ph}}\omega_{\mathrm{ph}}$ with the corresponding states $|n_1,n_2,n_{\mathrm{ph}}\rangle$. By pumping the QD via an external laser with detuning $\Delta = \omega_{\mathrm{ph}}$, several processes are energetically possible, when the energy shifts due to the interaction are neglected. In Fig. 5.2.1 the processes of interest for the case of two QDs are shown. The process that is known from the case of a single QD takes place by using the laser energy once to excite a single QD and create a phonon, cf. Fig. 5.2.1(a). The external coherent laser field may excite all phonon number states if the corresponding processes are efficient. In the setup of interest, the pump laser energy may be absorbed twice and excite two quantum dots and two phonons simultaneously, as depicted in Fig. 5.2.1(b). The more QDs are present the more simultaneous phonon

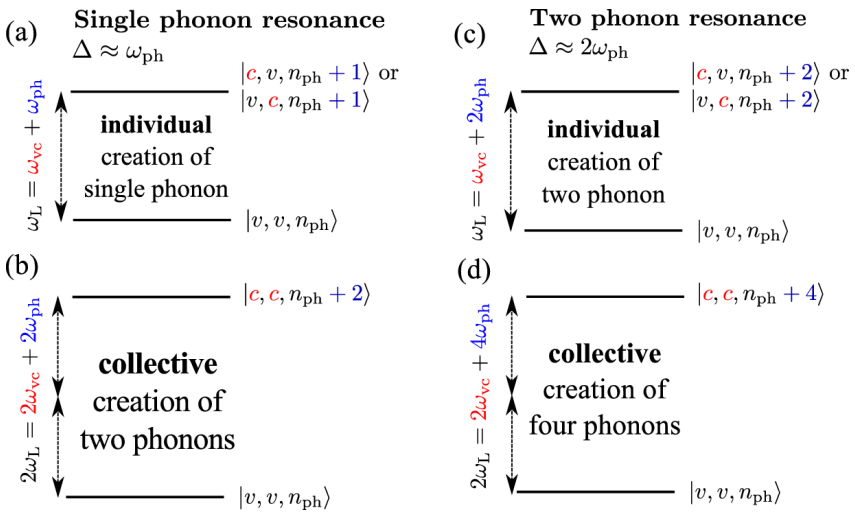

Figure 5.2.1.: Excitation scenarios leading to phonon generation illustrated for the case of small interactions, where certain energy levels are degenerate that split up for high coupling strenth g and driving E_1. For $\Delta \approx \Omega$, two cases are be investigated. A single phonon process (a), which corresponds to the single emitter case. One phonon is created using the excess energy when exciting a single QD. (b) For $\Delta \approx 2\omega_{\mathrm{ph}}$, two phonons are created collectively by exciting both QDs. If the detuning is chosen to be twice the phonon frequency, similar processes take place creating twice the phonons (c,d).

creation processes may occur, but at maximum as many as QDs are present. There are, however, also other resonances that may be addressed by an appropriate detuning. In the following the two phonon process will be of particular interest. When $\Delta = 2\omega_{\mathrm{ph}}$ (again this is valid if the shifts due to E_1 and g are neglected), then two phonons may be created by exciting one QD to the excited state, cf. Fig. 5.2.1(c). In the same manner as before also $2N_{\mathrm{QD}}$ phonons can be excited in the case of multiple QDs. Then each QD creates 2 phonons simultaneously, as shown in Fig. 5.2.1(d). There are several other processes to create a certain number of phonons within one cycle by certain choices for the detuning. In the following only the focus lied on the cases discussed in this section. The case with $\Delta = \omega_{\mathrm{ph}}$ is the prototypical process and it is investigated in what way this is influenced by multiple QDs. Furthermore, two phonon generation is considered as a process which is able to create more phonons than the single phonon process. As discussed in the last chapter in order to create a high number of phonons, the radiative decay of the QD is imperative. Without this incoherent process the system would oscillate between the states addressed by the frequency of the pump laser. By considering a large coupling strength g, in comparison to Sec. 4.3, the shifts due to the interactions become relatively large and lead to different energy shifts for different phonon creation processes. For the single phonon case, the shifts are estimated by an effective theory, as shortly discussed in Sec. 4.3 and presented in more detail in App. A.1. For the two phonon case an analogous behavior is observed.

5.3. Many emitter phonon lasing

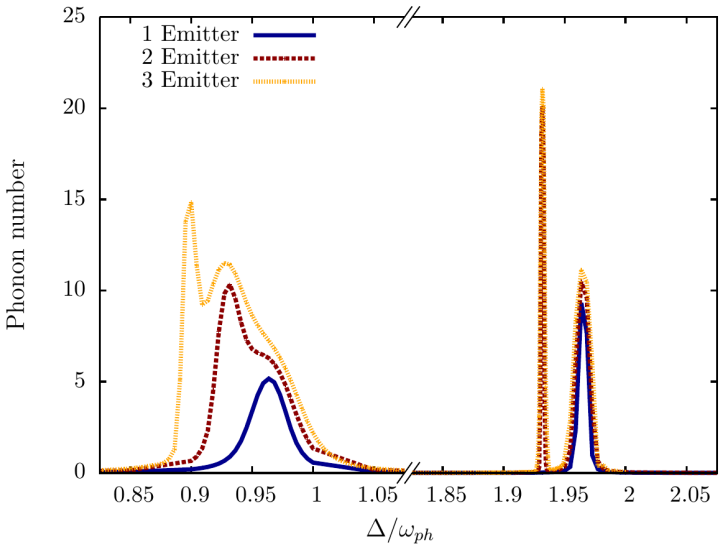

Figure 5.3.1.: Phonon number in the acoustic phonon mode for one (blue, solid line), two (red, dashed), and three (yellow, dotted) Emitters. When increasing the number of emitters new resonances appear, while the peaks observed for fewer emitters remain. The phonon number of the additional peaks is higher. while their width is smaller. This may be observed for the resonance at $\Delta \approx \omega_{\mathrm{ph}}$ and $\Delta \approx 2\omega_{\mathrm{ph}}$. The peaks at the two-phonon resonance are higher as multiple phonons may be created each cycle , cf. Fig. 4.3.1, Left. Parameters: $\omega = 2.281/\mathrm{fs}$, $\omega_{\mathrm{ph}} = 0.011/\mathrm{fs}$, $E_1 = 4.56 \times 10^{-4}/\mathrm{fs}$, $g = 2 \times 10^{-3}/\mathrm{fs}$, $\gamma = 10^{-5}/\mathrm{fs}$, and $\kappa = 5 \times 10^{-7}/\mathrm{fs}$. (This figure is previously published in Ref. [Dro+17]. Copyright 2017 American Physical Society, used with permission.)

In Fig. 5.3.1 the phonon number as a function of the optical detuning for a fixed external pump strength is shown for one, two and three QDs.

Several lines appear near the expected single- and two-phonon-resonances $\Delta \approx \omega_{\mathrm{ph}}$ and $\Delta \approx 2\omega_{\mathrm{ph}}$, for a single QD. At the single- and the two-phonon-resonance, only a single peak is observed. When increasing the number of quantum dots the number of peaks is also increased. At the single-phonon-resonance adding a QD leads to the appearance of a new peak. For the two-phonon-resonance only up to two peaks are observed for the choice of parameters. All peaks are red-shifted with respect to $\Delta = \omega_{\mathrm{ph}}$. The additional peaks appearing for multiple QDs are even more red-shifted. The peaks appearing by adding more QDs are attributed to collective effects, where all QDs emit a phonon collectively, and thus are called collective resonances. In the following this will be explained.

By inspecting Fig. 5.3.1 more carefully, it may be observed that the collective resonances lead to more narrow peaks. Furthermore, the two-phonon-processes exhibit narrower lines than the single-phonon-processes. However, while the peaks are narrower, they also become higher. At the two phonon resonance about twice the number of phonons are observed. Collective processes also have higher phonon numbers than the line that is present for the single QD case.

To test if the high phonon numbers are in fact due to a coherent phonon lasing process,

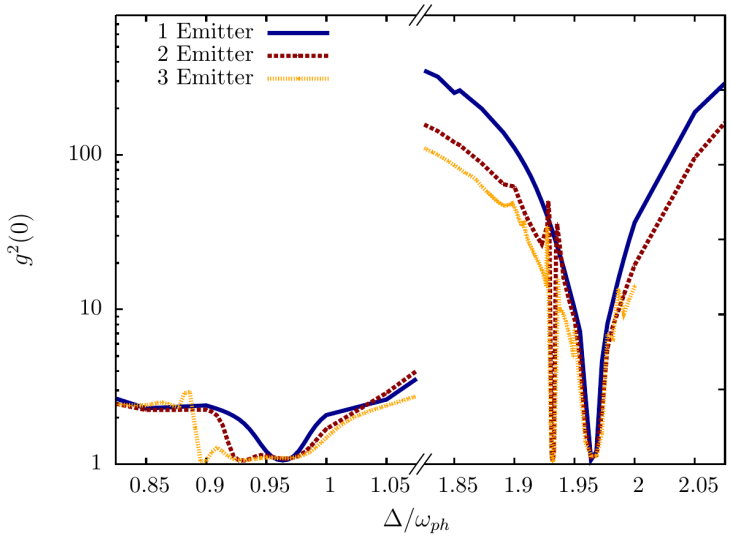

Figure 5.3.2.: The stationary second order correlation function is shown for one (blue, solid line), two (red, dashed), and three (yellow, dotted) Emitters. At the single as well as at the two phonon line the second order correlation function reaches unity, which indicates coherent statistics as expected for laser action.

the statistics of the phonon mode are studied. Thus, the second order correlation function is computed for the steady state. This is defined as, cf. Chapter 2,

$$g^{(2)}(\tau) = \lim_{t\to\infty} \frac{\langle b^\dagger(t) b^\dagger(t+\tau) b(t+\tau) b\rangle}{\langle b^\dagger(t) b(t)\rangle^2}. \tag{5.3.1}$$

The value for $\tau = 0$ is shown in Fig. 5.3.2 as a function of the detuning for the same parameters as in Fig. 5.3.1. A value of unity is an indicator of coherent statistics and a necessary condition for phonon lasing. At all observed peaks indeed a value of $g^{(2)}(0) \approx 1$ is observed also for the two-phonon-resonances. This indicates that also the two-phonon-process creates coherent phonons. The collective resonances also show $g^{(2)}(0) \approx 1$.

5.3.1. Effective approach

In the following, the properties of the collective processes will be studied in more detail using the effective Hamiltonian approach presented in App. A.1. After eliminating the non-energy-conserving terms for $\Delta = \omega_{\mathrm{ph}}$ for the case $N_{\mathrm{QD}} = 2$ and assuming alls coupling elements, driving strengths and frequencies to be equal for both QDs, Eq. (A.1.4) reads

$$\begin{aligned} H_{\mathrm{eff}} = \hbar\omega_{\mathrm{ph}} b^\dagger b - \hbar\left[\Delta + 2\frac{\hbar E_1^2}{\Delta} + \frac{\hbar g^2}{\omega_{\mathrm{ph}}}\right](\hat{p}_1^\dagger \hat{p}_1 + \hat{p}_2^\dagger \hat{p}_2) - \frac{\hbar g^2}{\omega_{\mathrm{ph}}}\left[\hat{p}_1^\dagger \hat{p}_1 \hat{p}_2^\dagger \hat{p}_2 + \hat{p}_2^\dagger \hat{p}_2 \hat{p}_1^\dagger \hat{p}_1\right] \\ + \frac{i\hbar g E_1}{2}\left(\frac{1}{\Delta} + \frac{1}{\omega_{\mathrm{ph}}}\right)\left[\left(\hat{p}_1^\dagger + \hat{p}_2^\dagger\right) b^\dagger - \left(\hat{p}_1 + \hat{p}_2\right) b\right]. \end{aligned} \tag{5.3.2}$$

In this Hamiltonian, the second term gives the effective energy of the emitters, the third term is a phonon induced interaction between different emitters and the last terms is the electron-phonon interaction. This interaction now has a form similar to the Tavis-Cummings interaction. However, in this case a phonon is created when an electron is brought to the excited state. This process is energetically possible due to the external pumping. The third term will be considered in more detail. This term reduces the resonance frequency, when both QDs are excited. The impact of this term on the phonon laser is shown in Fig. 5.3.3. Here, the resonances close to $\Delta \approx \omega_{\mathrm{ph}}$ are considered for the effective Hamiltonian Eq. (5.3.2) (dashed lines) as well as for the full Hamiltonian Eq. (3.2.1) (solid line). The third term in Eq. (5.3.2) corresponds to a QD-QD interaction. When considering the effective Hamiltonian without the this interaction, only one resonance is predicted and the intensity of the resonance is overestimated by a factor of two. When including the QD-QD interaction, both resonances exhibited by the full Hamiltonian are reproduced with a small deviation in height. The width is overestimated by the effective Hamiltonian. As the lower resonance is successfully predicted by including the phonon induced QD-QD interaction, this resonance is attributed to collective effects, since the QD-QD interaction only contributes to the shift, when both QDs are excited due to the operator product $\hat{p}_2^\dagger \hat{p}_2 \hat{p}_1^\dagger \hat{p}_1$. The effective Hamiltonian allows to estimate the energy shifts induced by the interactions. There are the shifts due to the electron-phonon interaction and due to the external pumping laser (i.e. electron-photon interaction). For the single phonon resonance they may be estimated from Eq. (5.3.2) as $-\frac{\hbar g^2}{\omega_{\mathrm{ph}}}$ and $-2\frac{\hbar E_1^2}{\Delta}$, respectively. The QD-QD interaction adds to the energy shift, if both QDs are in the excited state, increasing the shift to approximately twice the shift for two QDs in the case of equal coupling strengths.

This is consistent with the findings in Sec. 4.3, cf. Fig. 4.3.1, where the shift was estimated to go roughly with the number of QDs. In Sec. 4.3, the QDs were assumed to exhibit the same dynamics, which corresponds to the collective case. Due to the smaller electron-phonon coupling strength, the individual resonances can not be the resolved so that it is not clear which of the so far discussed processes are also included in the semiclassical model.

5.3.2. Collective Resonances

The discussion in Sec. 5.2 suggests that the collective resonance is enabled by a process of higher order in the pumping strength. Then, they would only be observed for higher pumping strengths. Fig. 5.3.4 shows that this is indeed true. For smaller pump strengths Fig. 5.3.4(a) only the single QD resonance may be observed. When increasing the pump, the resonance appears, at first not at maximal strength, cf. Fig. 5.3.4(b). With even more increasing pump it appears at full strength Fig. 5.3.4(c). Once it reaches twice the height of the single QD resonance, only the width of the collective resonance increases, cf. Fig. 5.3.4(d). In this case the single emitter resonance becomes higher for the case with two emitters as it overlaps with the collective resonance. This study shows that the two emitter case also includes the resonance of the single emitter case at the same strength.

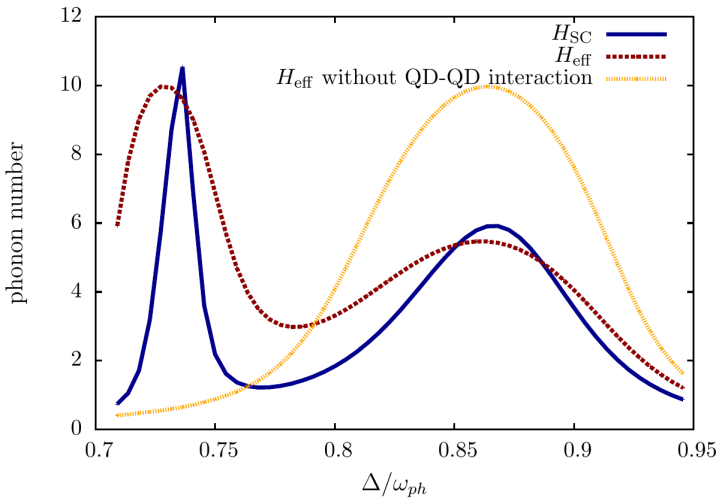

Figure 5.3.3.: The effective Hamiltonian H_{eff} Eq. (A.1.4)/(5.3.2) is compared with the full Hamiltonian Eq. (3.2.1). When the phonon induced QD-QD interaction (cf. third term in Eq. (5.3.2)) is neglected the position of one peak is predicted in accordance to the full Hamiltonian. However, the height is overestimated by the factor of two. When including the QD-QD interaction, the position and height of both peaks is predicted well, while their width is overestimated. (This figure is previously published in Ref. [Dro+17]. Copyright 2017 American Physical Society, used with permission.).

5.3.3. Two phonon resonance

With the above findings in mind, the resonances at $\Delta \approx 2\omega_{\mathrm{ph}}$ in Fig. 5.3.1 are considered once more. For the case with two and three QDs also at this resonance two peaks are present. While the effective Hamiltonian Eq. A.1.4 is not valid for this case, at it was derived with the assumption of a detuning $\Delta \approx \omega_{\mathrm{ph}}$, the size of the shifts seems in the same order as before. In analogy to the single phonon resonance $\Delta \approx \omega_{\mathrm{ph}}$ the processes involved in the two phonon case are the ones depicted in Fig. 5.2.1(c) for the smaller peak and the ones depicted in Fig. 5.2.1(d) for the more intense peak. The higher the order of the process, the smaller the width of the peak becomes, but the more phonons may be created in a single cycle.

As these peaks also correspond to higher order processes so that they also will appear at high pump strength, but a given peak may also appear more likely for more QDs. This is also discussed in Sec. 4.3, where the two phonon resonance is observed for higher pump strengths than the single phonon resonance, but also only for multiple QDs as the coupling is smaller. For the parameters used in this section, the two phonon resonance may already be observed for few emitters.

With these arguments there should be also a third peak for the case with three emitters at the two phonon resonance. This is indeed the case as it may be observed when the pump strengths is increased even further.

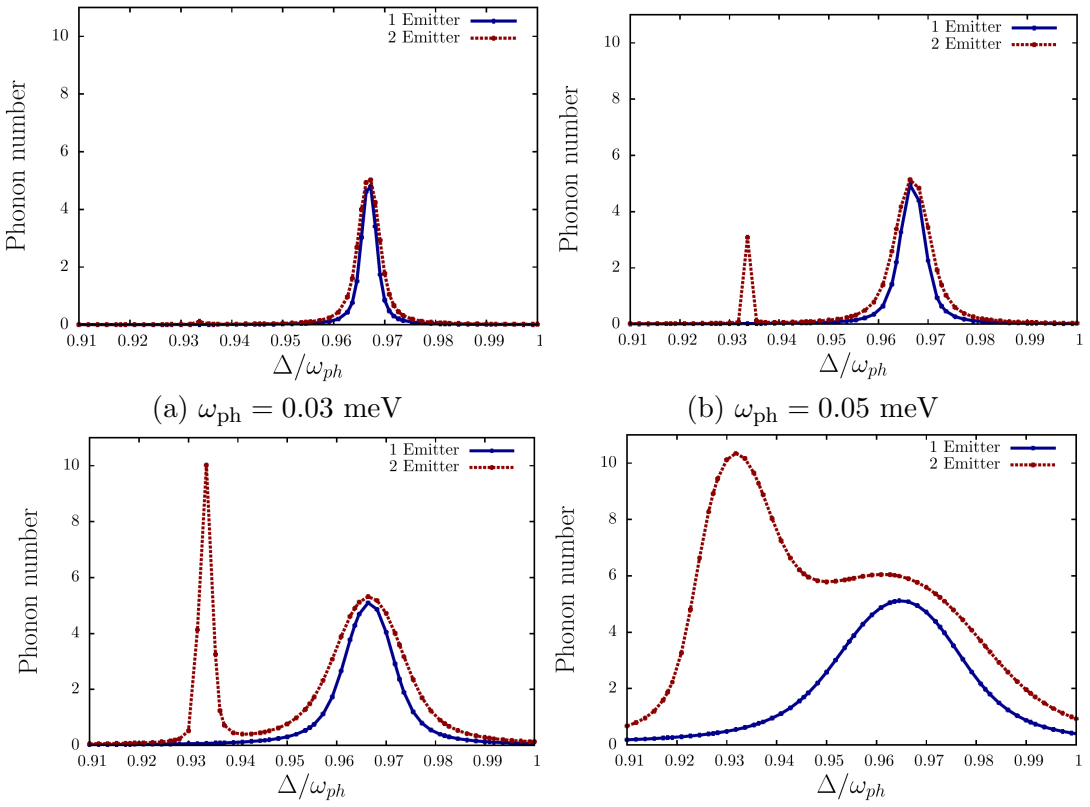

(a) $\omega_{\mathrm{ph}} = 0.03$ meV (b) $\omega_{\mathrm{ph}} = 0.05$ meV

(c) $\omega_{\mathrm{ph}} = 0.1$ meV (d) $\omega_{\mathrm{ph}} = 0.25$ meV

Figure 5.3.4.: The behavior of the resonances with increased pump strength is shown for one (solid, blue line) and two (dashed, red line) is shown. At small pump strengths (a) both cases coincide, as the pump is not strong enough to excite both QDs. When the pump is, increased at first (b) a small collective resonance appears, until it grows to its full height (c). Further increase in the pump strength only increases the width of the resonances (d). (Figures (a), (c), and (d) are previously published in Ref. [Dro+17]. Copyright 2017 American Physical Society, used with permission.)

5.3.4. Nonidentical emitters

So far the emitters were assumed to be identical. In experimental situations, however, the quantum dots which are manufactured are rarely identical [BGL99; Mic03; Jah12]. Therefore, this section considers deviations in the optical resonances and in the electron phonon coupling elements for the case of two quantum dots. As two individual quantum dots are considered, this treatment does not describe inhomogeneous broadening in an ensemble of quantum dots. The focus lies on two manufactured non-identical quantum dots. However, the following study gives an estimation about which deviations in transition energies and electron phonon may be tolerated.

First, a deviation in the transition energies $\omega_{\mathrm{vc},i}$ in Eq. (3.2.1) is considered. When considering different $\omega_{\mathrm{vc},i}$, this results in different $\Delta_i = \omega_{\mathrm{L}} - \omega_{\mathrm{vc},i}$ with respect to the driving laser frequency. In the following $\omega_{\mathrm{vc},1}$ will be assumed to be the energetically higher transition and will serve as reference so that the plots show the detuning from the

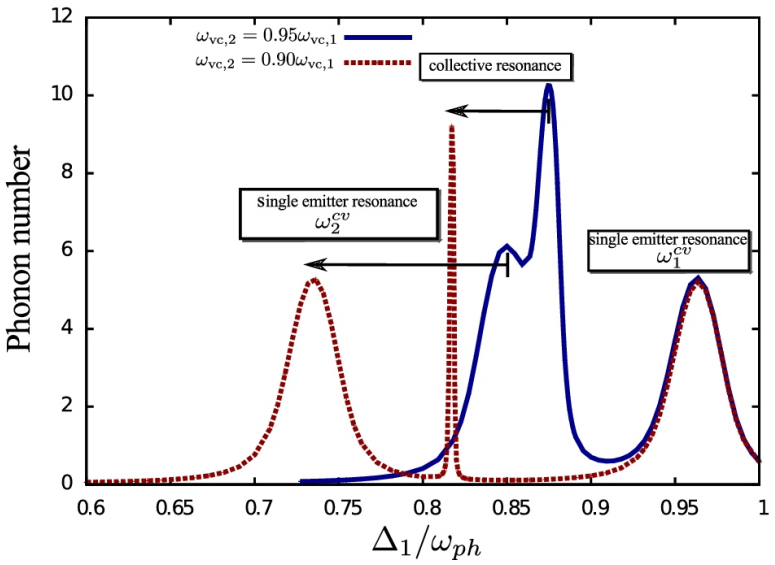

Figure 5.3.5.: The effect of different transition energies on the collective resonance is shown. As expected, the collective resonances becomes smaller when the difference becomes larger. When the transition energies differ by about 10%, the peak is significantly smaller. (This figure is previously published in Ref. [Dro+17]. Copyright 2017 American Physical Society, used with permission.)

energetically higher resonance. In Fig. 5.3.5 two cases are considered. First, a deviation of 5% in the transition frequency, i.e. $\omega_{\mathrm{vc},2} = 0.95\omega_{\mathrm{vc},1}$ and second a difference of 10%, i.e. $\omega_{\mathrm{vc},2} = 0.9\omega_{\mathrm{vc},1}$. The figure shows that an increasing difference in the transition frequencies leads to a reduced height and width of the collective resonance. Thus, the collective resonance vanishes for large deviations. The single emitter resonances shift so that they are at different resonances. The individual peaks may still be explained by the effective Hamiltonian Eq. (5.3.2) when taking into account the different transition energies. The collective resonance can be estimated by taking into account the mean transition energy as

$$\Delta_{\mathrm{coll}} = \omega_{\mathrm{ph}} - \frac{\omega_{\mathrm{vc},1} - \omega_{\mathrm{vc},2}}{2} - \frac{2g^2}{\omega_{\mathrm{ph}}}. \tag{5.3.3}$$

Thus, the collective resonance is between the individual resonances, but should become very narrow until disappearance.

Now, a deviation in the coupling strengths in Eq. (3.2.1) is considered. Here much larger differences may be tolerated without disappearance of the collective resonances. Here, g_1 will be used as reference with the value given in the caption of Fig. 5.3.1. In Fig. 5.3.6 the deviations $g_2 = 1.6g_1$, $g_2 = 2.0g_1$, and $g_2 = 4.0g_1$ are given. For a deviation of 60% (solid, blue curve) only a small deviation from the case $g_1 = g_2$ is observed. An additional shoulder is observed for the peak as the single emitter resonances split up. For the deviation of $g_2 = 2g_1$, the collective resonance is still at the same height. In this case the collective and one single phonon resonance are very close. For a high deviation with $g_2 = 4g_1$, the single emitter resonances are clearly separated due to the dispersive shift. The second single emitter resonance is higher than the first one due to the higher coupling strength. The collective resonance in this case is clearly smaller in height and

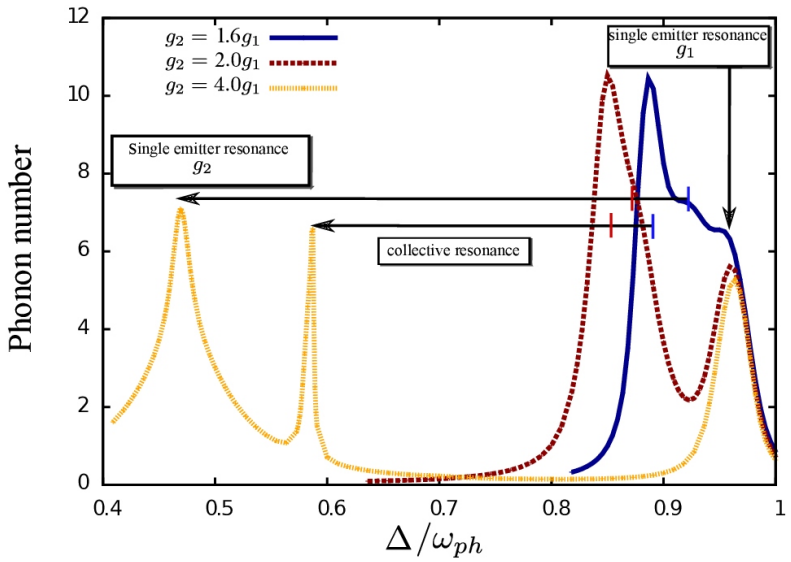

Figure 5.3.6.: The effect of different coupling strengths on the collective resonances is shown. In this case, a large relative difference between the coupling strength may be tolerated. For a coupling strengths four times as high, a significantly smaller collective peak is observed. (This figure is previously published in Ref. [Dro+17]. Copyright 2017 American Physical Society, used with permission.)

width. Interestingly, it is now located in between the single emitter resonances.

The single emitter resonances can still be described by the effective Hamiltonian Eq. (3.2.1) when accounting for the different coupling strengths in the dispersive shifts

$$\Delta_i \approx \omega_{\mathrm{ph}} - \frac{g_i^2}{\omega_{\mathrm{ph}}}. \tag{5.3.4}$$

The collective resonance, however, is not anymore described well by the effective Hamiltonian in the case of different coupling strengths. A heuristic formula for the collective resonance for the two emitter case with different coupling strengths is estimated from Fig. 5.3.6 by the mean of the coupling strengths as

$$\Delta_{\mathrm{coll}} \approx \omega_{\mathrm{ph}} - \frac{(g_1 + g_2)^2}{2\omega_{\mathrm{ph}}}. \tag{5.3.5}$$

For equal coupling strengths this agrees with the effective Hamiltonian Eq. (5.3.2).

5.4. Conclusion

In this chapter the collective resonances in a semiconductor acoustic cavity with multiple emitters are studied. The results agree qualitatively with the observations in Sec. 4.3, where a semiclassical approximation is used as in both cases the shifts are correctly modeled by the effective Hamiltonian for weak pump strengths. However, this chapter focuses on the additional resonances due to the many emitter setup. These may be demonstrated by using higher electron phonon coupling strengths than in Sec. 4.3. There,

individual peaks cannot be resolved. However, due to the approximations made there, it is an open question whether these would be observed at all. In particular the assumption of the same dynamics in each individual quantum dot should imply that in fact only collective processes are modeled. The increase of the peaks with the number of emitters suggests that indeed the collective resonance is observed there as the height of the individual resonances in this chapter are not proportional to the number of emitters. The shift of the collective resonance proportional to the number of quantum dots as estimated by the effective Hamiltonian in Sec. 4.3 is confirmed by the fully quantum mechanical model. This also showed that an analogous splitting of the two phonon resonance is observed. The fully quantum mechanical treatment also allows to consider the statistics of the phonons. The phonon statistics for the two phonon resonance is also coherent so that this peak can indeed be attributed to phonon lasing. Employing the quantum mechanical model, also an estimation for the possible deviations in emitter energies and coupling strengths for collective processes is estimated. While the emitters may not deviate more than 10% in their energy, the coupling strength is more robust against deviations. When the coupling strength for the second emitter is four times the one for the first emitter, the resonance is still present, even if it is considerably narrower. This is particularly interesting as the coupling strength is sensitive against the size and the placement of the emitters inside the acoustic cavity. By establishing the robustness against this deviation, an imperfect placement does not entail a massive degradation in phonon generation.

Due to the straightforward density matrix formalism, only up to three quantum dots are considered because many phonon number states are needed for the correct numerical evaluation, for incresing number of emitters. Algorithms exploiting permutation symmetries may be used to study higher numbers of emitters without inhomogeneous broadening [Car02; GR16]. Then, also direct diagonalization of the Liouville propagator is possible, which allows a speedup in the computation of the steady state [GR17]. As in the following inhomogenous broadening will be taken into account these techniques are not easily accessible.

This concludes the part about control of mechanical oscillators by coherent laser fields. In particular in case of coherent phonon generation the external laser is used to induce coherent statistics into the mechanical oscillator, which corresponds to a steering of the quantum statistics of the phonons. In the following parts the control of quantum statistics is still of major interest. However, there the control of the quantum statistics of optical fields is considered. In the next Part II, the influence of an optical emitter with given emission photon statistics on the emission statistics of a second quantum optical system is considered.

Part II.

Control by cascaded driving

6. Non-classical pumping via a dissipative channel

So far the environment to which the physical system is coupled only served as a channel to include losses from the system. Either in form of radiative decay or in the form of pure dephasing. The mechanical systems of Part I were manipulated to exhibit coherent statistics induced by a classical external pump laser. In general the light used to pump a system is not necessarily coherent. For example, systems may be incoherently driven, which will also be considered in this part. The main case of interest, however, is when antibunched light is used to pump a quantum system. Then, the quantum nature of the incoming light needs to be taken into account. In the following this will be done by using a cascaded setup [Gar93; Car93], where a source system is used to pump a target system. Both of the systems are modeled quantum mechanically.

This chapter follows the publication Ref. [Azi+17], where the results were published recently. Here, the quantum nature of the light emitted from the source is included as well as the influence of the channel transferring the light from source to target. The coupling channel is modeled as an electrodynamical environment. However, in contrast to Part I, where the environment was only responsible for dissipation and decoherence, now also to some degree coherence is transferred from the source to the target. The setup where a source quantum system unidirectionally excites a target system is called a cascaded setup. It simplifies the evaluation since the coupling channel is traced out and no back-action from the target on the source is considered.

The Jaynes-Cummings model that will be used in this chapter as a source is a prototypical source of antibunched light. However, there are various other examples for quantum light sources. In this context semiconductor nanostructures are of particular interest for possible applications. Next to single photon sources [Shi07; IDM16; Gai09; BRV12] light states with a certain fixed number of photons may be generated [Hei+17; Mun+14]. Furthermore, there are sources that produce polarization entangled photons [Sch+12] on demand [Shi07] or time ordered photon pairs [Bou+17]. Further light sources that offer the possibility to create quantum states of light are nanophotonic structures [Lod+17] and even biological systems are studied with respect to their emission properties [Sim+12].

There are several applications for quantum light sources. The most prominent being probably the use of single photon sources for cryptographic protocols [Kim08; Zol+05; Jen+00]. Quantum light is furthermore useful for probing the properties of targets as excitation with certain light states may, e.g., enhance the signal quality in spectroscopic setups [Wal15; KK06a; Kir+11; KK06b] or increased the resolution in double-quantum-coherence spectroscopy [RM10]. Furthermore, two photon sources are interesting from a fundamental point of view in quantum mechanics [PKM17] leading to time entangled-photons and corresponding Bell inequalities [Fra89], which may be used as another way of implementing quantum cryptographic protocols [Jay+14]. These two photon

transitions in turn are efficiently driven by entangled photons [SB15]. Another proposal is to purify non-classical states by suppressing fluctuations with single photon-pumping [LCn+15]. An application of high interest for quantum light is in the context of the optical implementation of quantum information science, where e.g. entangled photon pairs are proposed for implementing quantum gates by entanglement swapping for realization of quantum repeaters [Tro14].

Next to sources emitting light with nonclassical properties also well controllable thermal sources have been developed [BH84; Str+16; AB11; Jah+16] for spectroscopic applications [Kaz+15; Str+16] and for alternate probing techniques employing photon echoes [BH84].

After discussing different sources and their applications, a short overview of some of the previous investigations using the cascaded model will be given. The cascaded formalism was used to show that the response of the target system depends on the nature of the light statistics of the input for simple sources [KC94; GP94; Par96]. Following these investigations, recently the impact of the input statistics on correlations up to third order on a cavtiy mode [CnL16] and a two level system [Cn+16] was investigated. The use of higher order correlations for advanced characterization of the light field was proposed. These have become accessible in experiments e.g. via two photon spectroscopy [GT+13; DSM16].

This is the context for the chapter at hand. An incoherently driven Jaynes-Cummings model serves as source providing the input for a Tavis-Cummings model with two emitters as target. The emitters are again modeled by two level systems (TLSs). The Jaynes-Cummings model is used as a source as it exhibits a wide range of output statistics from antibunched to thermal statistics. The Tavis-Cummings model exhibits a large nonlinearity due to multiple emitters. In Chapter 10 of part III the Tavis-Cummings model will be considered again when feedback is used as a different way of manipulating the photon statistical output.

Using the quantum Langevin [Gar93] equation or the quantum stochastic Schrödinger equation [GZ04; Car09] in the cascaded approach the emission is self-consistently mapped to the input of the target system. This results in a coupling mechanism that mediates the excitation dissipatively from source to target. The cascaded setup does not destroy coherences completely. Rather the coherences are transferred to the target system, while they are necessarily degraded. Thus cascaded driving differs from thermal as well as from coherent excitation and constitutes an intermediate regime. In the following the intermixing of these regimes is discussed .

This Chapter is structured as follows. At first, in Sec. 6.1, the cascaded master equation is introduced. The derivation is sketched in App. B. The derivation may be conducted either using Langevin operators [GC85; CnL16] or the quantum stochastic Schrödinger equation [Car93; PZ16].

In Sec.6.1 the derived coupling is applied to the aforementioned example of two identical quantum emitters inside a cavity. When comparing this to the case of a single emitter, the observations for the intensity-intensity correlation are similar: The target follows the source in a classically degraded fashion, which is plausible for nonlinear quantum systems [ME15; MEK13]. When higher order intensity correlations are considered, which is done in Sec. 6.2, it becomes clear that the target does not simply follow the source in the trivial manner suggested by the $g^{(2)}$-function. The higher order correlations reveal a transitional regime in the statistical output of the target. In Sec. 6.3 this is compared to thermal and

coherent input light. Sec. 6.4 concludes the chapter.

6.1. Cascaded coupling of cQED systems

In this section the master equation used throughout the paper is introduced. A more detailed derivation can be found in App. B. In Fig. 6.1.1 a schematic depiction of the setup is shown. The output of an incoherently pumped optical cavity containing an emitter is used to drive the emitters inside a second cavity.

For the derivation of the coupling master equation the Born-Markov approximation is used and a thermal bath is assumed [CnL16; GC85; CG84; Gar86]. Then the bath degrees of freedom may be traced out when system and bath density matrix are assumed to factorize [BP02; Car02].

Considering general non-thermal bath states complicates the problem and other methods are needed to deal with the complexity [Ric+09; CC14; Kab+11a] especially when non-Markovian effects need to be included [Pri+10]. An example of a non-Markovian bath is presented in part III, where optical self feedback is considered. The formalism presented there can also be used for bidirectionally coupled systems with a delay [PZ16]. For the cascaded setup the delay between the systems can be neglected as they are assumed to only couple unidirectionally.

After the computation shown in App. B, the master equation is obtained as

$$\begin{aligned}\frac{d\rho}{dt} &= \frac{1}{i\hbar}[H_0 + H_s + H_t, \rho] \\ &\quad + \sum_{i=s,t} \frac{\gamma_i}{2}\left(2J_i\,\rho J_i^\dagger - \{J_i^\dagger J_i\,,\rho\}\right) - \sqrt{\gamma_s\gamma_t}\left([J_t^\dagger, J_s\rho] + [\rho J_s^\dagger, J_t\,]\right). \end{aligned} \tag{6.1.1}$$

Here, $a, b = ab + ba$ indicates the anticommutator and J_i is the flip operator of either source or target. This may be the annihilation operator of a single cavity mode or an electronic flip operators. The first term in this equation will give the dynamics of the closed systems. The second term is the loss of the modes coupled to the environment. The third term represents the coupling of between source and target mediated by the reservoir. To achieve a nonzero coupling between source and target both of them need to allow a dissipation of excitation into the mediating reservoir. While this is obvious for the source as the target cannot be excited if nothing is emitted the need for the target to be subject to losses is less intuitive.

Using this as the starting point for the following study different targets and sources may be considered. Now, the Hamiltonians for the systems discussed in the introduction are defined.

The Hamiltonian for the interactions in the source reads

$$H_\mathrm{s} = \hbar g_s\left(c_s^\dagger\sigma_s^- + \sigma_s^+ c_s\right). \tag{6.1.2}$$

The cavity mode is described by the creation and annihilation operators $c_s^\dagger$ and c_s, respectively. The emitter inside the cavity is described by a two level system with the flip operators $\sigma_s^+ = |e\rangle_s\langle g|_s$ and $\sigma_s^- = |g\rangle_s\langle e|_s$. Cavity and emitter are coupled with the strength g_s.

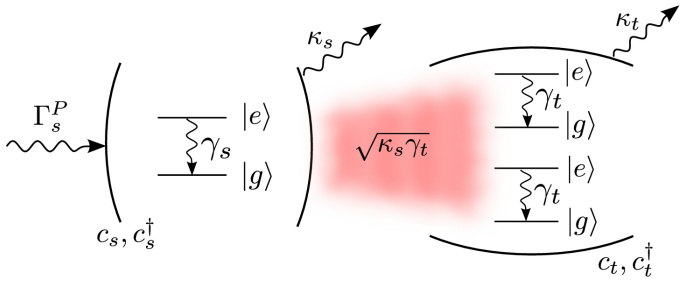

Figure 6.1.1.: Schematic depiction of the studied setup. The source cavity, which contains a TLS, is pumped incoherently with rate Γ_s^P. The emission of the source cavity is fed into the one or two emitters contained in the target cavity with the rate $\sqrt{\kappa_s\gamma_t}$ that depends on the decay rate of source cavity and target emitter.

In Eq. (6.1.1) $J_s := c_s$ is chosen so that the output of the cavity mode is emitted into the mediating bath. The statistical regime of the cavity output is tuned by incoherent driving. This can be done by either offresonant optical driving or electrical pumping [Shi07; Ste+06; Yua+02; Sch+14] and can be described in the form of Lindblad terms [DVL10; Gar11]

$$\mathcal{D}[\sqrt{\Gamma_s^P}\sigma_s^+]\rho := \Gamma_s^P\left(2\sigma_s^+\rho\sigma_s^- - \{\sigma_s^-\sigma_s^+,\rho\}\right). \tag{6.1.3}$$

This induces a transition of the emitter from the ground to the excited state. In the following the short hand notation $\mathcal{D}[J]\rho := 2J\rho J^\dagger - \{J^\dagger J,\rho\}$. is used for incoherent terms in the Lindblad form.

Finally, radiative decay in the source emitters is included by the Lindblad terms

$$\mathcal{D}[\sqrt{\gamma_s}\sigma_s^-]\rho := \gamma^s\left(2\sigma_s^-\rho\sigma_s^+ - \{\sigma_s^+\sigma_s^-,\rho\}\right). \tag{6.1.4}$$

For operation in the lasing regime this decay would imply an imperfect lasing where not all photons are emitted into the cavity mode.

After fixing the description of the source system now the target system is fixed. The single emitter Jaynes-Cummings model is considered briefly as a target, but the focus will be on the two emitter Tavis-Cummings model, as it exhibits stronger nonlinearities. The interaction Hamiltonian of the target is

$$H_\mathrm{t} = \hbar\sum_{j=1,2} g\left(c_t^\dagger\sigma_{j,t}^- + \sigma_{j,t}^+ c_t\right). \tag{6.1.5}$$

Similar to the source Hamiltonian, the emitters of the target system are approximated by two level systems with flip operators $\sigma_{j,t}^{-/+}$ that couple to the cavity mode with strength g, where the target cavity mode is described by the creation and annihilation operators $c_t^\dagger$ and c_t, respectively. In this case the emitters couple to the bath, i.e. $J_{i,t} := \sigma_{i,t}^-$ $(i = 1, 2)$ in Eq. (6.1.1).

This time the cavity is assumed to have an additional decay, again modeled by a Lindblad term

$$\mathcal{D}[\sqrt{\kappa_t}c_t]\rho := \kappa_t\left(2c_t\rho c_t^\dagger - \{c_t^\dagger c_t,\rho\}\right). \tag{6.1.6}$$

For the full description the Hamiltonian of the free evolution is defined as

$$H_0 = \hbar\omega_0 \sum_{i=s,t} c_i^\dagger c_i + \hbar\omega_e \sigma_s^+ \sigma_s^- + \hbar\omega_e \sum_{i=1,2} \sigma_{t,i}^+ \sigma_{t,i}^-, \tag{6.1.7}$$

The first term is the oscillation of the source and target cavity modes with the optical frequency ω_0. They are assumed to be resonant. The second term is the oscillation of the source and target emitters with frequency ω_e. All frequencies are assumed to be in resonance, i.e. $\omega_0 = \omega_e$.

With the above assumptions the master equation reads

$$\begin{aligned}\frac{d\rho}{dt} = \frac{1}{i\hbar}[H_0 + H_s + H_t, \rho] - \sqrt{\kappa_s\gamma_t} \sum_{i=1,2} \Big([\sigma_{t,i}^+, c_s\rho] + [\rho c_s^\dagger, \sigma_{t,i}] \Big) \\ + \mathcal{D}[\sqrt{\Gamma_s^P}\sigma_s^+]\rho + \mathcal{D}[\sqrt{\gamma_s}\sigma_s^-]\rho + \mathcal{D}[\sqrt{\kappa_s}c_s]\rho + \mathcal{D}[\sqrt{\kappa_t}c_t]\rho + \sum_{i=1,2} \mathcal{D}[\sqrt{\gamma_t}\sigma_{t,i}^-]\rho.\end{aligned} \tag{6.1.8}$$

The master equation is written in the basis $\langle e_s, p_s, e_t, p_t|\rho|e_s', p_s', e_t', p_t'\rangle$, where the indices e represent the emitter states and the indices p are the basis of the cavity mode. The indices s and t indicate source and target, respectively. For the numerical evaluation the master equation is again written in a rotating frame, cf. App. B in order to eliminate the fast oscillations. Thus, a system of first order differential equations needs to be solved. This is done numerically by a fourth order Runge-Kutta algorithm. The number of levels for the emitters is fixed as two level systems are assumed. However, the photonic degrees of freedom introduce an infinite number of levels. For the numerical investigation only a finite number of levels may be included. Thus, the number of states is increased until the numerical solution is converged. At maximum $n_{\mathrm{ph,s}} = n_{\mathrm{ph,t}} = 16$ photon states were needed to reach convergence in the investigated quantities. The density matrix contains $(8n_{\mathrm{ph,s}}n_{\mathrm{ph,t}})^2$ elements.

The main interest of the following discussion will be the response of the target to the source statistics. At first the stationary second order correlation function is considered. As discussed in Chapter 2, it is defined in this case as

$$g_i^{(2)}(s) = \lim_{t\to\infty} \frac{\left\langle c_i^\dagger(t) c_i^\dagger(t+s) c_i(t+s) c_i(t) \right\rangle}{\left\langle c_i^\dagger(t) c_i(t) \right\rangle^2}, \tag{6.1.9}$$

and can be measured by a Hanbury Brown-Twiss setup. The index i is either s for the source or t for the target cavity.

From now on all parameters but the incoherent pumping strength of the source cavity are fixed. In Tab. 6.1.1 the coupling strengths and damping rates for source and target are given. As the cavity frequencies and emitter resonances are all assumed to be in resonance, these parameters define the system.

The output field of the cavities can be characterized by the second order correlation function Eq. (6.1.9). Changing the pumping strength allows to tune the output statistics of the source cavity from the antibunched regime, where $g^{(2)}(0) < 1$, to the thermal regime, where $g^{(2)}(0) > 1$.

parameter	value (ps^{-1})
source coupling strength	$g_s = 0.1$
target coupling strength	$g_t = 0.1$
source emitter decay	$\gamma_s = 0.02$
target emitters decay	$\gamma_t = 0.5$
source cavity decay	$\kappa_s = 0.1$
target cavity decay	$\kappa_t = 0.005$

Table 6.1.1.: Parameters that are fixed throughout the chapter for source and target. As no detunings are present the optical frequency is eliminated by introduction of a rotating frame, cf. App. B.

Depending on the physical realization the assumption of a two level system may fail. In general, e.g., quantum dots are multi-level systems so that higher levels may be excited making the response of the second order correlation more complex. Considering more realistic quantum dot models potentially allows to produce other types of light [Jah+16]. However, this is beyond the scope of this study as it focuses on the cascaded interaction.

As quantum effects become most obvious for $s = 0$ in Eq. (6.1.9) this is the case that will be considered in the following.

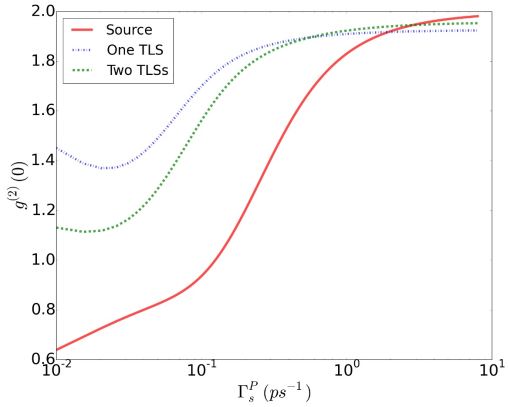

Figure 6.1.2.: The behavior of the second order correlation function Eq. (6.1.9) as a function of the incoherent pump strength Γ_s^P for the source cavity (solid, red) and the target cavity with one (blue, dashed dotted) and two (green, dashed) TLSs. In the regime of low pump rates the source cavity exhibits antibunching, while there is a transition to the bunching regime for higher pump strengths. For the target cavity there is no antibunching regime: The correlation function follows the source in a classically degraded fashion. The classical degradation becomes less pronounced with the higher nonlinearity in the two emitter case. (This figure is adpated from Ref. [Azi+17].

In Fig. 6.1.2 the second order correlation function $g(2)(0)$ for the source, a target with a single emitter, and a target with two emitters is shown. When increasing the external incoherent pump strength, the source goes from the antibunching regime to the thermal regime. In the antibunched regime only a single photon can be created before the decay

of the system due to the small pumping and the small coupling strength. The transition to the thermal regime is explained by the dephasing introduced due to the pumping so that the output statistics approach $g^{(2)}(0) = 2$ [Gar11; RC94; Rit+10]. Both targets seem to follow this trend with a classical degradation, i.e. quantum features are not observed in the target. For the two emitter target, the dip in the correlation is larger. For this reason the two emitter case will be used to illustrate the investigation. More emitters would lead to an even higher nonlinearity, however, the numerical evaluation would become even more involved, which can be avoided to some degree using symmetries, as mentioned before [GR17]. In Ref. [CnL16] it was proposed to characterize a systems output statistics in a more thorough manner by using higher order correlation functions. By considering higher order correlations a transitional behavior is observed which stems from the nature of the cascaded coupling that includes dissipative and Hamiltonian-like processes at the same time. Correlations up to the tenth order correlation function are considered, which reveal a qualitative transition also in the target which never reaches the nonclassical regime in the $g^{(2)}$-function.

6.2. Higher order photon correlations

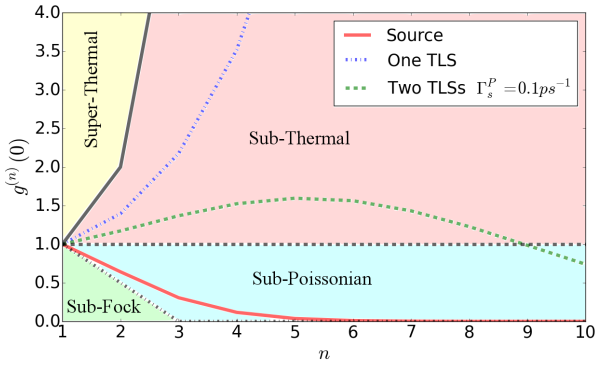

Figure 6.2.1.: Higher order steady state correlation functions $g^{(n)}(0)$, Eq. (6.2.1), for orders 1 to 10 with the pump strength $\Gamma_s^P = g$. The source is in the subpoissonian regime, where $g_s^{(n)}(0) < 1$ for all n (red, solid), and decreases monotonically with increasing correlation order. The single emitter target cavity is in the sub-thermal regime, where $g_t^{(n)} > 1$ for all n, and increases monotonically with increasing order (for $1 \leq n \leq 10$). However, the two emitter target cavity is in the sub-thermal regime for $n < 9$, but from then on the correlations are in the sub-possionian regime. Thus, there is no monotonicity for this case. For reference, coherent (gray, dashed) and thermal (gray, solid) statistics are shown. Furthermore, the statistics of the two photon Fock state (gray, dashed dotted) is shown exemplary for a nonclassical state of the light field. (This figure was originally published in Ref. [Azi+17]. Copyright 2017 American Physical Society, used with permission)

In order to characterize the light field more clearly and analyze the transition in the behavior of the target statistics as induced by the source statistics, higher order correlation functions are considered. These have become experimentally accessible in recent years

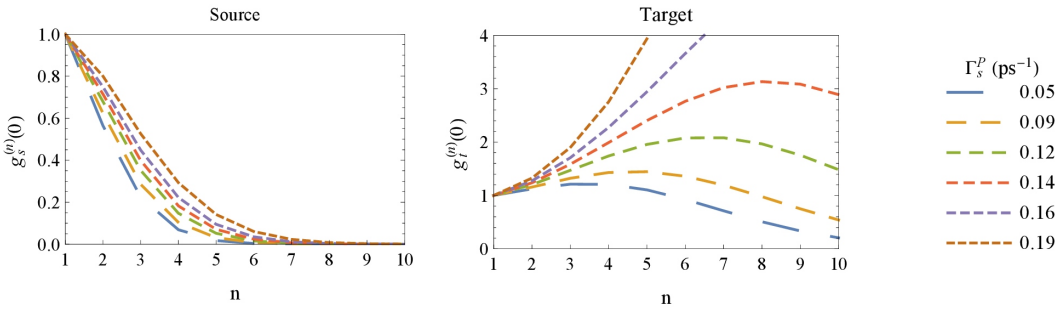

Figure 6.2.2.: Behavior of the correlation functions up to tenth order for the source and the target cavity in vicinity of $\Gamma_s^P = g$. When increasing the incoherent pump strength the source statistics become less antibunched, however it stays within the antibunched regime. The target cavity statistics show a more significant change: Starting out with statistics, where the higher order correlations ($n > 6$) are in the subpoissonian regime, increasing the pump strength leads to increased values for the $g^{(n)}$-functions. The lower order correlation functions cross to the sub-thermal regime until all leave this regime and the lower order correlations approach an upwards curve as expected for thermal statistics cf. Fig. 6.2.1. (This figure is previously published in Ref. [Azi+17]. Copyright 2017 American Physical Society, used with permission.)

[Aßm+09]. The stationary nth order correlation function is defined as

$$g^{(n)}(0) = \frac{\left\langle {c_i^\dagger}^n {c_i}^n \right\rangle}{\left\langle c_i^\dagger c_i \right\rangle^n}. \tag{6.2.1}$$

Here, i stands for either the source or the target. Using the higher order correlation functions states that have a similar value for the second order correlation function can be distinguished if they are not equal. E.g. a Fock state with high photon number is close to a coherent state in the second order correlation function.

With this states of the light field indistinguishable by only the $g^{(2)}(0)$ may be discriminated. For example a Fock state with a large number of photons produces a similar $g^{(2)}(0)$-function as a coherent field, cf. Chap. 2. The three prototypical cases of light statistics, coherent, thermal, and Fock are used for reference.

In Fig. 6.2.1, the correlation functions up to tenth order are shown for the source and the target cavity that contains one and two emitters. For comparison coherent and thermal statistics as well as a two photon Fock state are shown. The pump strength assumed here coincides with the electron photon coupling strength: $\Gamma_s^P = g$. For the source cavity the output statistics is in the sub-Poissonian regime and decreases monotonically with increasing correlation order, i.e. $g_s^{(n)}(0) > g^{(m)}(0)$ for all $n < m < 10$. This corresponds to a non-classical output field. For the output field of the target cavity with a single emitter, there is a monotonic increase of the value of the correlation function with increasing order, i.e. $g_s^{(n)}(0) < g^{(m)}(0)$ for all $n < m < 10$.

In contrast to this, the cavity output does not behave monotonically for the target with two emitters as $g_t^{(2)}(0) < g_t^{(3)}(0)$ while $g_t^{(2)}(0) > g_t^{(6)}(0)$. This shows that the target cavity, while clearly influenced by the source cavity is not just a mirror image. The influence

of the degradation is not equal for all orders in $g^{(n)}(0)$. In the following the two emitter case will be considered in more detail as the single emitter case does not exhibit the non-monotonicity for the parameters used here.

In order to gain more insight into the behavior of the target statistics in Fig. 6.2.2 the various correlation functions are shown for increasing pump strength. Here, the focus lies on the regime around $\Gamma_s^P = g$. For all cases the response of the target system differs strongly from the one of the source. Again the source shows monotonic statistics with $g_s^{(n)}(0) > g_s^{(m)}(0)$ for all $n < m \leq 10$. Higher order correlations become very small. This is expected, as the photon manifold that may be reached is limited due to the cooperativity [WM08] $C_s = g_s^2/(\Gamma_R \kappa_s)$. Thus, from some order on no significant contribution is expected.

For the target system there is a clear maximum in the photon correlations for a certain order m so that $g_t^{(m)}(0) \geq g_t^{(n)}(0)$ for all n. When increasing the pump strength, the maximum shifts to higher orders, i.e. m increases. From the maximum onwards, the correlations decrease. The maximum may shift to very large values, where for the source cavity the correlation is very small. In particular, the relation between the maximum in the target and the statistics of the source is not obvious.

As a first step towards quantifying the transitional behavior, the second order central difference is considered, which we use as an analog of the second order derivative to study the turning behavior. It is defined as [Olv13]

$$g^{(n)\prime\prime} = \frac{g^{(n+1)} - 2g^{(n)} + g^{(n-1)}}{(n+1-n)(n-(n-1))}. \tag{6.2.2}$$

This is the second order derivative at $n = 2$, where the first flip will occur so that the curve turns upwards. In Fig. 6.2.3 the finite difference for the pumping regime shown in Fig. 6.2.2 is presented. The source statistics exhibit a transition from an upward to a downward turning point. The target statistics, however, experiences a transition from a downward to an upward turning point. The curves cross when the pump strength equals the coupling strength $g = 0.1\text{ps}^{-1}$. This illustrates the influence of the source on the target statistics.

In the next section, the cascaded driving is compared with coherent and incoherent driving to show that the non-monotonic photon statistics is not trivially reproduced by these.

6.3. Comparison of cascaded driving with coherent and incoherent driving

In the last section, a non-monotonic behavior in the target statistics was shown and the transition was characterized. Now the behavior of the target statistics is compared to the case when the target system is driven either with coherent light or if the target system is directly driven incoherently. This is achieved by setting $\kappa_s = 0$ so that target and source do not couple anymore. The target system is now driven by the additional Hamiltonian term

$$H_{\text{pump}} = E_0 \left(c_t^\dagger e^{-i\omega_L t} + c_t e^{i\omega_L t} \right) \tag{6.3.1}$$

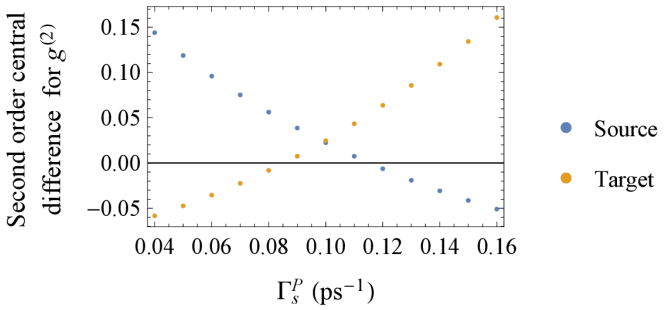

Figure 6.2.3.: When considering the second order central difference at the position of the $g^{(2)}(0)$-function, a change in the turning behavior is observed: The source goes from an upwards to a downwards turning point, while the target goes from an upward to a downward turning. The curves cross at $\Gamma_s^P = g = 0.1\text{ps}^{-1}$. (This figure is previously published in Ref. [Azi+17]. Copyright 2017 American Physical Society, used with permission.)

in the case of coherent driving, cf. Chap. 3, or by the incoherent pumping Term in Lindblad form

$$\mathcal{D}[\sqrt{\Gamma_s^P}\sigma_s^+]\rho \to \mathcal{D}[\sqrt{\Gamma_t^P}\sigma_t^+]\rho, \tag{6.3.2}$$

cf. Sec. 6.1. These scenarios are shown in Fig. 6.3.1 for an exemplary driving strength. All other parameters are kept equal to the cascaded case in order to allow for comparison. The observed behavior is stable for a wide parameter range, however, in comparison to the pumping with the source system the photon number may become larger so that states including higher photon numbers need to be taken into account for the numerical evaluation. Incoherent driving (Fig. 6.3.1, left) induces close to thermal statistics according to Eq. (2.0.7). This is expected, as it corresponds to driving by a thermal reservoir. Coherent driving (Fig. 6.3.1, right) induced coherent statistics, which is also expected. In both cases no maximum is observed for the parameters investigated here so that the cascaded driving allows to access part of the Hilbert space which are not accessible by the naive coherent or incoherent driving. In Ref. [CnL16] this was discussed for Hamiltonian coupling, which is similar to the case of coherent driving.

By taking a closer look at the coupling terms the behavior can be made intuitive. Coherent driving excites the emitters by creating coherences, while incoherent driving creates excitation while destroying existing coherences.

This can be compared to the cascaded driving by considering the master equation Eq. (6.1.8). By changing $\sqrt{\gamma_t\kappa_s} \to -\sqrt{\gamma_t\kappa_s}$ the system dynamics remains unchanged as for the exchange of $H_{t/s} \to -H_{t/s}$. This shows that part of the dynamics are like the ones introduced through a coupling in the Hamiltonian as they are invariant under the change of the time direction. This part of the dynamics preserves coherences especially for low pumping strengths, which is not necessarily expected from a dissipative coupling. However, to enable the coupling both, source cavity and target emitters, need a finite decay to the reservoir. This reservoir coupling introduces a loss of excitation and coherence to the reservoir and is not invariant under time inversion. Thus, the cascaded coupling exhibits properties of both driving scenarios which results in a statistics that illustrates the mixture of the properties of the two driving scenarios.

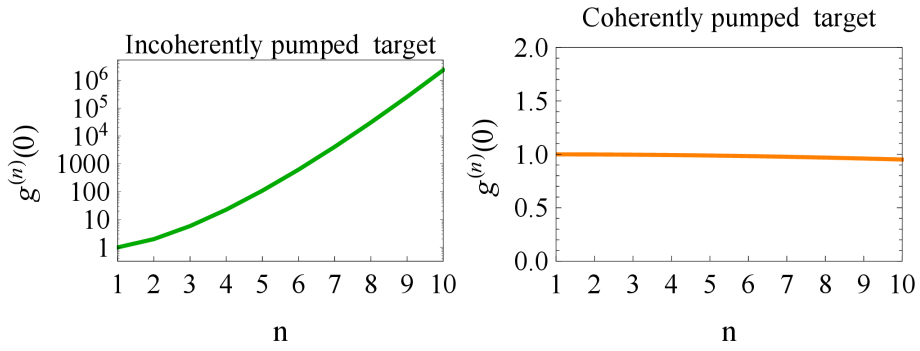

Figure 6.3.1.: Higher order correlation function for the target system with two emitters. Incoherent (left) and coherent (right) pump of the target emitters is considered, where no coupling to the source system is assumed. As exemplary pumping strength $\Gamma_t^P = \sqrt{\gamma_t \kappa_s}$ and $E_0 = \sqrt{\gamma_t \kappa_s}$ are used. However, the behavior is stable for a wide range of parameters. For incoherent pumping monotonously increasing nearly thermal statistics are observed, cf. Eq. (2.0.7). The coherent pumping induces close to coherent statistics without maximum. (These figures are previously published in Ref. [Azi+17]. Copyright 2017 American Physical Society, used with permission.)

For a different perspective on the statistical behavior the probability distribution corresponding to the non-monotonic correlations in Fig. 6.2.1 is shown in Fig. 6.3.2 in terms of the Fock states in blue. This distribution is very flat as the first few photon number states have a similar probability. For comparison the probability distribution for the coherent state with the same mean photon number is shown (dashed, orange). Here, the majority of the contribution is given by fewer number states.

6.4. Conclusion and outlook

In this chapter the influence of different output statistics on a target system was investigated. The output from the source may be in the nonclassical or in the thermal regime. Higher order stationary correlations showed a non-monotonic behavior that is not observed for simple incoherent and coherent driving. This non-monotonic behavior is the result of the mixing of Hamiltonian like coupling and incoherent processes both inevitably present for the cascaded setup. The cascaded driving does not allow to imprint the source statistics on the target without any degradation. Only higher order correlations are preserved while lower order correlations shift to high values in the correlation functions, which corresponds to an approach of more classical states of light. From this follows that the lower order correlations such as the $g^{(2)}(0)$ function do not reach the sub-Poissonian regime for the parameters studied here, while the higher order correlations do. This behavior leads to the no non-monotonicity of the correlations, which corresponds to a flat distribution of the photon number states.

A possible experimental realization of the discussed setup could be achieved by coupling microcavities containing emitters by a waveguide. If the unidirectionality of the coupling cannot be established by arguing from a thermodynamical perspective unidirectional photonic structures may be employed [LJS14]. The unidirectionality may also be designed

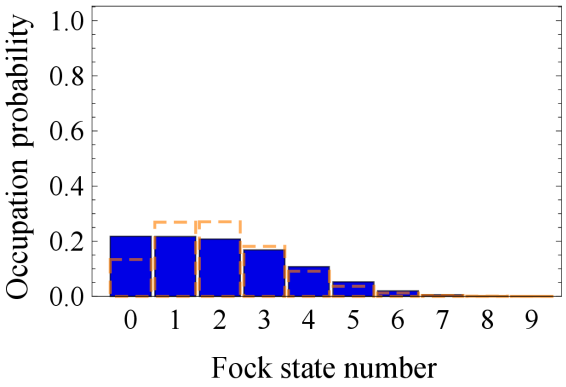

Figure 6.3.2.: Occupation probability of the Fock states for the target system with two emitter at $\Gamma_s^P = 0.1\text{ps}^{-1}$ corresponding to the photon statistics shown in Fig. 6.2.1 (solid, blue). Due to the cascaded coupling the photon number distribution is exceptionally flat. This illustrates the photon statistics that deviate from the prototypical cases. For reference (dashed, orange), the coherent distribution is shown. (This figure is previously published in Ref. [Azi+17]. Copyright 2017 American Physical Society, used with permission.)

using a combination of coherent and incoherent interactions [MC15; MC17].

The work presented here may be expanded in two directions. Either more realistic systems may be considered such as realistic quantum dots, which give rise to even more complex output statistics for the source cavity [Shi07] or allowing different bath states may give even more freedom for designing the statistics of the target cavity. E.g. squeezed states could be included in the formalism used here [Dra06]. For more complex cases, however, the bath degrees of freedom need to be considered. As this is an involved undertaking at first methods for including the bath degrees of freedom need to be considered.

In the next part of this thesis the effect of feedback on the emission statistics of quantum systems will be investigated. Then it is necessary to include the degrees of freedom of the bath explicitly as the non-Markovian nature of the bath needs to be taken into account. Using feedback the emission statistics may be manipulated to enhance certain properties. For feedback only single systems are considered, however, the formalism presented in the following may also be used to extend the cascaded coupling to bidirectional coupling. This becomes particularly involved when a time delay between the source and the target is considered, cf. App. B.

Part III.

Quantum coherent feedback

7. Controlling quantum systems via feedback

In the previous chapters two approaches for controlling quantum systems were presented. The mechanical systems in Part I were controlled by the frequency of an external optical laser. In this case it was possible to induce coherent phonon generation. If non-classical light is used to irradiate a system the light statistics become more complex as now correlations deviate from the laser like coherent statistics as seen in Part II of this thesis. However, in the case of interest, due to the degrading effect of the cascaded coupling, the light became more classical as the non-classical properties of the light field could not be fully transfered from source to target. Thus, a method is needed which does not degrade the correlations but preserves them.

A possible way to reinforce the quantum nature of light in form of Fock states is to use feedback on quantum systems [Say+11; Zho+12]. Here, the outcome of a measurement is used to correct the state of the controlled system. This scheme is widely used in quantum optics, however originally effects due to a finite feedback time have been neglected [WM06]. This approach is still often used and only recently time delay effects are considered in measurement based feedback [Ema13; Bra10].

In classical nonlinear systems Pyragas control [Pyr92] is a successful method for controlling dynamical systems [SS08; SKH16]. In Pyragas control the system dynamics is fed back as input into the system at a later time. It was first intended to stabilize unstable periodic orbits in dynamical systems by reinforcing the systems dynamics using a delay time $\tau = 1/\nu$, where ν is the frequency of the periodic solution. In the equations of motion Pyragas control typically has the from

$$\dot{x}(t) = F(x(t), t) + K\left(x(t) - x(t-\tau)\right), \tag{7.0.1}$$

where $x(t)$ is some dynamical variable describing the state of the system and F is the dynamical equation governing the system. The second term is the control term with strength K. When a solution with period τ is reached, the control term vanished. Using this also the stabilization of steady states is possible [HS05]. Time-delayed feedback control is often used for controlling laser dynamics [LK80; Gau+94; Oht06] and more recently for reducing the jitter in lasers [Ott+12]. Measurement based feedback in nanolasers may lead to chaos and pulsing [Mun+17].

Another way of controlling quantum systems is by shaping its environment [PCZ96]. These environment lead to non-Markovian effects [Bre+16; SDG99; RHP14]. From a control perspective, no measurement is necessary and the quantum state of the system is not perturbed. By placing a quantum system in front of a mirror a special type of environment is created that acts as a non Markovian bath where only discrete times are relevant for the current dynamics [DZ02]. The ideal case of a single feedback time from an environment can be motivated by a heuristic Hamiltonian that can be derived from

a setup with a microscopic mirror [FKC0]. This heuristic Hamiltonian is successfully used to describe experimental setups [Dub+07] and will the the basis of the studies performed throughout this thesis. In the spirit of the Pyragas control, a finite time delay is introduced by the heuristic Hamiltonian in the realm of quantum mechanics. In Chap. 8 the feedback Hamiltonian will be introduced and the efficient evaluation of the induced dynamics will be discussed before in the Chapter 10 a Tavis-Cummings model subject to feedback will be considered. In Chapter 11 a pulsed two level system subject to feedback will be considered. In both cases feedback is able to enhance the nonclassical signatures of the light states.

8. Modeling quantum optical feedback

In this chapter the problem of quantum feedback will be addressed, in particular the theoretical models, that may be used to describe it numerically. Parts of this chapter have been published in Ref. [Nau+17]. In this thesis feedback involving a single delay time will be addressed. In the quantum mechanical formulation this corresponds to an interaction with a non-Markovian bath with a single memory time. The standard approach to model this scenario is to include a Hamiltonian with a continuous number of modes that acts as reservoir [Wei12]. The full Hamiltonian is

$$H_{\text{tot}} = H_{\text{sys}} + H_{\text{fb}}, \tag{8.0.1}$$

where H_{sys} contains the subsystem of interest that feedback acts on and H_{fb} describes the degrees of freedom that lead to feedback. For non-Markovian interactions the reservoir can be traced out, as in Part II, However, in this part of the thesis the delay introduced by the bath will be considered explicitly. As discussed before, feedback on some system operator A is modeled by the bath Hamiltonian [DZ02; FKC0]

$$H_{\text{fb}} = \int_{\mathcal{B}} d\omega \hbar\omega b^\dagger(\omega) b(\omega) + \hbar \int_{\mathcal{B}} d\omega \left[G_{\text{fb}}(\omega) b^\dagger(\omega) A + \text{h.c.} \right]. \tag{8.0.2}$$

The integrals are over the frequency domain $\mathcal{B}$, which is around the resonance frequency ω_0 of the system. The coupling in case of feedback with equal in- and out-coupling reads

$$G_{\text{fb}} = g_0(\omega) \sin(\omega L/c_0) = \frac{g_0(\omega)}{2i} \left(e^{i\omega L/c_0} - e^{-i\omega L/c_0} \right), \tag{8.0.3}$$

where ω is the frequency of a mode, L is the distance between the system and the back reflecting surface, and c_0 is the speed of light. For the situation of possibly different in- and out-coupling-rates, the ansatz [PZ16]

$$G_{\text{fb,asymm}} = i \left(\kappa_R(\omega) e^{i\omega L/c_0} - \kappa_L(\omega) e^{-i\omega L/c_0} \right) \tag{8.0.4}$$

is made. In the following, the coupling coefficients κ_R and κ_L will be assumed to be constant over this domain, which is approximatively valid when small bandwidths are considered. However, in the present case, the overall coupling constant still has a sinusoidal dependence and the dynamics are not Markovian.

8.1. Overview of different approaches

In this section a short overview of different methods used to model time delayed feedback in quantum systems is given. For high intensities semiclassical approximations are possible, however, when the full quantum dynamics is considered. The most direct approach is to

compute the dynamics using the Schrödinger equation by including all degrees of freedom explicitly. To achieve a more tractable and general approach solutions using the density matrix and in the Heisenberg picture were proposed as well as the method considered in more detail in Chapter 8.2.

8.1.1. Semiclasscial approximation

When considering the Hamiltonian Eq. (8.0.2) in the regime of coherent fields a form similar to Pyragas control Eq. (7.0.1) is obtained. As the coherent fields naturally appear in optomechanical systems with high field intensities, Pyragas control in the classical limit can be used in optomechanics to stabilize unstable solutions. This was considered in Ref. [Nau+14] and establishes a close connection to Part I of this thesis.

8.1.2. Direct evaluation in the Schrödinger picture

When considering feedback given by the Hamiltonian Eq. (8.0.2) fully quantum mechanically, the most straightforward method to evaluate feedback numerically is by evaluating the Schrödinger equation directly. For closed systems with a fixed number of excitations a set of differential equations may be derived once the width of the frequency interval and sampling rate of the frequency have been chosen. These two parameters are to be chosen with care for a certain physical system. The number of equations scales with the number of modes needed to characterize the bath to the power of the number of excitations: While the regimes of a single excitation [Car+13] or two excitations [Hei+14] are manageable, multiple excitations become very involved. Furthermore, this approach is not immediately suitable for open or pumped systems. Thus, in the following sections, the focus lies on methods which allow for a solution of systems with a variable number of excitations subject to feedback.

While the straightforward evaluation of the Schrödinger equation is not easily applicable for general pumped systems, in the very low excitation regime, an approximative approach may be employed. This will be shown in Chapter 10 together with a benchmark using the matrix product state evolution approach from Sec. 8.2.

8.1.3. Feedback with the density matrix via Liouville propagator

A first approach to treat feedback in Liouville space to compute the full density matrix allows to consider pumped systems as well as incoherent effects such as pure dephasing and additional decay channels [Gri15]. In this approach the dynamics of the system subject to feedback are viewed as a sequence of n cascaded systems in the time interval between $[(n-1)\tau, n\tau)$. This is connected to the approach in Part II, however the systems in the cascade represent not real systems but rather the past version of the same system [Gri15]. However, due to the back-action between the systems, the system dynamics is computed via a trace-like operation from a Liouville space propagator that needs to be evolved first. As for the nth interval n cascaded identical systems are needed, the propagator in the nth interval has $(d_{\mathrm{scs}})^{4n}$ matrix elements. This system of coupled first order differential equations is solved via a fourth order Runge-Kutta algorithm, as in Part II. A systematic use of sparse matrices mitigates this scaling, but the number of intervals in τ that can be computed in practice is limited by this scaling. As this was the first numerical solution

that was proposed for the pumped two level system subject to feedback, it will be used in Sec. 8.3 to benchmark the method presented in Sec. 8.2.

8.1.4. Feedback in the Heisenberg picture

Treating feedback in the Heisenberg picture is another approach to evaluate general open systems subject to feedback. The Heisenberg picture is successful for the approximative treatment in the many excitation regime, where correlations can be treated perturbatively [Sch+14]. Recently the single excitation regime was studied [Kab+16]. The Heisenberg picture may allow to only keep track of the observables of interest reducing the complexity in comparison to an approach employing the full density matrix equation. There are, however, complications due to the reservoir induced noise. This problem relates to the matrix product state evolution method introduced in the next section.

8.2. Open system dynamics using matrix product state evolution

In this thesis, the focus lies on modeling feedback using matrix product state evolution by starting from the quantum stochastic Schrödinger equation (QSSE) [PZ16]. With this, the long time limit in the numerical simulations of Chapters 10 and 11 can be evaluated. In this section a more thorough overview of the method is given and deviations from the original scheme in [PZ16] are documented in detail. The approach relies on techniques developed in the context of spin systems, were the time evolution of a system with a large Hilbert space can be computed via matrix product states, when the correlations are relatively small [Vid03; Vid04]. When modeling a quantum optical setup, the external field is expressed in the time domain instead of the frequency domain used in the methods based on the direct evaluation of Eq. (8.0.2). This was suggested in Refs. [Sch+05; Sch+07], where the external field is viewed as a chain of multi-level systems. Since the model relies entirely on the Schrödinger picture, incoherent processes can not be included immediately. Decay channels may be added by adding the respective bath mode, cf. Chap. 10, but processes such as pure dephasing can only be included via additional effort, e.g. in form of a quantum jump approach [DCM92]. Here, the focus lies on the presentation of the theory not incorporating incoherent processes to emphasize the significance of the entanglement of the system with the non-Markovian reservoir. To solve the resulting equations of motion in a tractable manner, a stroboscopic map is performed and the quantum state of the system is expressed as a matrix product state (MPS). In Sec. 8.2.1, the derivation of the quantum stochastic Schrödinger equation will be shown exemplary for the Jaynes-Cummings model subject to self-feedback. Afterwards, in Sec. 8.2.4, the expression via the MPS for the numerical implementation will be considered.

8.2.1. Feedback in the time domain

Here, the equations for feedback on the cavity mode of a Jaynes-Cummings model, cf. Chap. 6, are derived exemplary, as a prototypical system. In the numerical simulations different systems will be considered as well, however the basic approach remains the same.

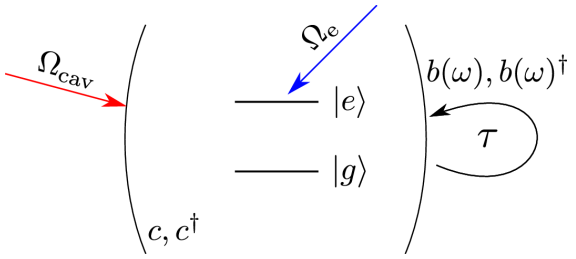

Figure 8.2.1.: Schematic depiction of the system under study: A single cavity mode with operators $c, c^\dagger$ containing an emitter is coupled to external reservoir modes (operators $b(\omega), b^\dagger(\omega)$) inducing feedback. Possibly either the cavity is pumped with strength Ω_{cav} or the two level system (TLS) is pumped with strength Ω_{e} via an external coherent laser.

The Hamiltonian for this system reads

$$H_{\mathrm{tot}} = H_{\mathrm{sys,JCM}} + H_{\mathrm{fb}} \tag{8.2.1}$$

with

$$\begin{aligned} H_{\mathrm{sys,JCM}} = {} & \hbar\omega_{\mathrm{cav}} c^\dagger c + \hbar\omega_{\mathrm{e}}\sigma_+\sigma_- + \hbar g\left(c^\dagger\sigma_- + \sigma_+ c\right) \\ & + \frac{\hbar\Omega_{\mathrm{cav}}}{2}\left(ce^{i\omega_L t} + c^\dagger e^{-i\omega_L t}\right) + \frac{\hbar\Omega_{\mathrm{e}}}{2}\left(\sigma_- e^{i\omega_L t} + \sigma_+ e^{-i\omega_L t}\right) \end{aligned} \tag{8.2.2}$$

and

$$\begin{aligned} H_{\mathrm{fb}} = {} & \int d\omega \hbar\omega b^\dagger(\omega) b(\omega) \\ & + i\hbar \int d\omega \left[b^\dagger(\omega) c\left(\sqrt{\frac{\gamma_R}{2\pi}} e^{-i\omega\tau/2} - \sqrt{\frac{\gamma_L}{2\pi}} e^{i\omega\tau/2}\right) - \mathrm{h.c.}\right]. \end{aligned} \tag{8.2.3}$$

The c and $c^\dagger$ may destroy or create a photon in the cavity mode with ω_{cav}, respectively. The two level system with transition energy ω_{e} may be brought to the excited state by the flip operator $\sigma_+ = |e\rangle\langle g|$ and to the ground state by $\sigma_- = |g\rangle\langle e|$. Cavity and two level system are coupled via the electron-photon coupling with strength g. Either the two level system or the cavity may be pumped by a coherent laser with frequency ω_{L} and strength Ω_{e} or Ω_{cav}, respectively. For the interaction with the reservoir, the decay rates γ_L and γ_R are introduced. They are related to the coupling strengths κ_i

$$\kappa_i = \sqrt{\frac{2\gamma_i}{\pi}}. \tag{8.2.4}$$

The operators fulfill the commutation relations

$$\left[c^\dagger, c\right] = 1 \tag{8.2.5}$$

$$[\sigma_+, \sigma_-] = 2\sigma_z \tag{8.2.6}$$

$$\left[b(\omega), b^\dagger(\omega')\right] = \delta(\omega - \omega'). \tag{8.2.7}$$

Introduction of rotating frame and transformation to the time domain

In the first step, the Hamiltonian is transformed to a rotating frame using the unitary transformation

$$U_{\mathrm{rf}} = \exp\left(+iH_{\mathrm{B}}t/\hbar + i\omega_L c^\dagger ct + i\omega_L \sigma_+\sigma_- t\right), \tag{8.2.8}$$

in order to eliminate the high-frequency oscillations. The new Hamiltonian is derived from $H_{\mathrm{tot,rf}} = U_{\mathrm{rf}} H_{\mathrm{tot}} U_{\mathrm{rf}}^\dagger - i\hbar U_{\mathrm{rf}} \frac{\partial}{\partial t} U_{\mathrm{rf}}^\dagger$ and becomes

$$H_{\mathrm{tot,rf}} = H_{\mathrm{sys,rf}} + H_{\mathrm{fb,rf}} \tag{8.2.9}$$

$$H_{\mathrm{sys,rf}} = \hbar\Delta_{\mathrm{cav}} c^\dagger c + \hbar\Delta_{\mathrm{e}}\sigma_+\sigma_- + \hbar g\left(c^\dagger\sigma_- + \sigma_+ c\right) + \frac{\hbar\Omega_{\mathrm{cav}}}{2}\left(c + c^\dagger\right) + \frac{\hbar\Omega_{\mathrm{e}}}{2}\left(\sigma_- + \sigma_+\right)$$

$$H_{\mathrm{fb,rf}} = i\hbar \int d\omega \left[b^\dagger(\omega) e^{i(\omega-\omega_L)t} c \left(\sqrt{\frac{\gamma_R}{2\pi}} e^{-i\omega\tau/2} - \sqrt{\frac{\gamma_L}{2\pi}} e^{i\omega\tau/2} \right) - \mathrm{h.c.} \right]. \tag{8.2.10}$$

In the next step, the unitary transformation $U_{\tau/2} = \exp\left(-i\int d\omega\omega\tau/2 b^\dagger(\omega)b(\omega)\right)$ is used to shift the the time dependence of the bath operators, which are defined as $b(t) = \frac{1}{\sqrt{2\pi}}\int_{\mathcal{B}} d\omega b(\omega) e^{-i(\omega-\omega_L)t}$. With this, the interaction Hamiltonian becomes

$$H_{\mathrm{fb,rf}} = -i\hbar\left[\left(\sqrt{\gamma_R} b(t-\tau)e^{-i\phi} + \sqrt{\gamma_L} b(t)\right) c^\dagger - \left(\sqrt{\gamma_R} b^\dagger(t-\tau)e^{i\phi} + \sqrt{\gamma_L} b^\dagger(t)\right) c\right]. \tag{8.2.11}$$

Now the Hamiltonian is in the time-domain instead of the frequency domain, and the new bath-operators already show the feedback explicitly in their time-arguments. Here, the feedback phase $\phi = \pi - \omega_L\tau$ was introduced, which determines, whether the interference of the system with the feedback field is constructive or destructive. This formulation is closely related to the formulation via quantum Langevin equations. Here, the explicit time dependence is eliminated from the system Hamiltonian. Only the implicit time dependence of the operators c, $c^\dagger$ due to the rotating frame is left, which is just the frequency of the driving laser. In the following, frequencies are given relative to the driving frequency, so that this time dependence is not taken into account any further.

From the commutation relation Eq. (8.2.7), the commutation relation for the bath operators in the time-domain follow as

$$\left[b(t), b^\dagger(t')\right] = \delta(t-t'). \tag{8.2.12}$$

When $b(t)$ is interpreted as noise term, this corresponds to the correlation of Gaussian white noise. This is the case, since the coupling to the bath is mostly Markovian, so that the noise operators represent Gaussian correlation. The non-Markovianity of the bath is contained solely in the delay term and not within a correlation describing colored noise. In the following, however, the full bath dynamics is considered and the bath variables are not treated stochastically. Then, $b(t)$ may be interpreted as the operator destroying of a photon at time t. This aspect will be discussed in more detail in the following.

System-bath dynamics in the Schrödinger picture

In order to evaluate the dynamics of the system coupled to the feedback bath, the dynamics of the compound system is evaluated at discrete times. The time evolution operator is

then applied to the state at time t_k and evolves it to the time t_{k+1}, where $t_{k+1} - t_k = \Delta t$. To do this the time evolution operator in the iterative equation

$$|\Psi(t_{k+1})\rangle = U(t_{k+1}, t_k)|\Psi(t_k)\rangle, \tag{8.2.13}$$

has to be determined. Here, $|\Psi\rangle$ will be written in the form of a matrix product state, which will be discussed in Sec. 8.2.4. Before that the time evolution operator will be derived. In principle time ordering has to be considered, when evaluating the evolution operator

$$U(t_{k+1}, t_k) = \hat{T}\left[\exp\left(-\frac{i}{\hbar}\int_{t_k}^{t_{k+1}} dt' H_{\mathrm{tot,rf}}(t')\right)\right], \tag{8.2.14}$$

where $\hat{T}$ is the time ordering operator. In the original scheme, the operator is evaluated up to first order in Δt [PZ16]. This is shown explicitly in App. C. For the following discussion the important definitions and the final result is shown here. When evaluating Eq. (8.2.14) explicitly in first order of Δt creation operators for a photon inside this time interval are defined and by this the time is discretized. The time intervals will also be called photon bins and the operator for the destruction of a photon in the time interval Δt between time $t_k = k\Delta t$ and $t_{k+1} = (k+1)\Delta t$ is $\Delta B(t_k) = \int_{t_k}^{t_{k+1}} dt b(t)$. The full evolution operator for the Jaynes-Cummings model with feedback reads

$$\begin{aligned}
U(t_{k+1}, t_k) = \mathbb{1} &- \frac{i}{\hbar} H_{\mathrm{sys,rf}} \Delta t \\
&- \Big[\left(\sqrt{\gamma_R}\Delta B(t_{k-l}) e^{-i\phi} + \sqrt{\gamma_L}\Delta B(t_k)\right) c^\dagger \\
&\quad - \left(\sqrt{\gamma_R}\Delta B^\dagger(t_{k-l}) e^{i\phi} + \sqrt{\gamma_L}\Delta B^\dagger(t_k)\right) c \Big] \\
&+ \frac{1}{2}\Big[\gamma_L \Delta B^\dagger(t_k)\Delta B^\dagger(t_k) + \sqrt{\gamma_L\gamma_R} e^{i\phi}\Delta B^\dagger(t_k)\Delta B^\dagger(t_{k-l}) \\
&\quad + \sqrt{\gamma_R\gamma_L} e^{i\phi}\Delta B^\dagger(t_{k-l})\Delta B^\dagger(t_k) + e^{2i\phi}\gamma_R \Delta B^\dagger(t_{k-l})\Delta B^\dagger(t_{k-l})\Big] cc \\
&- \frac{1}{2}\Big[\gamma_L \Delta B^\dagger(t_k)\Delta B(t_k) + \sqrt{\gamma_L\gamma_R} e^{-i\phi}\Delta B^\dagger(t_k)\Delta B(t_{k-l}) \\
&\quad + \sqrt{\gamma_R\gamma_L} e^{i\phi}\Delta B^\dagger(t_{k-l})\Delta B(t_k) + \gamma_R \Delta B^\dagger(t_{k-l})\Delta B(t_{k-l})\Big] cc^\dagger \\
&- \frac{1}{2}\Big[\gamma_L \Delta B(t_k)\Delta B^\dagger(t_k) + \sqrt{\gamma_L\gamma_R} e^{i\phi}\Delta B(t_k)\Delta B^\dagger(t_{k-l}) \\
&\quad + \sqrt{\gamma_R\gamma_L} e^{-i\phi}\Delta B(t_{k-l})\Delta B^\dagger(t_k) + \gamma_R \Delta B(t_{k-l})\Delta B^\dagger(t_{k-l})\Big] c^\dagger c \\
&+ \frac{1}{2}\Big[\gamma_L \Delta B(t_k)\Delta B(t_k) + \sqrt{\gamma_L\gamma_R} e^{-i\phi}\Delta B(t_k)\Delta B(t_{k-l}) \\
&+ \sqrt{\gamma_R\gamma_L} e^{-i\phi}\Delta B(t_{k-l})\Delta B(t_k) + e^{-2i\phi}\gamma_R \Delta B(t_{k-l})\Delta B(t_{k-l})\Big] c^\dagger c^\dagger.
\end{aligned} \tag{8.2.15}$$

The first line represents the zeroth order of the exponential and the first order of the system evolution. As $H_{\mathrm{sys,rf}}$ is not time-dependent, it is proportional to Δt. The second line is the first order of the exponential for the bath Hamiltonian. The time dependent bath operators $b(t)$ are transformed with the above transformation into time discrete operators. The new operators obey the commutation relations

$$\left[\Delta B(t_k), \Delta B^\dagger(t_j)\right] = \Delta t \delta_{k,j}$$

as shown in App. C. Due to the normalization the discretized photon operators are proportional to $\sqrt{\Delta t}$, so that the first order terms of the exponential expansion of the bath Hamiltonian are proportional to $\sqrt{\Delta t}$. Then the second order expansion of the bath Hamiltonian (cf. lines 3–10 in Eq. (8.2.15)) also needs to be taken into account for the evolution matrix to be in first order of Δt. This is further discussed and systematized in Sec. 8.2.2, where higher order expansions are considered. For the numerical evaluation Eq. (8.2.15) is expressed as a matrix using the basis states for the Jaynes-Cummings model $|i_\mathrm{T}, i_\mathrm{cav}\rangle$ and the basis states (cf. App. C)

$$|i_p\rangle = \frac{\left(\Delta B^\dagger(t_p)\right)^{i_p}}{\sqrt{i_p! \Delta t^{i_p}}} |\mathrm{vac}\rangle \tag{8.2.16}$$

for the reservoir, where $|\mathrm{vac}\rangle$ is the vacuum state. The full basis is then given by $|i_\mathrm{T}, i_\mathrm{cav}\rangle \bigotimes_{p=-\infty}^{\infty} |i_p\rangle$. The use of matrix product states and the assumption of an initial vacuum state will allow to only treat a finite number of the infinitely many bath modes. In the appendix, cf. Eq. (C.0.5), the explicit matrix form of the time evolution operator in this basis for the Jaynes-Cummings model in first order is shown.

In the next Sec. 8.2.2, it will be shown how the evolution may be evaluated systematically in higher order to speed up the numerical computation. Before that some general comments on the time evolution scheme are in order. Note, that there are no stochastic elements in the above evolution operator Eq. (8.2.15). As mentioned before, the full bath dynamics are considered to treat the non-Markovian part of the bath dynamics. Nonetheless, this formulation is called the QSSE picture, since for a Markovian bath, this formulation leads directly to the master equation. In that case, the bath would be interpreted as white noise (which is not done here). Then, the dynamics of a single trajectory could be computed which would be one realization the ensemble treated in the density matrix picture [GZ04]. However, to emphasize again, in the case at hand, the dynamics of the reservoir modes are fully taken into account. Nonetheless, some issues of a trajectory approach are relevant. The evolution matrix derived from Eq. (8.2.15) is not unitary, if a finite Δt is considered, as necessary for a numerical evaluation. This leads to a deviation of the norm of the global state $|\Psi\rangle$ from unity. Thus, in the numerical evaluation the error $E_\Psi = \langle\Psi|\Psi\rangle - 1$ is an important measure for the correctness of the simulation. For the evolution in first order of Δt the error in each step will be proportional to Δt^2. The behavior in this case differs from the behavior of the density matrix, whose evolution is described by a master equation. The master equation is constructed such that the trace of the density matrix will be unity for a valid numerical evaluation. In the here employed picture using the quantum state, the norm of the state will always deviate from unity, so that this measure is even more important than when using the density matrix.

Furthermore, from Eq. (C.0.5) it becomes clear, that in a single photon bin a single time step at maximum two photons can be created. Since a single photon may only interact at maximum twice with the system, not more than four photons may be excited. Thus, only the photon states $i_\mathrm{cav} = 0, ..., 4$ have to be considered.

In Fig. 8.2.2, an intuitive interpretation of the time evolution is shown. the system at a given time t_k interacts only with the photons from time t_k and t_{k-l}. Since the future photon bins are in a vacuum state, they do not need to be considered explicitly before the interaction with the system. Furthermore, the bins, which are in the distant past before

$t - \tau$ do not contribute to the dynamics anymore, so that they can also be neglected. In the next section, it will be shown how this can be done in practice.

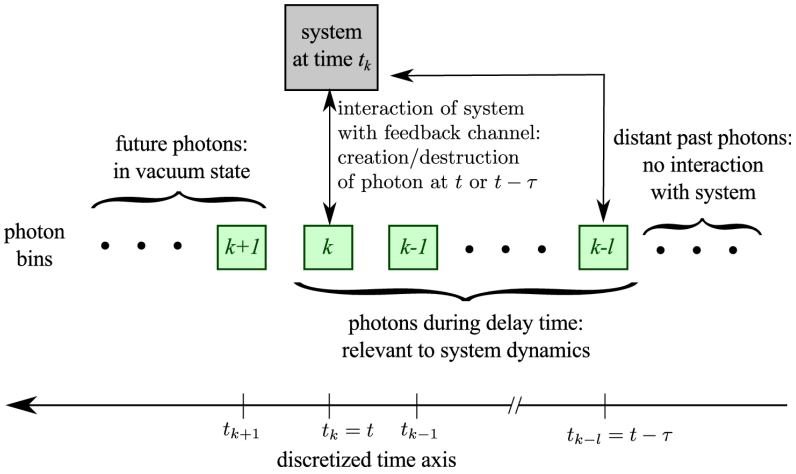

Figure 8.2.2.: The time evolution of the system subject to feedback in an intuitive picture.

8.2.2. Higher order time evolution

In App. C the time evolution operator in first order in Δt is derived explicitly to show how the arguments come into play in detail. In this section, Eq. (8.2.14) is considered from a more general point of view in order to obtain the time evolution operator in higher order of Δt. This will allow to speed up the numerical computation.

The time ordering in Eq. (8.2.14) may be dropped, if the Hamiltonians at different times commute, i.e. $[H_{\mathrm{tot,rf}}(t), H_{\mathrm{tot,rf}}(t')] = 0$, $t \neq t'$ [Sch01]. As only the operators in the bath Hamiltonian are explicitly time-dependent, only the commutation of the bath operator with itself at different times has to be considered. The argument is similar to the ones used for the first order expansion in App. C. As the bath Hamiltonian contains the bath operators $b(t)$ and $b^\dagger(t' - \tau)$, they may potentially not commute, if $t = t' - \tau$ due to the commutation relation Eq. (8.2.12). However, as the evolution operator evolves the system from t_k to t_{k+1}, the integration time is only Δt. Thus, the case $t = t' - \tau$ will not occur in the integral of Eq. (8.2.14), when $\Delta t < \tau$.

With these arguments, the time ordering in Eq. (8.2.14) can be neglected, so that the exponent can simply be integrated

$$
\begin{aligned}
U(t_{k+1}, t_k) &= \exp\left(-\frac{i}{\hbar} \int_{t_k}^{t_{k+1}} dt' H_{\mathrm{tot,rf}}(t') \right) \qquad (8.2.17) \\
&= \exp\Bigg(-\frac{i}{\hbar} H_{\mathrm{sys,rf}} \Delta t + \Big[\left(\sqrt{\gamma_R} \Delta B(t_{k-l}) e^{-i\phi} + \sqrt{\gamma_L} \Delta B(t_k) \right) c^\dagger \\
&\qquad - \left(\sqrt{\gamma_R} \Delta B^\dagger(t_{k-l}) e^{i\phi} + \sqrt{\gamma_L} \Delta B^\dagger(t_k) \right) c \Big] \Bigg).
\end{aligned}
$$

Here, the second part of the exponent giving the interaction is the same as the first order part of the expansion of the exponential in Sec. C.

Recall that the first term is proportional to Δt as given explicitly and that the second term is in order of $\Delta t^{1/2}$ as only a product of two time bin operators is proportional to Δt. This is a peculiar situation as in order to obtain a consistent perturbative formulation with respect to the time step terms from different orders in the exponential function have to be taken into account (as can already be seen in the first order computation of Sec. C). However, for higher order evaluation of the exponential function also mixing terms will occur.

The advantage of the above formulation in terms of the time bin operators is, that now the Hamiltonian can be expressed as a matrix in the same basis as U in Eq. (C.0.5), so that the whole evolution operator can be determined in a given order by considering only matrix multiplications:

$$\begin{aligned}\mathbf{U} &= \exp\left(\mathbf{M}_S + \mathbf{M}_B\right) \\ &= \sum_{n=0}^{\infty} \frac{1}{n!}(\mathbf{M}_S + \mathbf{M}_B)^n. \end{aligned} \tag{8.2.18}$$

Here, $\mathbf{M}_S$ is the matrix containing the system part of the dynamics with the matrix elements

$$(\mathbf{M}_S)_{j_S,j_k,j_\tau;i_S,i_k,i_\tau} = -\frac{i}{\hbar}\langle j_S, j_k, j_\tau| \int_{t_k}^{t_{k+1}} H_{\mathrm{S}} dt |i_S, i_k, i_\tau\rangle \tag{8.2.19}$$

and is in order of Δt. The interaction with the feedback reservoir $\mathbf{M}_B$ is in order of $\Delta t^{1/2}$ and the matrix elements are

$$(\mathbf{M}_{\mathrm{fb}})_{j_S,j_k,j_\tau;i_S,i_k,i_\tau} = -\frac{i}{\hbar}\langle j_S, j_k, j_\tau| \int_{t_k}^{t_{k+1}} H_{\mathrm{fb}} dt |i_S, i_k, i_\tau\rangle \tag{8.2.20}$$

With this, the different orders in Δt have to be taken into account and the fact that the matrices do not commute. In second order in Δt, the evolution matrix reads

$$\begin{aligned}\mathbf{U} = \mathbb{1} + \mathbf{M}_B + \mathbf{M}_S + \frac{1}{2}\mathbf{M}_B^2 + \frac{1}{2}\left(\mathbf{M}_S\mathbf{M}_B + \mathbf{M}_B\mathbf{M}_S\right) + \frac{1}{2}\mathbf{M}_S^2 + \frac{1}{6}\mathbf{M}_B^3 \\ + \frac{1}{6}\left(\mathbf{M}_S\mathbf{M}_B^2 + \mathbf{M}_B\mathbf{M}_S\mathbf{M}_B + \mathbf{M}_B^2\mathbf{M}_S\right) + \frac{1}{24}\mathbf{M}_B^4 + \mathcal{O}(\Delta t^{5/2}).\end{aligned} \tag{8.2.21}$$

The first four terms coincide with the previous result Eq. (C.0.5) including contributions of orders Δt^0, $\Delta t^{1/2}$, and Δt. The next terms add the orders $\Delta t^{3/2}$ and Δt^2. Here, the interaction and system Hamiltonian mix. Note, that terms in the expansion of the exponential up to fourth order contribute.

When considering the higher order time evolution operator, the number of photon states taken into account for the photon bins need to be increased, as not in a single time step more photon processes may occur. This increases the memory usage and the possible maximal complexity of the state for a given number of time steps, however, fewer time step need to be used in order to simulate a given realization. In the problems studied in this thesis, the gain in reducing the number of SVDs in a single time step due to the higher order evaluation outweighs the increased complexity of the photon bath by far.

8.2.3. Pulsed excitation

In order to simulate pulsed excitation efficiently using the MPS evolution, the Hamiltonian can be divided into a time-independent and a time-dependent part

$$H_{\mathrm{tot}} = H_{\mathrm{sys}} + H_{\mathrm{pump}}(t) + H_{\mathrm{fb}}. \tag{8.2.22}$$

The time dependent pump Hamiltonian that will be used in this thesis is the semiclassical pump Hamiltonian in rotating wave approximation with a time-dependent enveloping amplitude $\Omega(t)$

$$H_{\mathrm{pump}}(t) = \frac{\hbar}{2}\Omega(t)\left(p e^{i\omega_{\mathrm{L}}t} + p^{\dagger}e^{-i\omega_{\mathrm{L}}t}\right). \tag{8.2.23}$$

Here, p may be a bosonic or fermionic creation operator depending on the pumped system. After transforming the Hamiltonian to the rotating frame with ω_{L}, as done in Sec. 8.2.1 for the Hamiltonian without time dependent envelope, the only time-dependence of the enveloping function is left. When writing the Hamiltonian in matrix form, the enveloping time-dependent factor is valid for the whole matrix of the pump Hamiltonian. By writing the time evolution matrix as the exponential function of the time independent system part $\mathbf{M}_S$, the time dependent part $\Omega(t_k)\mathbf{M}_P$, and the bath part $\mathbf{M}_B$, again the relevant terms in the expansion can be identified. The relevant terms in, e.g., second order of Δt are

$$\begin{aligned}
\mathbf{U} &= \exp\left(\mathbf{M}_S + \Omega(t_k)\mathbf{M}_P + \mathbf{M}_B\right) \\
&\approx \mathbb{1} + \mathbf{M}_B + \mathbf{M}_S + \frac{1}{2}\mathbf{M}_B^2 + \frac{1}{2}\left(\mathbf{M}_S\mathbf{M}_B + \mathbf{M}_B\mathbf{M}_S\right) + \frac{1}{2}\mathbf{M}_S^2 \\
&+ \frac{1}{6}\mathbf{M}_B^3 + \frac{1}{6}\left(\mathbf{M}_S\mathbf{M}_B^2 + \mathbf{M}_B\mathbf{M}_S\mathbf{M}_B + \mathbf{M}_B^2\mathbf{M}_S\right) + \frac{1}{24}\mathbf{M}_B^4 \\
&+ \Omega(t_k)\left[\mathbf{M}_P + \frac{1}{2}\left(\mathbf{M}_P\mathbf{M}_B + \mathbf{M}_B\mathbf{M}_P\right) + \frac{1}{6}\left(\mathbf{M}_P\mathbf{M}_B^2 + \mathbf{M}_B\mathbf{M}_P\mathbf{M}_B + \mathbf{M}_B^2\mathbf{M}_P\right)\right] \\
&+ \Omega(t_k)^2\mathbf{M}_P^2.
\end{aligned} \tag{8.2.24}$$

The first two lines are just the terms known from the time-independent case. The third line is the part that is linear in the expansion with the pump amplitude, while the last line is the part that is quadratic in the amplitude. For the numerical evaluation a similar approach to the time-independent problem may be used, however, for each order in $\Omega(t)$ a separate matrix is used. Thus, the time evolution matrix can be written as $\mathbf{U} = \mathbf{U}_0 + \Omega(t)\mathbf{U}_1 + \Omega(t)^2\mathbf{U}_2$. Then the total change of the state vector is given by the sum of these terms. For numerical efficiency, the time-evolution matrix can be saved as a sparse matrix. After computing the full evolution matrix $\mathbf{U}$, only the nonzero elements together with the corresponding indices are saved. This allows a significant speedup of the application of the evolution matrix on the state as in the problems at hand only few matrix elements are nonzero, especially if the Hilbert space of interest becomes large as in the problem of Chapter 10.

When evaluating the time dependent Hamiltonian one sparse matrix for each order in $\Omega(t)$ is used. The time dependent factor only needs to be evaluated once every time step and not the whole matrix has to be created anew. As each order is represented by a sparse matrix only few additional computations in comparison to the time-independent evolution have to be employed in each time step.

8.2.4. Exploring feedback dynamics using MPS techniques

With the evolution given by Eq. (C.0.5), one could take the initial state

$$|\Psi(0)\rangle = \sum_{i_{\mathrm{cav}},i_{\mathrm{T}},\{i_k\}} \psi_{...,i_{\mathrm{cav}},i_{\mathrm{T}},i_0,i_{0-1},...,i_{0-l},...}|..., i_{\mathrm{cav}}, i_{\mathrm{T}}, i_0, ..., i_{0-l-1}, i_{0-l}, ...\rangle \tag{8.2.25}$$

to compute the time evolution of the system numerically. Here, $\psi_{...,i_{\mathrm{cav}},i_{\mathrm{T}},i_0,i_{0-1},...,i_{0-l},...}$ is the probability amplitude for the basis state $|..., i_{\mathrm{cav}}, i_{\mathrm{T}}, i_0, ..., i_{0-l-1}, i_{0-l}, ...\rangle$, where i_{cav} is the number of photons in the cavity, i_{T} indicates whether the two level system in the excited state, and i_p gives the number of photons in bin p. However, there are still an infinite number of photon modes. Even, if only the system with up to n_{ph} photon number states and the bath with five photon states for each photon bin that lies inside the τ-interval are taken into account, the relevant part of the state would still have $n_{\mathrm{el}} = 2n_{\mathrm{ph}}5^l$ elements. In case of e.g. $\tau/dt = 100$ and $n_{\mathrm{ph}} = 10$, this would be $n_{\mathrm{el}} \approx 1.58 \times 10^{71}$, which corresponds to approximately 3×10^{63} GB of memory. This is obviously not practical. Thus, the concept of matrix product states is introduced to deal with this complication.

Schmidt-decomposition and notational conventions

As the concept underlying matrix product states, first the Schmidt-decomposition is introduced. It is also called singular value decomposition (SVD). The name Schmidt-decomposition is used customary in the context of quantum physics, while from the linear algebra point of view, the name singular value decomposition is used more often. It was introduced to describe and analyze entangled states [EK95; Sch11]. When a composite quantum system consists of several subsystems, these subsystems may be entangled. This leads to the general representation of the state involving superposition states. If $|i\rangle_A$ and $|j\rangle_B$ $(i, j = 0, 1, ...)$ are orthonormal basis sets of the subsystems with dimensions N_A and N_B, the state may be written as

$$|\Phi\rangle = \sum_{i,j} C_{i,j}|i\rangle_A \otimes |j\rangle_B. \tag{8.2.26}$$

Here, i and j may be multiindices incorporating several physical subsystems, as it will be the case in the following. When the state is written like this, there is a sum of several possible states. This may get quite involved if the subsystems are not two simple two level systems. The most simple state is a product state in the form $|\Phi\rangle = |\phi_A\rangle \otimes |\phi_B\rangle$. Then, only one of the coefficients C is nonzero. The goal of matrix product states is to try to keep the complication due to the superposition of states as small as possible, i.e., to remember as few nonzero coefficients as necessary. It turns out, that this is possible by using products of matrices instead of simple products of states. This will lead to the concept of matrix product states. The coefficients of the state are now considered as the coefficients of a matrix:

$$\mathbf{C} = \begin{pmatrix} C_{0,0} & C_{0,1} & C_{0,2} & \dots \\ C_{1,0} & C_{1,1} & & \\ C_{2,0} & & C_{2,2} & \\ \vdots & & & \ddots \end{pmatrix}. \tag{8.2.27}$$

With the singular value decomposition, the matrix $\mathbf{C}$ can be represented by the product

$$\mathbf{C} = \mathbf{V}\mathbf{S}\mathbf{W}^\dagger. \tag{8.2.28}$$

In the following, the tensor-notation is used relying on the use of indices, as this is clearer in the case of tensors containing more than two indices. Then, Eq. (8.2.28) becomes

$$C_{i,j} = \sum_{\alpha=1}^{r}\sum_{\beta=1}^{r} V_{i,\alpha} S_{\alpha,\beta} W^*_{\beta,j}. \tag{8.2.29}$$

The matrices on the right hand side have the following properties;

- $\mathbf{V}$ is a $N_A \times \min(N_A, N_B)$-matrix with orthonormal columns: $\mathbf{V}^\dagger\mathbf{V} = \mathbb{1}$, if $N_A \leq N_B \Rightarrow \mathbf{V}\mathbf{V}^\dagger = \mathbb{1}$
- $\mathbf{S}$ is a diagonal $\min(N_A, N_B) \times \min(N_A, N_B)$-matrix. The singular values on the diagonal of this matrix are nonnegative values. In the numerical computation, a decomposition with r nonzero singular values s_i in the order $s_1 \geq s_2 \geq ... \geq s_r > 0$ is done
- $\mathbf{W}$ is a $\min(N_A, N_B) \times N_B$-matrix with orthonormal rows: $\mathbf{W}\mathbf{W}^\dagger = \mathbb{1}$, if $N_A \geq N_B \Rightarrow \mathbf{W}^\dagger\mathbf{W} = \mathbb{1}$
- by neglecting small singular values, the matrix $\mathbf{C}$ is approximated optimally with respect to the norm $\sum_{i,j} |C_{i,j}|^2$

The reduced density matrices are $\rho_A = \mathrm{Tr}_B|\Psi\rangle\langle\Psi|$ and $\rho_B = \mathrm{Tr}_A|\Psi\rangle\langle\Psi|$. To compute the bipartite Schmidt-decomposition of the state $|\Psi\rangle = \sum_{i,j} C_{i,j}|i,j\rangle$, where i and j are the (compound) indices of the subsystems, which are to be separated. As stated above, the coefficients $C_{i,j}$ are regarded as entries of a rectangular matrix $\mathbf{C}$, so that the reduced density matrices may be written as $\rho_A = \mathbf{C}\mathbf{C}^\dagger$ and $\rho_B = \mathbf{C}^\dagger\mathbf{C}$. This is relevant, since for the singular value decomposition of $\mathbf{C}$, the following two relations hold [TB97]

$$\mathbf{C}^\dagger\mathbf{C} = \mathbf{W}\mathbf{S}^\dagger\mathbf{V}^\dagger\mathbf{V}\mathbf{S}\mathbf{W}^\dagger = \mathbf{W}\mathbf{S}^\dagger\mathbf{S}\mathbf{W}^\dagger \tag{8.2.30a}$$

$$\mathbf{C}\mathbf{C}^\dagger = \mathbf{V}\mathbf{S}^\dagger\mathbf{W}^\dagger\mathbf{W}\mathbf{S}\mathbf{V}^\dagger = \mathbf{V}\mathbf{S}^\dagger\mathbf{S}\mathbf{V}^\dagger. \tag{8.2.30b}$$

As this corresponds to the diagonalization of the reduced density matrices, $\mathbf{W}$ is the contains the eigenvectors of $\mathbf{C}^\dagger\mathbf{C}$, while $\mathbf{V}$ contains the eigenvectors of $\mathbf{C}\mathbf{C}^\dagger$. The singular values s_α in $\mathbf{S}$ are the square roots of the eigenvalues of $\mathbf{C}^\dagger\mathbf{C}$ and $\mathbf{C}\mathbf{C}^\dagger$. Because the relations Eqs. (8.2.30) hold, the singular value decomposition can be computed from the eigenvalues of the reduced density matrices, as done in Refs. [EK95; Vid03].

Using the singular value decomposition, a given matrix or tensor can be approximated by considering only the largest of the nonzero singular values. Then,

$$C_{i,j} = \sum_{\alpha=1}^{r}\sum_{\beta=1}^{r} V_{i,\alpha} S_{\alpha,\beta} W^*_{\beta,j} \approx \sum_{\alpha=1}^{d}\sum_{\beta=1}^{d} V_{i,\alpha} S_{\alpha,\beta} W^*_{\beta,j} = \tilde{C}_{i,j}. \tag{8.2.31}$$

The matrix C is approximated by $\tilde{C}$, where only the first $d < r$ singular values are taken into account. The error ϵ made in using the approximate matrix $\tilde{C}$ is estimated by the Frobenius norm $\mathcal{N}(\cdot)$, which can be evaluated directly from the singular values as

$$\epsilon = \sqrt{\mathcal{N}(C) - \mathcal{N}(\tilde{C})} = \sqrt{\sum_{\alpha}^{r} s_\alpha^2 - \sum_{\alpha}^{d} s_\alpha^2}. \tag{8.2.32}$$

Thus ϵ only depends on the neglected singular values, as the norm can be computed directly from the singular values. In practice, we will give a cutoff error, which should not be exceeded, however for controlling the memory use, we will also give a maximal number of singular values which are taken into account. We will discuss the numerical errors in more detail in Sec. 8.2.5.

By applying a singular value decomposition to the matrix $\mathbf{C}$, the state reads

$$\begin{aligned} |\Psi\rangle &= \sum_{i,j} \sum_{\alpha,\beta=1}^{\min(N_A,N_B)} V_{i\alpha} S_{\alpha\beta} W^*_{\beta j} |i\rangle_A |j\rangle_B = \sum_{i,j} \sum_{\alpha,\beta=1}^{\min(N_A,N_B)} V_{i\alpha} s_\alpha \delta_{\alpha,\beta} W^*_{\beta j} |i\rangle_A |j\rangle_B \\ &= \sum_{\alpha=1}^{\min(N_A,N_B)} \left(\sum_i V_{i\alpha} |i\rangle_A \right) s_\alpha \left(\sum_j W^*_{j\alpha} |j\rangle_B \right) = \sum_{\alpha=1}^{\min(N_A,N_B)} s_\alpha |\alpha\rangle_A |\alpha\rangle_B. \end{aligned}$$

The last term is the Schmidt-decomposition of a composite state into sums of product states.

The close relation of the Schmidt-decomposition to entanglement can be seen by considering the von Neumann entropy as a measurement for the entanglement between the two subsystems. By comparison with the relations Eqs. (8.2.30), and using the definition if the entropy, the entropy may be written as

$$S_{A|B} = -\mathrm{Tr}(\rho_A \log_2 \rho_A) = -\mathrm{Tr}(\rho_B \log_2 \rho_B) = -\sum_\alpha s_\alpha^2 \log_2 s_\alpha^2. \tag{8.2.33}$$

Diagrammatic tensor notation

In addition to the notation as matrices and the index notation, the diagrammatic notation for tensors is now introduced, which will be more instructive for more complex operations on the matrix product state. Every mathematical object will be represented by a geometric shape. The above SVD (8.2.29) can be expressed in a diagrammatic form, which is shown in Fig. 8.2.3. The matrix $\mathbf{C}$ has two physical indices, which are represented by vertical lines. It is decomposed into the matrices $\mathbf{V}$ and $\mathbf{W}$ with each one physical and one link index. These matrices are represented by rectangular shapes (possibly with rounded edges). The diagonal matrix $\mathbf{S}$ has two link indices and is represented by a circle. The rounded edges of the rectangular represent the orthonormality of the matrix: $\mathbf{V}$ is left-normalized (with orthonormal columns) and $\mathbf{W}$ is right-normalized (with orthonormal rows). The unitary matrix $\mathbf{V}'$ is computed as the product $\mathbf{V}' = \mathbf{VS}$ by contracting the index α. The rounded edges correspond effectively to the contraction of the tensor with the physical index with the neighboring diagonal matrix of singular values.

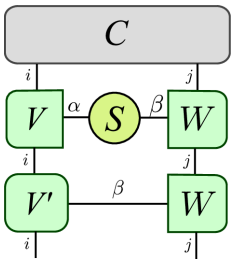

Figure 8.2.3.: Diagrammatic form of the SVD of a matrix.

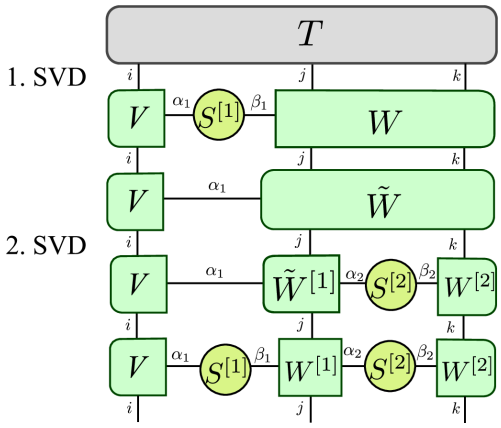

Figure 8.2.4.: Diagrammatic form of the SVD of the tensor $T_{i,j,k}$ of rank three.

Not only matrices, but also tensors of higher order can be decomposed by regarding two indices as a compound index of a matrix. This is more easily expressed in the diagrammatic and in tensor notation. The tensor $T_{i,j,k}$ may be decomposed as follows

$$T_{i,j,k} \overset{\text{SVD}}{=} V_{i,\alpha_1} S^{[1]}_{\alpha_1,\beta_1} W_{\beta_1,j,k} \overset{\text{SVD}}{=} V_{i,\alpha_1} S^{[1]}_{\alpha_1,\beta_1} W^{[1]}_{\beta_1,j,\alpha_2} S^{[2]}_{\alpha_2,\beta_2} W^{[2]}_{\beta_2,k}. \tag{8.2.34}$$

In the following, the Einstein summation convention is used, where it is summed over indices occurring twice. In Fig. 8.2.4 this is shown in form of the corresponding diagram. Here, an important technical detail is, that the tensor $W_{\beta_1,j,k}$ cannot be decomposed directly. In this form the basis of $W_{\beta_1,j,k}$ is not normalized correctly, yet. To do this, $\tilde{W}_{\beta_1,j,k} = S^{[1]}_{\alpha_1,\beta_1} W_{\beta_1,j,\alpha_2}$ needs to be computed, this tensor decomposed, and $\tilde{W}^{[1]}_{\alpha_1,j,\alpha_2}$ has to be multiplied with the inverse of $S^{[1]}_{\alpha_1,\beta_1}$, which then gives $W^{[1]}_{\beta_1,j,\alpha_2}$. This necessity leads to technical issues which are discussed in Sec. 8.2.5.

From the product state to the Matrix product state

In the previous section, the Schmidt-decomposition was introduced, which gives a new set of eigenvectors for the subsystem to express the state. The advantage of this formulation is not obvious, yet, but will be illuminated in the following. During the time evolution, the state of the total system Eq. (8.2.25) will be in a form, such that each subsystem has its own matrix. The initial state of the whole system is a product state, where the Jaynes-Cummings part is in an arbitrary state, while the photon bins are in the

zero-photon state. With the eigenstates of the photon bins defined in Eq. (8.2.16) and the state of the Jaynes-Cummings system $|\psi_\mathrm{S}\rangle$, the initial product state can be written as

$$|\Psi\rangle = ... \otimes |0_1\rangle \otimes |0_0\rangle \otimes |\psi_\mathrm{S}\rangle \otimes |0_{-1}\rangle \otimes ... \otimes |0_{-l}\rangle \otimes ... \tag{8.2.35}$$

In the matrix representation, this becomes

$$\begin{aligned}\mathbf{\Psi}(0) &= ... \begin{pmatrix}1\\0\\0\\0\\0\end{pmatrix}_1 \otimes \begin{pmatrix}1\\0\\0\\0\\0\end{pmatrix}_0 \otimes \mathbf{A}^{[\mathrm{S}]} \otimes \begin{pmatrix}1\\0\\0\\0\\0\end{pmatrix}_{-1} \otimes ... \otimes \begin{pmatrix}1\\0\\0\\0\\0\end{pmatrix}_{-l} \otimes ... \\ &= \ldots \mathbf{A}^{[1]} \otimes \mathbf{A}^{[0]} \otimes \mathbf{A}^{[\mathrm{S}]} \otimes \mathbf{A}^{[-1]} \otimes \cdots \otimes \mathbf{A}^{[-l]} \ldots \end{aligned} \tag{8.2.36}$$

The vectors are ordered, such that in the total state vector the system index is between the index of the photon bin at 0 and -1. This ordering of the vectors is important in the numerical implementation. The vector representing the state Ψ is a product of vectors representing the local states. Starting from this initial state, the application of the evolution operator Eq. (C.0.5) will then introduce correlations (or entanglement) between the system and the environment. Even though these cannot be described in the form of a product state, the goal is to deviate as little as possible from this form. In the above form, for each part of the total system (i.e. the local system and each photon bin) is described by an individual vector. In the following mainly the tensor notation will be used, as it facilitates dealing with the indices. The initial state vector can be written as

$$\psi(0)_{\{i\}} = \ldots A^{[1]}_{i_1} A^{[0]}_{i_0} A^{[\mathrm{S}]}_{i_\mathrm{s}} A^{[-1]}_{i_{-1}} \ldots A^{[-l]}_{i_{-l}} \ldots \tag{8.2.37}$$

Here, the compound index $i_\mathrm{s} \to i_\mathrm{T}, i_\mathrm{cav}$ is introduces for the system. The notation $\{i\}$ indicates the indices i for the system and all photon bins.

The application of the evolution operator in the form of the matrix Eq. (C.0.5) corresponds to the multiplication of this matrix with the total state vector

$$\psi(\Delta t)_{...,j_1,j_\mathrm{s},j_0,j_{0-1},...,j_{0-l},...} = \sum_{\{i\}} U^{...,i_0,i_\mathrm{s},...,i_{-l},...}_{...,j_0,j_\mathrm{s},...,j_{-l}...} \psi(0)_{...,i_\mathrm{s},i_0,i_{0-1},...,i_{0-l},...} \tag{8.2.38}$$

In the matrix U the only non-diagonal block exists for the index pairs including the local system and all of the photon bins inside the τ-interval (in the above case it is $-l$ up to 0). When thinking of the above total system as a chain of multilevel systems, the interaction induced by the evolution is a long range interaction. After the application of the evolution matrix Eq. (C.0.5), the state vector is in the form

$$\mathbf{\Psi}(\Delta t) = ...\mathbf{A}^{[1]} \otimes \mathbf{\Theta} \otimes \mathbf{A}^{[-l-1]} \otimes ..., \tag{8.2.39}$$

$$\theta_{j_0,j_s,j_{-1},...,j_{-l}} = U^{...,i_0,i_\mathrm{s},...,i_{-l},...}_{...,j_0,j_\mathrm{s},...,j_{-l}...} A^{[0]}_{i_0} A^{[\mathrm{S}]}_{i_\mathrm{s}} A^{[-1]}_{i_{-1}} \ldots A^{[-l]}_{i_{-l}}$$

and it is summed over all i. The future (photon bins after 0) and the distant past (photon bins before $-l$) are not influenced by the time evolution, so this will be the same as before. The part of the system, which is altered by the time evolution, may be represented by a

composite state vector Θ, where correlations between the system and the bath are present. Now a bipartite SVD is performed such that the left hand site matrix will include the system index and the right hand site matrix will include all indices of the bath. This can be written in the tensor notation as

$$\theta_{j_0,j_\mathrm{s},j_{-1},\ldots,j_{-l}} = \Gamma^{[\mathrm{S}]}_{j_\mathrm{s},\alpha_\mathrm{s}} \Lambda_{\alpha_\mathrm{s},\beta_\mathrm{s}} w_{\beta_\mathrm{s},(j_0,\ldots)}. \tag{8.2.40}$$

The diagonal matrix $\Lambda_{\alpha,\beta}$ contains the Schmidt coefficients, which may be interpreted as the amount of entanglement of the system with the relevant part of the bath. If the above state was a product state, there would be only one nonzero Schmidt coefficient. There may be maximally as many Schmidt coefficients as the dimension of the system (if the bath part is larger than the part of the local system, which is normally the case). This procedure is repeated for each photon bin. Multiple Bipartite decompositions are performed, dividing the subsystem into the next photon bin and the rest of the bath. In the end, this reads

$$\theta_{j_0,j_\mathrm{s},j_{-1},\ldots,j_{-l}} = \Gamma^{[\mathrm{S}]}_{j_\mathrm{s},\alpha_\mathrm{s}} \Lambda_{\alpha_\mathrm{s},\beta_\mathrm{s}} \Gamma^{[0]}_{\beta_\mathrm{s},j_0,\alpha_0} \Lambda_{\alpha_0,\beta_0} \ldots \Lambda_{\alpha_{1-l},\beta_{1-l}} \Gamma^{[-l]}_{\beta_{1-l},j_{-l}}. \tag{8.2.41}$$

In Eq. (8.2.41) the system and each photon bin of the bath have its own tensor Γ. The correlations with the other parts of the total system are encoded in the coefficients Λ. After this procedure, the indices are ordered such that the system index is between the indices for the photon bins at times 1 and 0. Now, the unitary evolution matrix may be applied again to the state vector and the procedure is repeated. Due to the MPS form of the state vector, the unitary evolution may only be applied to the relevant part of the state

$$\begin{aligned}
\psi(2\Delta t)_{\{j\}} &= \sum_{\{i\}} U^{\ldots,i_0,i_\mathrm{s},\ldots,i_{-l},\ldots}_{\ldots,j_0,j_\mathrm{s},\ldots,j_{-l},\ldots} \psi(\Delta t)_{\{i\}} \\
&= \sum_{\{i\}} \ldots \delta_{j_2,i_2} U^{i_0,i_\mathrm{s},\ldots,i_{1-l}}_{j_1,j_\mathrm{s},\ldots,j_{-l}} \delta_{j_{1-l},i_{1-l}} \ldots \psi(\Delta t)_{\{i\}} \\
&= \ldots A^{[2]}_{j_2} \left(\sum_{i_1,\ldots,i_{1-l}} U^{i_0,i_\mathrm{s},\ldots,i_{1-l}}_{j_1,j_\mathrm{s},\ldots,j_{-l}} \Gamma^{[\mathrm{S}]}_{i_\mathrm{s},\alpha_\mathrm{s}} \Lambda_{\alpha_\mathrm{s},\beta_\mathrm{s}} \Gamma^{[0]}_{\beta_\mathrm{s},i_0,\alpha_0} \Lambda_{\alpha_0,\beta_0} \ldots \Gamma^{[1-l]}_{\beta_{2-l},i_{1-l},\alpha_{1-l}} \Lambda_{\alpha_{1-l},\beta_{1-l}} \right) \\
&\times \Gamma^{[-l]}_{\beta_{1-l},j_{-l}} \ldots
\end{aligned} \tag{8.2.42}$$

The same procedure as before is applied. The correlations with the distant past (for photon bins $< 1-l$), are encoded in the index β_{1-l}. The vector resulting from the application of the evolution matrix is again decomposed. This is the basic technique for performing the time evolution of the system.

8.2.5. Implementation of the evolution algorithm

To implement the time evolution algorithm, at first the basic operations are introduced, which may be performed on the MPS and the relevant technical issues are discussed. Afterwards it is shown how these operations may model the time evolution of the state vector.

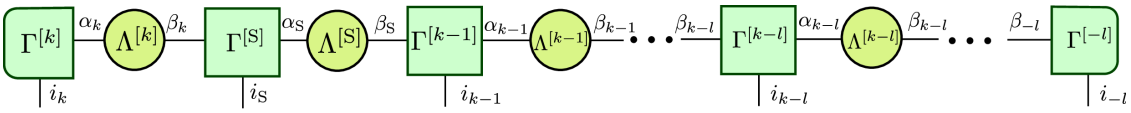

Figure 8.2.5.: State vector at time step k in canonical form.

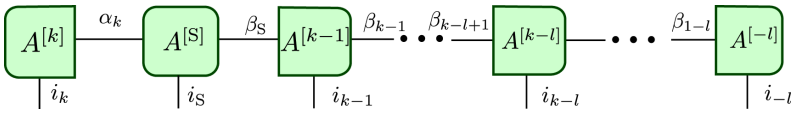

Figure 8.2.6.: State vector at time step k in the mixed normalized form, where the orthogonality center is at the system bin.

Operations on the MPS

In the diagrammatic form the state vector constructed from the above formalism is depicted in Fig. 8.2.5. This form of the MPS is called the canonical form. Note, it suffices to consider a MPS of finite length, even though there are infinitely many photon bins present in the system. Due to the choice of the initial state as a product state, only the part of the state, in which correlations are build up by application of the evolution, has be to considered as the MPS. In the numerical scheme, a slightly different approach is employed to save the state. When introducing the tensor notation in Sec. 8.2.4, it became clear, that before applying a SVD to only a part of the tensor, the normalization has to be ensured by contraction with the matrix containing the singular values. To go back to the canonic form the inverse matrix (containing the inverse singular values) has then to be contracted with the newly decomposed tensor. This poses a problem, when the singular values become small. Then, their inverse becomes large and numerical errors in the small singular values become significant. This could be handled by employing criteria to avoid too small singular values becoming important or by computing also the small singular values to a very high precision [SW13]. However, by writing the state in a different form, this problem can be avoided altogether. Before saving the tensors, they are always contracted with their neighboring singular values. This leads to the representation in the form

$$\psi(t_k)_{\{i\}} = A^{[k]}_{i_k,\alpha_k} A^{[\mathrm{S}]}_{\alpha_k,i_\mathrm{S},\beta_\mathrm{S}} A^{[k-1]}_{\beta_\mathrm{S},i_{k-1},\beta_{k-1}} \dots A^{[k-l]}_{\beta_{k-l+1},i_{k-l},\beta_{k-l}} \dots A^{[-l]}_{\beta_{1-l},i_{-l}}. \tag{8.2.43}$$

Now all the A contain a Γ and a Λ. However, in this representation one site is special. In the above case this is the system tensor, which is contracted with the right hand site as well as the left hand side Λ. This unitary tensor is called the orthogonality center of the state. All operations may be applied to this one. The ones on its left hand side are left-normalized and the ones on its right hand side are right-normalized. To apply operations to other sites, the orthogonality center has to be shifted by doing singular value decompositions. However, as mainly the system observables are of interest not many additional SVDs are needed, cf. Fig. 8.2.9.

The left normalized tensor may fulfills

$$A^{[k]}{}_{i_k,\alpha_k} A^{[k]*}{}_{i_k,\tilde{\alpha}_k} = \delta_{\alpha_k,\tilde{\alpha}_k} \tag{8.2.44}$$

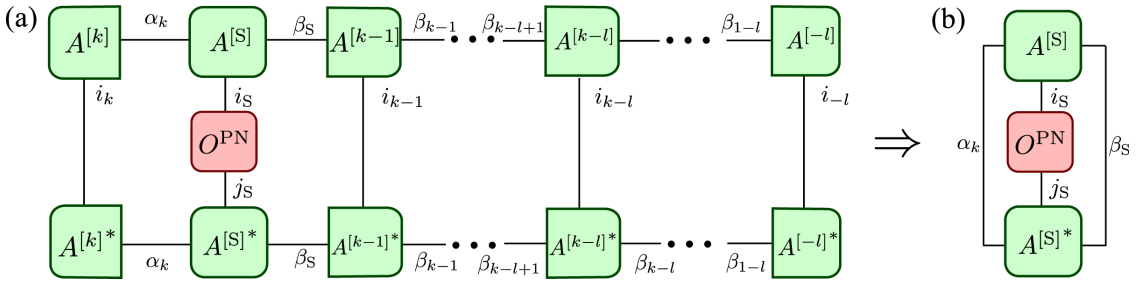

Figure 8.2.7.: (a) Diagram for the computation of the photon number. (b) By tracing out the parts of the system that do not need to be taken into account the simple form is obtained.

while the right normalized obeys

$$A^{[-l]}{}_{\alpha_{-l},i_{-l}} A^{[-l]*}{}_{\tilde{\alpha}_{-l},i_{-l}} = \delta_{\alpha_{-l},\tilde{\alpha}_{-l}}. \tag{8.2.45}$$

The most simple operation that can be performed on the MPS is a single site expectation value. From the above relation it follows, that the computation of e.g. the photon number may be simplified. The photon number operator may be expressed in matrix form as

$$O^{\mathrm{PN}}_{j_{\mathrm{cav}},i_{\mathrm{cav}}} = i_{\mathrm{cav}} \delta_{j_{\mathrm{cav}},i_{\mathrm{cav}}}. \tag{8.2.46}$$

In the diagrammatic notation, in Fig. 8.2.7(a) the computation of the expectation value is shown. Due to the relations Eq. (8.2.44) and Eq. (8.2.45), this can be simplified as shown in Fig. 8.2.7(b). Instead of the $3(k+l)+5$ contractions, only four contractions have to be performed. The simplicity of this operation represents the fact, that a simple operation on the system may not introduce correlations between the system and the bath.

Realization of the evolution algorithm

In the computation of the time evolution, Eq. (8.2.42), there is still a technical issue. As τ becomes larger the part of the state vector, which is influenced by the evolution, becomes larger. Thus, large matrices have to be decomposed. Already for reasonably large values for $\tau/\Delta t$ this becomes unfeasible, so that a different approach will be used. The time evolution introduces an interaction between the system, the photon bin at time t_k and at time t_{k-l}. If the bins at t_k and t_{k-l} were neighbors, the intermediate bins would not be influenced. When employing the analogy to a spin chain, this would correspond to a long range interaction. This can be dealt with in the way proposed in Ref. [Sch+10]. The method is based on the fact, that the ordering due to the decomposition into single site tensors performed in Eq. (8.2.41) is in principle arbitrary and these bins can in fact be made neighbors by simply changing the order of the indices in the tensor representing the state. The initial state is in the form of Eq. (8.2.6) but with the orthogonality center

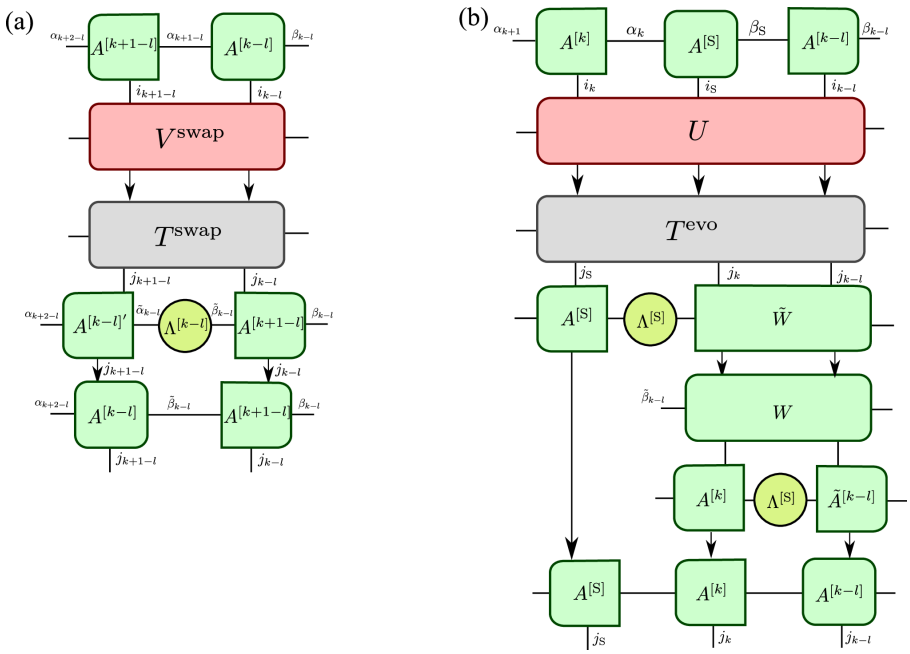

Figure 8.2.8.: (a) Swap operation performed on two photon bins to reorder the MPS. (b) Diagrammatic representation of the operations needed to perform the reduced unitary evolution.

at the bin $k-l$. A swap gate is applied on the photon bins at $k+1-l$ and $k-l$:

$$\begin{aligned} & A^{[k+1-l]}_{\alpha_{k+2-l},i_{k+1-l},\alpha_{k+1-l}} A^{[k-l]}_{\alpha_{k+1-l},i_{k-l},\beta_{k-l}} V^{\text{swap}}_{j_{k+1-l},j_{k-l};i_{k+1-l},i_{k-l}} \\ =& T^{\text{swap}}_{\alpha_{k+1-l},j_{k-l},j_{k+1-l},\beta_{k-l}} \\ \overset{\text{SVD}}{=}& A^{[k-l]'}_{\alpha_{k+1-l},j_{k-l},\tilde{\alpha}_{k-l}} \Lambda^{[k-l]}_{\tilde{\alpha}_{k-l},\tilde{\beta}_{k-l}} \tilde{A}^{[k+1-l]}_{\tilde{\beta}_{k-l},j_{k+1-l},\beta_{k-l}} \\ =& \tilde{A}^{[k-l]}_{\alpha_{k+1-l},j_{k-l},\tilde{\beta}_{k-l}} \tilde{A}^{[k+1-l]}_{\tilde{\beta}_{k-l},j_{k+1-l},\beta_{k-l}} \end{aligned} \tag{8.2.47}$$

This computation is also depicted in detail in Fig. 8.2.8(a). In this figure, the arrows represent the physical indices, which go into a new tensor, which is used for further calculations. The vertical lines for the link indices are kept. This operation is performed again until the photon bin $k-l$ is next to the system bin. Now the evolution matrix is a matrix only covering three physical indices instead of $l+2$, which is more feasible. In the numerical implementation, the evolution matrix is treated as a sparse matrix. Depending on the physical situation this can be much more efficient, especially for large Hilbert spaces, where only very few elements in the unitary evolution are nonzero. This is especially important in the case where additional losses need to be considered, as then the Hilbert space grows extraordinarily unfavorably. After the application of the evolution, the tensor $T^{\text{evo}}_{i_k,i_s,i_{k-l},\beta_{k-l}}$ has to be decomposed. Here, two SVDs are needed, which is depicted in Fig. 8.2.8(b).

Putting all these elements together, the total time evolution algorithm is represented diagrammatically in Fig. 8.2.9 for the exemplary case $\tau/\Delta t = 3$. The expectation values

of the systems are computed in the step before applying the evolution operator, where the orthogonality center is at the system bin.

When using this approach, the state grows as the system is time evolved. In order to avoid a huge state for long run-times, as the part of the state with the photon bins $< k - l$ are not used anymore and may be discarded. When only system expectation values are computed, the distant past can just be forgotten, as one would expect from a bath with a finite memory time.

Error handling in MPSs

In the above algorithm there are two main sources of errors. The first error source is due to the time evolution operator itself. Since the evolution operator is solved perturbatively in lowest order of Δt, an error is introduced for finite Δt. To account for the system-bath interaction, the evolution operator becomes non-unitary. This non-unitarity would vanish in the limit $\Delta t \to 0$. However, this limit has, strictly speaking, only a restricted relevance, since $1/\Delta t$ has to be smaller than the bandwidth $\mathcal{B}$. It leads to a deviation of the norm of the state from unity. So, an important measure for the error is the deviation of the state from unity

$$E_{\text{state}} = \langle \Psi | \Psi \rangle - 1. \tag{8.2.48}$$

The other source of errors is the truncation of the singular values, cf. Eq. (8.2.31). This error is controlled by two values: ϵ, the total relative error allowed in the singular values, and $d_{\max}$, the maximal number of singular values, that are kept during a decomposition. The value $s_{\min}$ is necessary to avoid problems due to numerical precision. The number of singular values has to be limited so that it is possible to save the state to memory. Thus, the method is applicable, if the part of the state that is cut off remains small. Truncating the singular values ultimately also leads to a deviation of the norm of the state from unity, since a part of the state is cut off. Thus, E_{state} is the quantity, that has to be monitored.

8.2.6. Computing correlation functions and the spectrum

In addition to the time evolution of the system, also the steady state spectrum and the (stationary) correlation functions are of interest. As the environment is not traced out in the treatment of feedback used here, but considered explicitly, the correlation functions may be computed directly from the external field. Alternatively, the correlations may be computed by approximating the output field and internal field as proportional, which is commonly done when considering master equations [Lou00]. In many cases this will be justified, depending on the observables of interest. However, in some cases this approach might fail, as when the external photon number distribution is considered [Fis+17]. This will be discussed in more detail in Chapter 11.

Spectrum

To compute the spectrum, the Wiener-Khinchin theorem is used, which relates the spectrum to the first order autocorrelation function [MW95]. The steady state spectrum

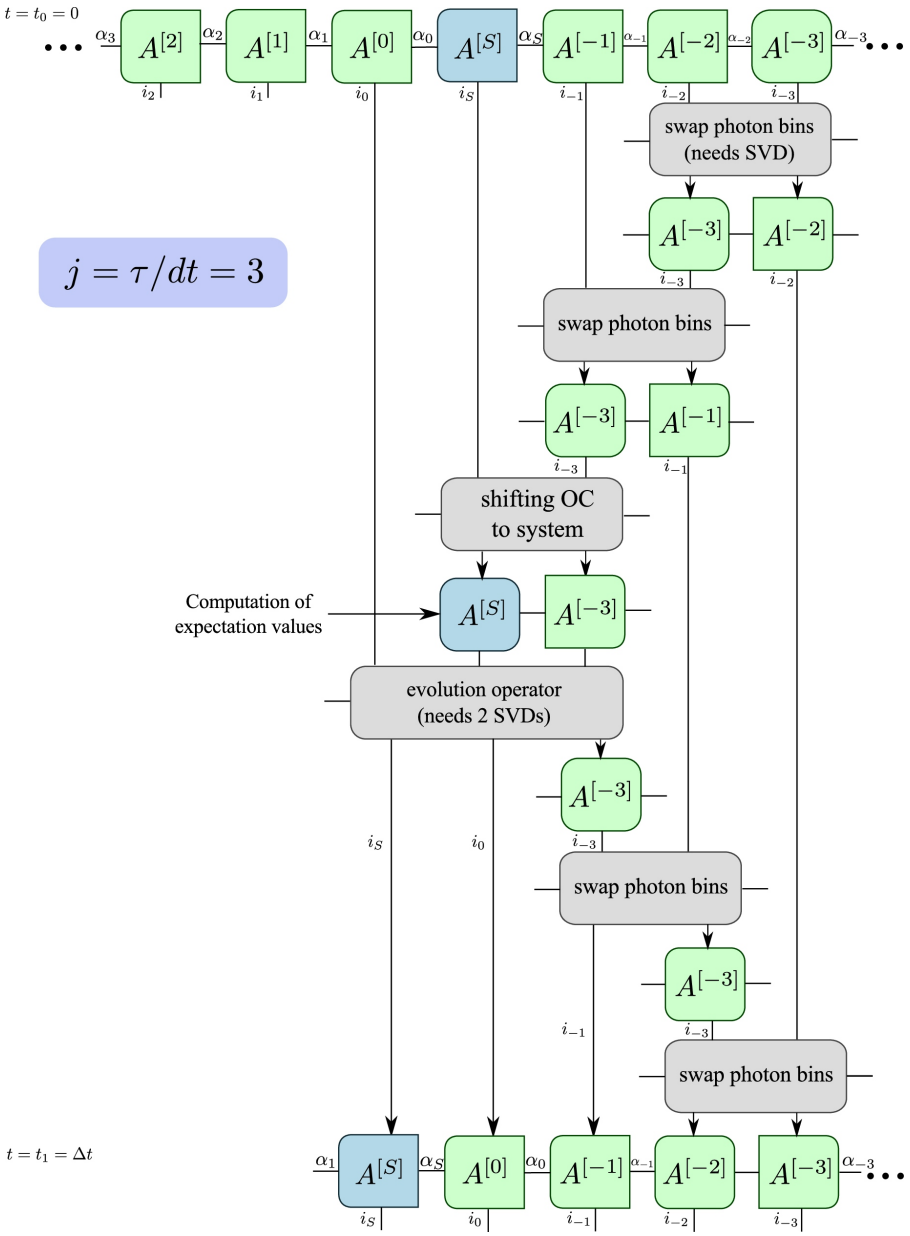

Figure 8.2.9.: Diagrammatic representation of the time evolution algorithm in the MPS form for the case $\tau/\Delta t = 3$, cf. Ref. [Nau+17].

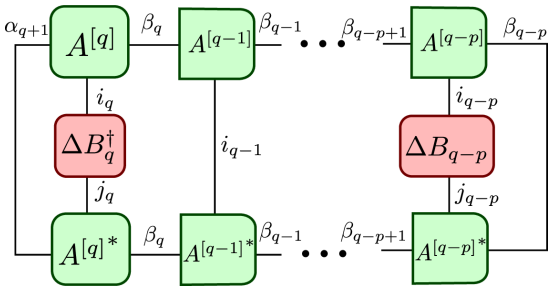

Figure 8.2.10.: Diagram for the computation of the first order correlation function from the MPS. To compute the spectrum, two times are involved, which corresponds to a non-local expectation value. The orthogonality center needs to be at one of the bins involved in the computation. Since two operators are involved they act on the bins at the edges of the tensor train, as the other bins may be traced out.

could be computed directly from the output field by evaluating [PZ16]

$$S(\omega) = \frac{2}{\Delta t}\Re\left(\sum_{p=0}^{M-1}\langle\Delta B^\dagger(t_q)\Delta B(t_{q-p})\rangle e^{i\omega p\Delta t}\right), \tag{8.2.49}$$

where M has to be chosen large enough for the spectrum to be converged and $q = k_{\max}-l-1$ (then, the output field at time t_k is computed). This requires the evaluation of nonlocal expectation values (involving different times). The advantage of this approach is that first the evolution is done and afterwards from the bath bins, the correlations can be computed. In case of $p = 0$, the expectation value in Eq. (8.2.49) is just the photon number at time t_q. This may be computed in the same manner as shown in Fig. 8.2.7(b) for the system. When $p \neq 0$, a true two-timed expectation value is computed, which corresponds to a nonlocal expectation value. The diagram for this is shown in Fig. 8.2.10. The larger p the longer the numerical evaluation takes. The nonlocal expectation value is evaluated in practice by iterating over all involved photon bins and contract the result of each bin, where either an operator is applied or the tensors are contracted immediately. When contracting the final tensor a scalar is left, which is the result of the computation. It is important to note that the orthogonality center needs to be at a photon bin that is involved in the contraction as otherwise no meaningful value is computed due to the non-unitarity of the total tensor that is contracted.

When assuming the proportionality between output field and internal field, the spectrum may be evaluated from

$$S(\omega) = 2\Re\left(\sum_{p=0}^{N-1}\langle c^\dagger(t_{\text{stat}})c(t_{\text{stat}}+p\Delta t)\rangle e^{i\omega p\Delta t}\right), \tag{8.2.50}$$

where c is some system field operator, e.g. the cavity mode. In this case, t_{stat} is the time, after which the system is stationary and N has to be chosen such that, the spectrum is

converged. To evaluate this, the expectation value is rewritten using the state vector

$$\begin{aligned}\langle c^\dagger(t)c(t+\tau)\rangle =&\langle\Psi(0)|c^\dagger(t)c(t+\tau)|\Psi(0)\rangle\\ =&\langle\Psi(0)|U^\dagger(t,0)c^\dagger(0)U(t,0)U^\dagger(t+\tau,0)c(0)U(t+\tau,0)|\Psi(0)\rangle\\ =&\langle\Psi(0)|U^\dagger(t,0)c^\dagger(0)U^\dagger(t+\tau,t)c(0)U(t+\tau,t)U(t,0)|\Psi(0)\rangle\\ =&\langle\Psi(t)|c^\dagger(0)U^\dagger(t+\tau,t)c(0)U(t+\tau,t)|\Psi(t)\rangle.\end{aligned}$$

The spectrum can now be computed in five steps:

1. compute the stationary state vector $|\Psi(t_{\text{stat}})\rangle$ (for which the system observables are stationary)
2. compute the state at time $|\Psi(t_{\text{stat}}+p\Delta t)$
3. compute the state vector $|\Psi_c(t)\rangle = c|\Psi(t)\rangle$ on which the destruction operator is applied
4. compute the next step of the time evolution of this state $|\Psi_c(t_{\text{stat}}+p\Delta t)\rangle$
5. evaluate $\langle\Psi_c(t_{\text{stat}}+p\Delta t)|c|\Psi(t_{\text{stat}}+p\Delta t)\rangle$.

Second order correlation function

For the unnormalized second order correlations, in general there may be four different time arguments

$$G^{(2)} = \langle\Delta B^\dagger(t_k)\Delta B^\dagger(t_l)\Delta B(t_m)\Delta B(t_n)\rangle. \tag{8.2.51}$$

The corresponding diagram is shown in Fig. 8.2.11. Due to the commutation relations of the time bin operators,

$$\Big[\Delta B^\dagger(t_k), \Delta B^\dagger(t_l)\Big] = 0,$$

the correlation is invariant under swapping the time arguments t_k and t_l as well as t_m and t_n. In most cases only the symmetric correlation with $k = n$ and $l = m$ is of interest, as it represents the intensity-intensity correlation in the popular Hanbury Brown-Twiss setup [BT56; Fox06]. The symmetric correlation allows a simplification in the numerical evaluation, as only $\Delta B(t_m)\Delta B(t_n)|\Psi(\infty)\rangle$ needs to be evaluated. This is particularly simple, as in the case $m = n$, only one photon bin is involved and the computation is similar to that of the photon number, while in the case $m \neq n$ operators act only on two photon bins. For the case with four times this is more involved, as at some intermediate bin an operator needs to be applied.

The steady state correlation function may also be computed from the proportionality between internal an external field. This can be done similarly as for the spectrum in the last step. When having evaluated $|\Psi_c(t_{\text{stat}}+p\Delta t)\rangle$, the normalized time-dependent second order correlation function may be evaluated from

$$\begin{aligned}g^{(2)} =&\frac{\langle c^\dagger(t_{\text{stat}})c^\dagger(t_{\text{stat}}+p\Delta t)c(t_{\text{stat}}+p\Delta t)c(t_{\text{stat}})\rangle}{\langle c^\dagger(t_{\text{stat}})c(t_{\text{stat}})\rangle^2}\\ =&\frac{\langle\Psi_c(t_{\text{stat}}+p\Delta t)|c^\dagger c|\Psi_c(t_{\text{stat}}+p\Delta t)\rangle)}{\langle c^\dagger(t_{\text{stat}})c(t_{\text{stat}})\rangle^2}\end{aligned}$$

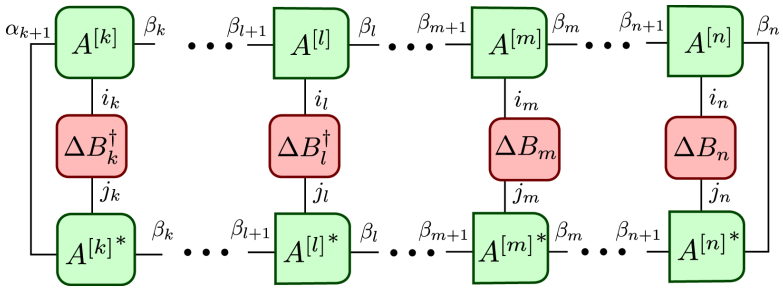

Figure 8.2.11.: Diagram for the computation of the second order correlation function from the MPS. In this case four operators with possibly different times are involved. For the general case with four different operators an operators acts at four different photon bins. For the simpler symmetric case, when $k = n$ and $l = m$, the photon number operators acts only a the bins at the borders.

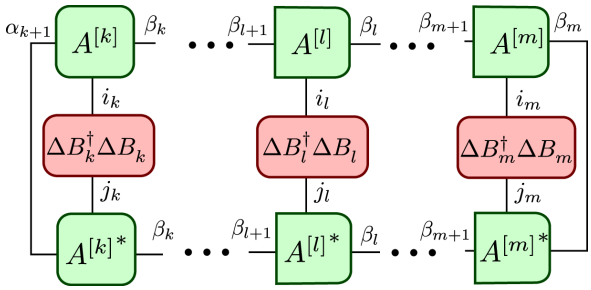

Figure 8.2.12.: Diagram for the computation of the symmetric third order correlation function from the MPS. In this case only three different times are involved simplifying the evaluation as the photon number operator is applied to the three photon bins.

Third order correlation function

The unnormalized third order correlation function reads in general

$$G^{(3)} = \langle \Delta B^\dagger(t_k) \Delta B^\dagger(t_l) \Delta B^\dagger(t_m) \Delta B(t_p) \Delta B(t_q) \Delta B(t_r) \rangle. \tag{8.2.52}$$

In this thesis only the symmetric case of the third order correlation function with $k = r$, $l = q$, and $m = p$ will be considered, which will be used in Chapter 11 to compute the photon number distribution of the output field. In Fig. 8.2.12 the diagram for the symmetric third order correlation function is shown. Here, a photon number operator acts on the photon bin.

8.2.7. Inclusion of additional decay channels

When setups are considered, where different subsystems are coupled, each of them may be subject to a decay. For example the Jaynes-Cummings model presented previously contains a cavity mode and a two level system. Before, the cavity mode was subject to feedback, while the two level system only coupled to the cavity mode and did not have an

additional decay channel. Since this might be the case in a physical system the inclusion of additional decay channels in the QSSE picture is shown. This is used in Chapter 10, where a cavity mode subject to feedback is coupled to two emitters and both emitters are subject to an additional radiative decay into other optical modes.

As the evolution algorithm presented so far stays within the Schrödinger picture, the convenient density matrix techniques to include decays via the Lindblad form (cf. Parts I and II of this thesis) can not be used straightforwardly. There are three possible ways to include additional decays. One may employ the quantum jump approach as discussed in Sec. 8.2, where trajectories would be computed. Another possibility would be to express the whole theory presented so far in terms of the density matrix. These two approaches in fact trace the degrees of freedom introduced by the additional decay channels out. The third ways is to include the additional decay channel explicitly in the computation as it is done with the decay channel for feedback, but without the non Markovian back-action. In this thesis the last approach is used, as it is the most straightforward extension of the theory presented so far.

An additional decay channel for the TLS in the Jaynes-Cummings model is included by considering an additional set of bath modes in the Hamiltonian Eq. (8.0.1), i.e. $H_{\mathrm{tot}} = H_{\mathrm{sys}} + H_{\mathrm{fb}} + H_{\mathrm{dc}}$, where

$$H_{\mathrm{dc}} = \int d\omega \hbar\omega b_2^\dagger(\omega) b_2(\omega) + i\hbar \int d\omega \sqrt{\frac{\Gamma}{2\pi}} \left[b_2^\dagger(\omega)\sigma_- - \mathrm{h.c.} \right]. \tag{8.2.53}$$

After the introduction of the rotating frames in the same manner as for Eq. (8.2.9), the time dependent reservoir operators may be defined as $b_2(t) = \frac{1}{\sqrt{2\pi}} \int_{\mathcal{B}} d\omega b_2(\omega) e^{-i(\omega-\omega_L)t}$ leading to

$$H_{\mathrm{dc,rf}} = i\hbar\sqrt{\Gamma} \left[b_2^\dagger(t)\sigma_- - \sigma_+ b_2(t) \right]. \tag{8.2.54}$$

When evaluating the time evolution operator in first order, this leads to the matrix $\mathbf{M}_{\mathrm{dc}}$ with the elements

$$\begin{aligned}
&(\mathbf{M}_{\mathrm{dc}})_{j_S,j_k,j_{2,k},j_\tau,j_{2,\tau};i_S,i_k,i_{2,k},i_\tau,i_{2,\tau}} \\
&= -\frac{i}{\hbar} \langle j_S, j_k, j_{2,k}, j_\tau, j_{2,\tau}| \int_{t_k}^{t_{k+1}} H_{\mathrm{dc,rf}} dt |i_S, i_k, i_{2,k}, i_\tau, i_{2,\tau}\rangle. \\
&= \sqrt{\Gamma} \langle j_S, j_k, j_{2,k}, j_\tau, j_{2,\tau}| \left[\Delta B_2^\dagger(t_k)\sigma_- - \sigma_+ \Delta B_2(t_k) \right] |i_S, i_k, i_{2,k}, i_\tau, i_{2,\tau}\rangle \\
&= \sqrt{\Gamma}\sqrt{\Delta t} \left(\sqrt{j_{2,k}} \delta_{j_{2,k},i_{2,k}+1} \delta_{j_{\mathrm{T}},0} \delta_{i_{\mathrm{T}},1} - \sqrt{i_{2,k}} \delta_{j_{2,k}+1,i_{2,k}} \delta_{j_{\mathrm{T}},1} \delta_{i_{\mathrm{T}},0} \right) \\
&\qquad \times \delta_{j_k,i_k} \delta_{j_\tau,i_\tau} \delta_{j_{2,\tau},i_{2,\tau}} \delta j_{\mathrm{cav}}, i_{\mathrm{cav}}
\end{aligned}$$

Here, the new set of bath operators $\Delta B_2(t_k) = \int_{t_k}^{t_{k+1}} dt b_2(t)$ is introduces in the same manner as before. Note, that an additional set of indices needs to be included for the additional decay channel. As expected from a simple decay, it only acts on the photon bin at the current time and does not influence the past of the reservoir. This matrix then needs also to be considered in the exponential Eq. (8.2.18).

For the time evolution algorithm the photon reservoir is decomposed into photon bins at discrete times. As the times for the reservoir inducing the decay are the same times, which are used for the feedback time, the compound index $\tilde{i}_k = i_k, i_{2,k}$ may be introduced.

By doing this, both photon baths are treated by considering a common Hilbert space and when performing the SVD all photon modes at a given time are treated as one entity. This allows to keep the MPS structure presented before in the same manner, with the only difference that one photon bin contains multiple photon modes.

When writing the state in MPS form for this case it reads

$$\psi(t_k)_{\{i\}} = A^{[k]}_{i_k,i_{2,k},\alpha_k} A^{[\mathrm{S}]}_{\alpha_k,i_\mathrm{s},\beta_\mathrm{S}} A^{[k-1]}_{\beta_\mathrm{S},i_{k-1},i_{2,k-1},\beta_{k-1}} \dots A^{[k-l]}_{\beta_{k-l+1},i_{k-l},i_{2,k-l},\beta_{k-l}} \dots A^{[-l]}_{\beta_{-l},i_{-l},i_{2,-l}}. \tag{8.2.55}$$

Here, each tensor contains the indices of two bath bins at the same time.

8.2.8. SVD with LAPACK

In practice, the numerical singular value decomposition as implemented in LAPACK will be used. When using LAPACK with C it is important to note that LAPACK is written in Fortran and the ordering of matrices in the memory are different for C and Fortran. The decomposition of tensors of higher ranks corresponds to the decomposition of rectangular matrices. Then, the ordering of the indices is important as well as whether the matrix or its transposed is decomposed.

In the program used for the numerical calculations of this thesis, a singular value decomposition in two steps is used. Here, two functions from the LAPACK library are available that are suitable. On the one hand, there is the function `zgesvd` that uses a QR algorithm and on the other hand there is the function `zgesvd` that uses a divide an conquer method, dividing the matrix into submatrices, computing the SVD of them and putting the result together.[1] As the latter algorithm is generally faster and thus used for most SVDs. However, in some cases this algorithm fails to converge. Then, the function `zgesvd` is used as the fall-back algorithm.

8.3. Benchmark of MPS evolution

In this section the MPS evolution as presented in the previous section is benchmarked with some solutions given by the methods mentioned in Sec. 8.1. The known results can be reproduced which gives confidence in the method.

One of the most simple problems, which nonetheless already incorporates the essence of the problems which feedback poses with respect to the numerical description is the two level system subject to feedback. For this case the system Hamiltonian

$$H_{\mathrm{sys,TLS}} = \hbar\omega_\mathrm{TLS}\sigma_+\sigma_- + \hbar\Omega_\mathrm{TLS}\left(e^{-i\omega_\mathrm{L}t}\sigma_+ + e^{i\omega_\mathrm{L}t}\sigma_-\right), \tag{8.3.1}$$

where ω_TLS is the transition frequency of the two level system, ω_L is the frequency of a possible driving laser, and Ω_TLS is the pump strength. The total Hamiltonian is then given by Eq. (8.0.1) with the feedback part Eq. (8.0.2), whre $A = \sigma_-$.

First, the case without pump is considered as this is the most simple case and an analytical solution exists in the regime where the two level system is most probably decayed when feedback sets in [DZ02]. In Fig. 8.3.1 the comparison between the analytical solution (solid, blue) and the evolution from the MPS method (dashed, red) is shown.

[1] http://www.netlib.org/utk/people/JackDongarra/etemplates/node193.html

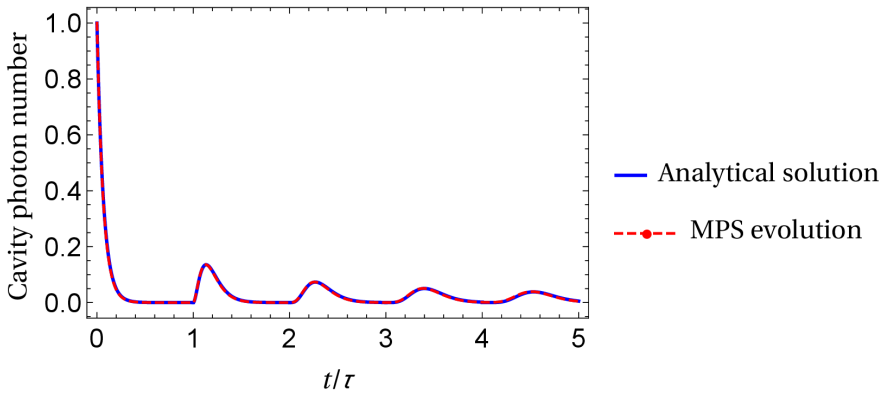

Figure 8.3.1.: Decay of two level system with feedback for the case $\gamma_L/\tau = \gamma_R/\tau = 7.5$, $\Omega_{\mathrm{TLS}} = 0$. The frequency ω_{L} is eliminated by introducing a rotating frame, cf. Sec. 8.2.1. The analytical solution (solid, blue) is taken from Ref. [DZ02] and fits the numerical solution form the MPS evolution well. The discretization for the MPS evolution is $\tau/\Delta t = 100$

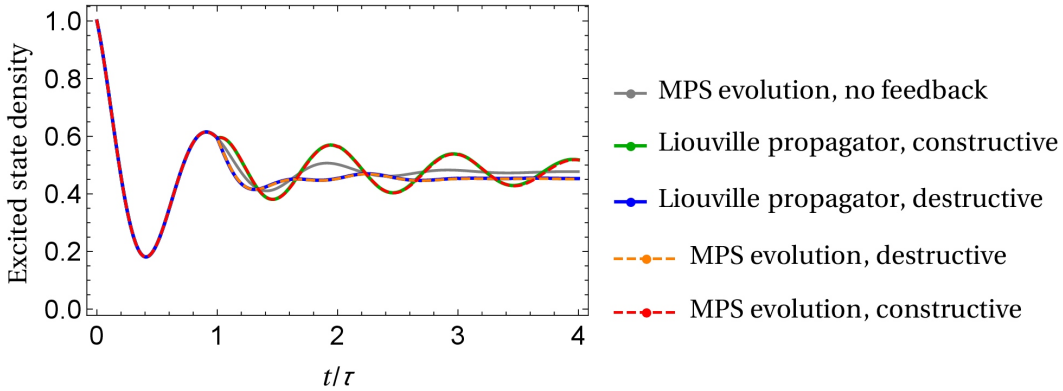

Figure 8.3.2.: Pumped two level system subject to feedback. The dashed solutions are obtained from the MPS evolution for destructive (orange) and constructive (red) interference. The solid curves are the reference solution by the Liouville space method discussed in Sec. 8.1.3. The parameters are, cf. Eq. (8.3.1), $\Omega_{\mathrm{TLS}} = \pi\gamma_L$, $\tau\gamma_L = \tau\gamma_R = 1$. For the MPS evolution $\tau/\Delta t = 100$ is used. The detuning of the pump laser from the TLS frequency is $\omega_{\mathrm{L}} - \omega_{\mathrm{TLS}} = 0$. For constructive interference $e^{i\omega_{\mathrm{L}}\tau} = 1$ and for destructive $e^{i\omega_{\mathrm{L}}\tau} = -1$. For reference the evolution without feedback is shown in gray.

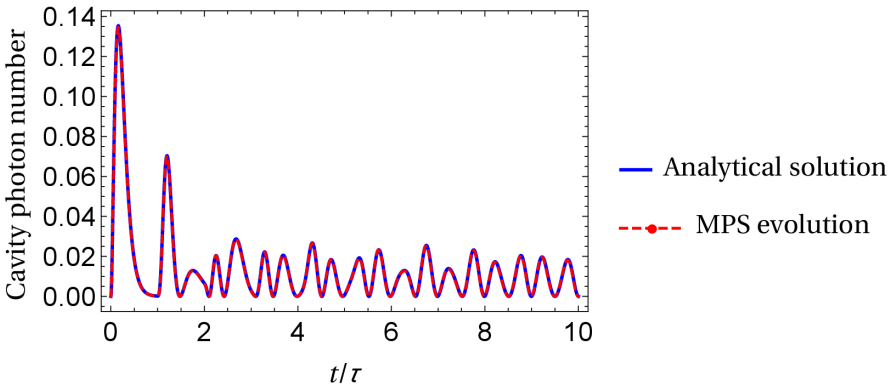

Figure 8.3.3.: The photon number is shown for the single excitation regime for the Jaynes-Cummings model with feedback, i.e. Hamiltonian Eq. (8.0.1) with the system given by the Hamiltonian Eq. (8.2.2). The numerical evaluation via the MPS evolution is compared to the analytical solution taken from [Kab+15]. The solution is reproduced well for several τ-intervals. The parameters are taken as $\tau = 2\pi/g$, $\gamma_L/g = \gamma_R/g = 2$, $\omega_{\text{cav}} = \omega_{\text{e}}$, $\Omega_{\text{cav}} = \Omega_{\text{e}} = 0$, and $e^{i\omega_{\text{cav}}\tau} = 1$ with the TLS being initially in the excited state. The time is discretized with $\tau/\Delta t = 50$.

The next important case is the driven two level system, which was first studied numerically in Ref. [Gri15]. Here, the excitation does not decay in a single τ-interval. Thus, in Fig. 8.3.2 the solution given by the MPS method is compared with the solution from the algorithm given in Ref. [Gri15]. Here, the cases $e^{i\omega_{\text{L}}\tau} = 1$ and $e^{i\omega_{\text{L}}\tau} = -1$ are considered. As the former increases the excited state density, this is called the case of constructive interference, while the latter is called the deconstructive case as it decreases the density.

This section is concluded by considering the Jaynes-Cummings model with feedback introduced in the previous section. There, Rabi oscillations may be stabilized by tuning the feedback as given in the caption of Fig. 8.3.3. In the single excitation regime this was first considered in Ref. [Car+13] and in Ref. [Kab+15] an analytical solution was given. Here, the numerical solution via the MPS evolution method is found to be in excellent agreement with the analytical case. As in the following effects with more than two photon are of particular interest, the MPS evolution is compared to the brute force evaluation of the Hamiltonian Eq. (8.0.1), when initially two photon are present in the cavity mode. For the brute force evaluation, the integral in the feedback part of the Hamiltonian is discretized. This is done in the same way as for the approximate solution in Chapter 10, where more details are given. Additional information on the brute force evaluation of the feedback Hamiltonian may be found in Refs. [Sch14; Hei16]. In Fig. 8.3.4, the time evolution of the photon number using the MPS method is shown to coincide well with the reference solution.

The single photon case is used to illustrate the speedup of the computation due to the second order evolution algorithm presented in Sec. 8.2.2. When the cumulative error in the norm of the MPS, as discussed at the end of Sec. 8.2.5, should stay in a similar order of magnitude, the evaluation time differs strongly. In Fig. 8.3.5 the error in the MPS

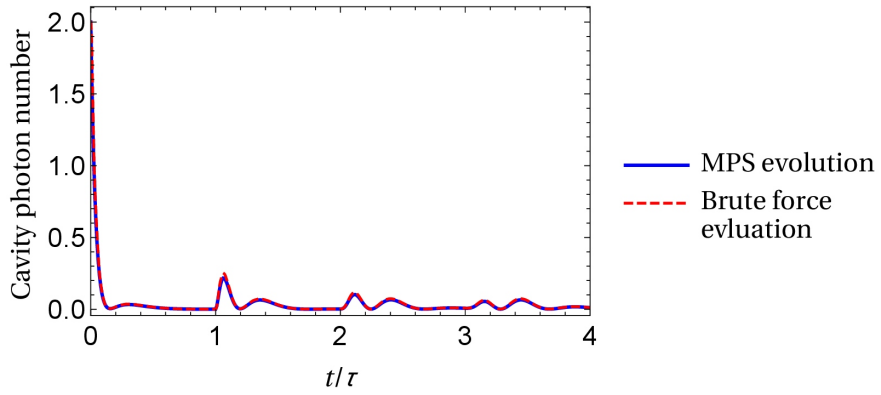

Figure 8.3.4.: In the case corresponding to Fig. 8.3.3, where initially two photons are in the cavity mode, the MPS evolution is compared to the brute force evaluation of Hamiltonian Eq. (8.0.1) as done in Chapter 10 for the approximate solution. The solution is reproduced well for several τ-intervals. The parameters are taken as $\tau = 2\pi/g$, $\gamma_L/g = \gamma_R/g = 2$, $\omega_{\text{cav}} = \omega_{\text{e}}$, $\Omega_{\text{cav}} = \Omega_{\text{e}} = 0$, and $e^{i\omega_{\text{cav}}\tau} = 1$ with the TLS being initially in the excited state. The time is discretized with $\tau/\Delta t = 50$. For the brute force evaluation 3600 momentum values are used with the discretization $\Delta k/g = \frac{3}{40\pi c_0}$.

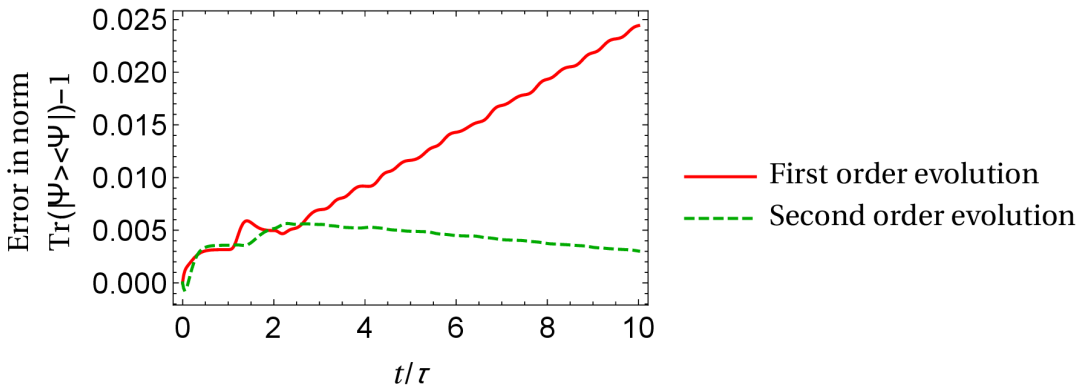

Figure 8.3.5.: The error in the norm of the MPS, cf. Eq. (8.2.48), for the time evolution shown in Fig. 8.3.3 for the case of first order evolution in Δt (red, solid) and second order evolution in Δt (green, dashed). If the relative error in the MPS is kept in a similar order of magnitude, the first order evolution takes about 9 min 30 s, while the second order evolution only takes 2 s on the same machine.

norm is shown for the case of evolution operator, where terms up to first order in Δt are considered and for the case, where terms up to second order in Δt are considered. For the first order case the numerical evaluation takes about 9 minutes and 30 seconds, while the second order evaluation on the same computer is finished after about 2 seconds. In the second order case, the discretization $\tau/\Delta t = 50$ is sufficient to reproduce the analytical solution very well, cf Fig. 8.3.3, while in the first order case $\tau/\Delta t = 2000$ is necessary for a similar error E_{state}. In both cases the singular values are cut off, when the error given by Eq. (8.2.32) due to neglecting them is less than 10^{-10}. However at maximum 32 singular values are taken into account for each SVD. This computational speedup allows to address more complex problems, which will be done in the following.

In this chapter of the thesis the method to solve time-delayed quantum coherent feedback in the picture of the quantum stochastic Schrödinger equation via matrix product state evolution was presented. The method first introduced in Ref. [PZ16] was extended to higher order terms in the time evolution and to systems with time dependent Hamiltonians. In Chapter 10 this method will be applied to the two emitter Jaynes-Cummings model already considered in Part II together with an approximate method in the Schrödinger picture. This will serve to further test both methods and to show enhanced antibunching when feedback is applied. Furthermore, in Chapter 11, the impact of feedback on the output field of a two level system is studied. This will reveal that feedback can be used to switch between increased two photon emission and single photon emission.

9. Control of photon statistics via quantum coherent feedback

In Part I mechanical oscillators and in Part II a cavity quantum electrodynamcis (cQED) setup are subject to an optical input field allowing to control internal degrees of freedom of the irradiated system. For manipulating the mechanical oscillator a laser field was used modeled by a classical field, which induces, e.g., laser dynamics in the mechanical oscillators through the optomechanical or the electron-phonon interaction. The laser dynamics correspond to coherent statistics. Steering the systems towards lasing is possible by choosing the correct laser power and frequency, which serve as control parameters in this case.

In case of the cQED setup, consisting of a cavity with two emitters, the photon statistics were manipulated by driving this target system with a source system exhibiting a photon statistics of choice. When the emitted light from the source is transmitted along a dissipative channel, the source characteristics may only be partially imprinted onto the target system, as the dissipation is detrimental for light exhibiting quantum features such as antibunching. However, higher order correlations prove to be more robust against this decoherence. The main control parameter in this setup is the driving strength of the source system.

While the modeling of the light source in Part II proofs to be more complex as the full quantum dynamics are taken into account, no delay effects are considered as a cascaded setup is assumed [Car93; Gar93]. Thus, the dynamics of the target system do not influence the source.

In the present chapter time delay effects will be considered explicitly. In particular systems subjected to self-feedback will be investigated. In order to treat the evaluation numerically, the methods presented in Chapter 8 will be employed. When feedback is used to manipulate the dynamics of systems, the main control parameter of interest is the feedback time τ, which simultaneously affects the feedback phase. In contrast to the treatment of the cascaded setup, where the system is not affected by its past, in the feedback case this has to be considered explicitly. In the following, some of the possibly exploitable effects feedback may have on an optical system are explored with particular focus on the manipulation of the the photon statistics.

In the next section the cQED setup used as target in Part II is now subject to self-feedback. Here the focus lies on the question how states with photon statistics deviating from the coherent case are influenced by employing optical feedback. The results presented in Chapter 10 were previously published in Ref. [Lu+17] in collaboration with Yiping Lu. Of particular interest is the case where the system exhibits antibunching as feedback allows to control the extend of the antibunching to a certain degree. In this part also an approximative solution in the Schrödinger picture is used. In the regime of few excitations the approximative solution agrees well with the MPS evolution method.

In Chapter 11, a pulsed two level system subjected to feedback is considered using the MPS evolution method. Here, feedback allows to tune the output state of the two level system between two and single photon emission. In particular the two photon emission is enhanced in comparison to the case without feedback.

10. Increasing antibunching

The main problem in exploiting quantum effects for applications is the limited time for which quantum correlations dominate the system dynamics [Zol+05; WM06]. In order to overcome this restriction several proposals have been made. In this context, purification of quantum gates [ECZ97], correction of errors [Sho95], and measurement-based feedback [WM06] have been proposed. Instantaneous feedback, as discussed earlier, allows to stabilize single photon Fock states [Zho+12].

Recently, the effect of time-delayed feedback close to the quantum regime is addressed in optical systems [Alb+11a; Hop+13; Hoi+15; Alb+11b].

After having introduced the MPS evolution method in Chapter 8, it is now applied to a cavity quantum electrodynamical system. Alongside the numerically exact method, an approximative numerical scheme in the Schrödinger picture is used to gain further insight into the system dynamics and the modeling. This scheme is valid in the regime of few excitations. As the dissipation is taken into account in form of an effective non-Hermitian Hamiltonian, only weak decay rates may be considered [ZZC16; GZ04]. In the regime of low pumping rates the approximative model agrees well with the MPS evolution. This is shown by additional benchmarks in order to test both models in this regime where it is difficult to use other models. After showing the agreement of the models in certain regimes, the approximative model is used in the limit of short time delays to control the output statistics of the light field. Here, antibunching and bunching can be enhanced and diminished as well as the amount of entanglement between the emitters inside the cavity. The focus lies on the possibility to have additional control over the system emission rather than maximizing, e.g., bunching.

In the system studied in this chapter, a connection between the photon statistics and the entanglement between the two emitters inside the cavity was shown [ZZC16]. This connection allows to probe to some extend the entanglement between the two emitters which is not easily addressable in experiments. This may be done by probing the full density matrix of a system which contains all information [Jam+01; The+02], but which is only reconstructed with some additional effort [LLZ15; LZ16]. The entanglement observed in the following, however is very small and cannot be exploited for applications. Here, it will rather serve to establish whether the connection between entanglement and correlation still exists when feedback is applied.

In Sec. 10.1, the approximative model will be introduced and in Sec. 10.2 the case without feedback will be shortly considered. Then, in Sec. 10.3, the regime of validity of the approximative solution is estimated using the MPS evolution. Afterwards the approximative solution is employed in the limit of short time delays to illustrate that feedback serves as additional degree of freedom that can be used for controlling the photon statistics of the system in Sec. 10.4. In certain cases this is compared with the solution obtained via the MPS evolution. In Sec. 10.5 the relation between the statistics and entanglement will be briefly discussed.

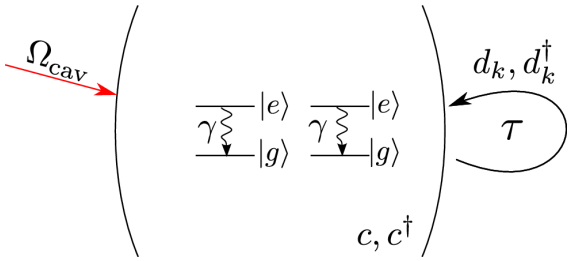

Figure 10.1.1.: A quantum optical many-emitter system with a cavity mode subjected to feedback is investigated with respect to the emission statistics of the cavity mode. Two two-level systems are placed in a cavity that is subjected to feedback, e.g., by coupling to a semi-infinite waveguide. The emitters decay with rate γ and the cavity is pumped with a weak coherent laser with strength Ω_{cav} and frequency ω_{L}. Cavity and emitters are coupled via the electron photon interaction with strength g.

10.1. Model

The system investigated in this chapter is in principle the target system from Part II of this thesis. It may be realized experimentally, e.g., as a nanophotonic device [Sap+15]. However, in the present case the regime where the coupling is much larger than the losses is considered. Then, a detuning between a coherent pump laser and the cavity resonance enables antibunching and bunching.

The model with feedback is sketched in Fig. 10.1.1. The cavity, which is subjected to feedback, contains two two-level systems. It is furthermore pumped by an external coherent laser. After introducing a rotating frame, cf. Eq. (8.2.8), the system Hamiltonian reads [ZZC16]

$$H_{\mathrm{sys,2em}} = \hbar\Delta c^\dagger c + \hbar\sum_{i=1}^{2}\delta\sigma_i^+\sigma_i^- + \hbar\sum_{i=1}^{2} g_i(\sigma_i^+ c + c^\dagger\sigma_i^-) + \hbar\Omega_{\mathrm{cav}}(c^\dagger + c). \tag{10.1.1}$$

As in Part II the emitters are assumed to be identical and in resonance with the cavity mode, i.e. $\delta = \Delta$ and $g_1 = g_2 = g$. However, the cavity is now pumped coherently so that it has a frequency, which may differ from the system resonance. This will be exploited to drive the system into different regimes. In the Hamiltonian Eq. (10.1.1), $\Delta = \delta = \omega_0 - \omega_{\mathrm{L}}$ is the detuning of pump laser from the frequency of the cavity mode and the emitters. The g_i are the coupling strengths between cavity and emitters and Ω_{cav} is the pump strength. The operators $c^\dagger$ and c create and annihilate a photon in the cavity mode, respectively. The ith emitter is brought to the excited state by the flip operator $\sigma_i^+ = |e_i\rangle\langle g_i|$ and brought to the ground state by $\sigma_i^- = |g_i\rangle\langle e_i|$. This is all in analogy to the Jaynes-Cummings model, Eq. (8.2.2). Feedback is also included in the same manner so that the derivation for the feedback algorithm does not change. As the emitters are also assumed to be subjected to decay additional loss channels are included as described in Sec. 8.2.7.

For the approximative model, the feedback and system Hamiltonian remain the same. However, the feedback part is not rewritten in the time domain, rather the Hamiltonian

is used in the form obtained after the introduction of the rotating frame. This reads, cf. Eq. (8.2.10),

$$H_{\mathrm{fb,rf}} = \int dk (G(k,t) c^\dagger d_k + G^*(k,t) d_k^\dagger c), \tag{10.1.2}$$

where $G(k,t) = G_0 \sin(\omega_k \tau/2) \exp[i(\omega_\mathrm{L} - \omega_k)t]$ is the k-dependent coupling strength of the cavity mode to the environment. Note, that G_0 differs from the $g_0(\omega)$ in Eq. (8.0.3) as here the integral is over the momentum k. Furthermore, the Hamiltonian was rewritten using the momentum of the photons instead of the frequency as done in Refs. [Car+13; Hei+14]. This can be done by employing the dispersion relation $\omega_k = c_0|k|$, where c_0 is the speed of light. Thus, the new operators $d_k, d_k^\dagger$ are introduced for annihilation or creation of a photon with momentum k. The investigation is restricted to the one-dimensional case.

To include the decay of the emitter in the Schrödinger picture an approximative effective Hamiltonian is used, which is valid as long as $\gamma \ll g_i$ [ZZC16]. The Hamiltonian for the emitter decay reads

$$H_{\mathrm{decay}} = -\frac{i}{2}\gamma \sum_{i=1}^{2} \sigma_i^+ \sigma_i^-. \tag{10.1.3}$$

In order to describe the system approximately in the Schrödinger picture as in Ref. [ZZC16], it is assumed here that maximally two excitations are present so that the Hilbert space is finite. When choosing the basis $|i_1, i_2, i_{\mathrm{photon}}, k, k'\rangle$, where i_1 and i_2 indicate whether the first, respectively the second, emitter is in the ground state g or the excited state e. The index i_{photon} indicates the number of photons in the cavity and k and k' indicate that in the kth or k'th mode of the environment a photon is present. With this basis the ansatz for the state in the reduced Hilbert space reads

$$\begin{aligned}|\varphi(t)\rangle = &\int dk \int dk' C_{gg0kk'} |g,g,0,\{k\},\{k'\}\rangle + \int dk C_{eg0k} |e,g,0,\{k\}\rangle \\ &+ \int dk C_{gg0k} |g,g,0,\{k\}\rangle + \int dk C_{gg1k} |g,g,1,\{k\}\rangle + \int dk C_{ge0k} |g,e,0,\{k\}\rangle \\ &+ C_{ge10}|g,e,1,\{0\}\rangle + C_{eg10}|e,g,1,\{0\}\rangle + C_{gg10}|g,g,1,\{0\}\rangle + C_{gg20}|g,g,2,\{0\}\rangle \\ &+ C_{ee00}|e,e,0,\{0\}\rangle + C_{eg00}|e,g,0,\{0\}\rangle + C_{ge00}|g,e,0,\{0\}\rangle + C_{gg00}|g,g,0,\{0\}\rangle.\end{aligned} \tag{10.1.4}$$

Thus, the coefficients $C_{i_1,i_2,i_{\mathrm{photon}},k,k'}(t)$ correspond to the probability amplitudes of the basis states, where the time dependence was omitted for clarity. The equations of motion for the probability amplitudes are derived from the Schrödinger equation

$$i\hbar \frac{\partial}{\partial t} |\varphi(t)\rangle = H |\varphi(t)\rangle. \tag{10.1.5}$$

The full set of equations of motion is given in App. D.1.

In this part the normalized second order correlation function for the cavity mode is considered using Eq. (2.0.3)

$$g^{(2)}(t,s) = \frac{\langle c^\dagger(t) c^\dagger(t+s) c(t+s) c(t)\rangle}{\langle c^\dagger(t) c(t)\rangle^2}. \tag{10.1.6}$$

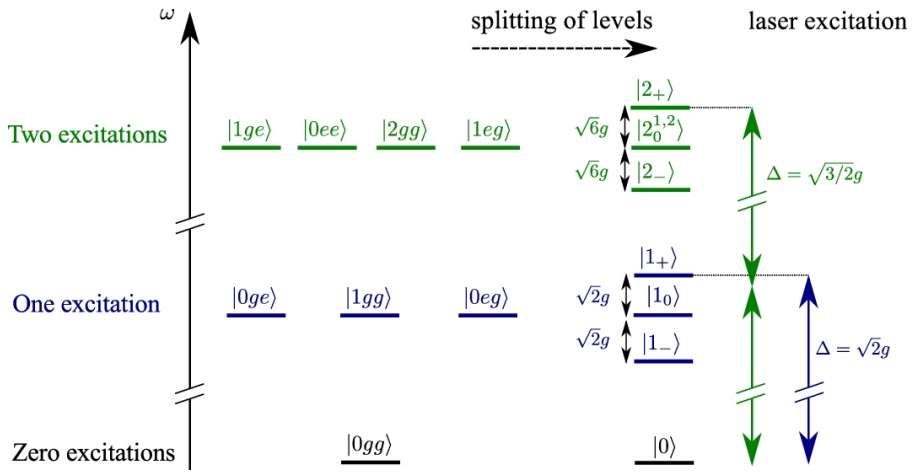

Figure 10.2.1.: Due to the electron-photon interaction the Hamiltonian is diagonal in a new basis, cf. App. D.2, when losses and pumping are neglected. This basis reveals the energy splitting that is caused by the interaction. The single excitation state $|1_+\rangle$ can be addressed by the detuning $\Delta = \sqrt{2}g$ and the two excitation state $|2_+\rangle$ is addressed by the detuning $\Delta = \sqrt{3/2}g$. This is a second order process as twice the energy from the coherent pump laser is needed for this transition. This figure is adapted from Ref. [Lu+17].

The value of interest is again the steady-state value of the correlation function without time offset, i.e. $g^{(2)}_{\text{stat}} = \lim_{t\to\infty} g^{(2)}(t,0)$. In the Schrödinger picture this reads

$$g^{(2)}(t,0) = \frac{\langle\varphi(t)|c^\dagger c^\dagger cc|\varphi(t)\rangle}{\langle\varphi(t)|c^\dagger c|\varphi(t)\rangle^2}. \tag{10.1.7}$$

The explicit version of the correlation function is given in App. D.1.

Furthermore, the entanglement between the two emitters will be of interest. This is quantified by the concurrence which is defined as [Woo98]

$$C(\rho_{AB}) = \max\{0, \sqrt{\lambda_1} - \sqrt{\lambda_2} - \sqrt{\lambda_3} - \sqrt{\lambda_4}\}. \tag{10.1.8}$$

In this equation the matrix $\rho_{AB} = \text{Tr}_{\text{photonic modes}}(\rho)$ is the reduced density matrix of the emitters. The total density matrix can be obtained from $\rho = |\varphi(t)\rangle\langle\varphi(t)|$. With this the matrix $\mathbf{M}_C = \rho_{AB}(\sigma_{y,1}\otimes\sigma_{y,2})\rho^*_{AB}(\sigma_{y,1}\otimes\sigma_{y,2})$ is computed, where $\sigma_{y,i} = i\left(|e_i\rangle\langle g_i| - |g_i\rangle\langle e_i|\right)$ is the second Pauli spin matrix. By diagonalizing the matrix $\mathbf{M}_C$, the eigenvalues λ_i are obtained which are numbered in order of decreasing absolute value.

10.2. Photon statistics of emission without feedback

Before considering the impact of feedback on the photon statistics the behavior without feedback is briefly addressed as done in Ref. [ZZC16]. In Fig. 10.2.2, the photon number and the second order correlation function are shown as a function of the detuning. Two points of interest are present. First, the case $\Delta = \sqrt{2}g$, where the photon number exhibits

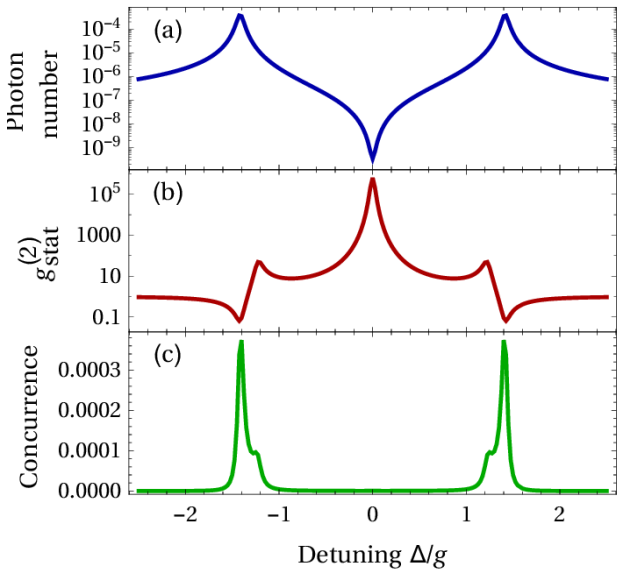

Figure 10.2.2.: (a) When considering the behavior of the photon number with respect to the detuning two peaks are observed at the resonances $\Delta = \pm\sqrt{2}g$. (b) the stationary second order correlation function shows antibunching for $\Delta = \pm\sqrt{2}g$ and bunching for $\Delta = \pm\sqrt{3/2}g$. A very high bunching is observed for $\Delta = 0$, which will not be considered in the following, as here the approximations that are made may fail. (c) In the concurrence peaks are observed for $\Delta = \pm\sqrt{2}g$ and $\Delta = \pm\sqrt{3/2}g$. This may be explained by considering Fig. 10.2.1, cf. Ref. [ZZC16].

a maximum and the correlation shows a minimum. Here, the system behaves similarly as a single photon emitter. Second, the case $\Delta = \sqrt{3/2}g$, where the correlation exhibits a maximum, i.e., strong bunching. These observations can be explained by considering the energy levels of the system. As $\omega_0 \gg g$ the energy splitting due to the interaction can be treated perturbatively. The splitting due to the external pump laser is neglected as $g \gg \Omega_{\mathrm{cav}}$. Thus the states with one and two excitations split up as shown in Fig. 10.2.1. The full expressions for the states are given in App. D.2. By tuning the laser to the resonance $\Delta = \sqrt{2}g$, the state $|1_+\rangle$ is addressed. This state contains only a single excitation so that the cavity field is antibunched. For the detuning of $\Delta = \sqrt{3/2}g$, however, the state $|2_+\rangle$ is addressed, which contains two excitations. This leads to strong bunching. Here a two photon process is necessary to excite the state with the energy $2\omega_0 + \sqrt{6}g$. Due to the small pump strength the probability for the system to be in the ground state is still very large. However, the signatures of the states with one and two excitation are clearly visible in Fig. 10.2.2.

In the following the impact of feedback on these two cases, i.e., the case with antibunching

and the case with bunching is investigated. This is done in the limit of short time delays $\tau \leq \frac{1}{\gamma}$.

10.3. Comparison with MPS evolution method

In this section the approximative method is compared with the MPS evolution introduced in Chapter 8. In order to compare the two approaches the decay rate needs to be related to the coupling to the feedback environment. From comparison of Eq. (8.2.4) and Eq. (10.1.2) the relation $G_0 = \sqrt{\frac{2\gamma_L}{\pi}}$ follows. As the approximative approach is expected to fail for high pump rates, the regime of validity of the approximative solution is estimated by comparing the photon number for both cases with increasing pump strength. This is shown in Fig. 10.3.1 for the case of antibunching with constructive and destructive interference as there the photon number is larger. A similar picture is obtained when feedback is applied in the case of bunching. For low pump strengths both solutions coincide for constructive and destructive interference, cf. Sec. 10.4. In the case of constructive interference the photon number is overestimated by the approximate solution, while it is underestimated for the case of destructive interference. With increasing pump the solutions deviate, which is in agreement with the expectation, as for higher pump strengths higher numbers of excitations become relevant. In the following, the pump strength $\Omega_{\text{cav}} = 0.035\gamma$ will be considered for the case of feedback, as the deviation is negligible for this value in all cases.

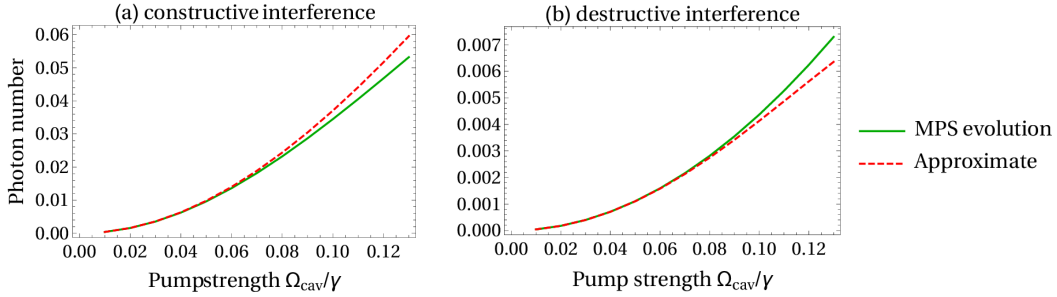

Figure 10.3.1.: Comparison of the MPS evolution and the approximative model for the dependence of the steady-state photon number with increasing pump strength Ω_{cav} in the cases of (a) constructive and (b) destructive interference. Both methods agree well for low pump strengths. With increasing pump strength the approximate model overestimates the photon number in the constructive case, while it is underestimated in the deconstructive case. The parameters are $\Delta = \delta = \sqrt{2}g$, $\tau = 0.01/\gamma$, $G_0 = \sqrt{2c\gamma/\pi}$, $\gamma_L = \gamma_R = 0.5\gamma$, and $g = 40\gamma$. For constructive interference $\omega_0 = 350 \times 100\gamma\pi$, while for destructive interference $\omega_0 = (350 + 1) \times 100\gamma\pi$.

10.4. Control of photon statistics via feedback

After introducing the behavior of the system without feedback, the impact of feedback in the system is investigated. Most of the discussion will be based on the approximative

solution, however, for some important cases the result will be compared to the one obtained from the MPS evolution. As discussed before two situations are studied. First the case, where antibunching is observed and afterwards the case of bunching. By applying feedback the signatures of the respective state can be amplified or, to a certain degree, suppressed.

10.4.1. Enhancement of antibunching

Now, the impact of feedback on the system in case of the detuning $\Delta = \sqrt{2}g$ is considered, where the state with a single excitation is addressed. In Fig. 10.4.1, the time evolution of the photon number (a) and of the second order correlation function (b) are considered in the regime of short time delays. For this choice of feedback, the photon number is increased, while at the same time bunching is increased, when comparing this to the case without feedback. As reference the non-feedback case is shown. There, the parameters are chosen such that the dynamics in the interval $[0, \tau)$ coincide for the cases with and without feedback. Note, that for the second order correlation function the time evolution is shown for the first time argument, cf. Eq. (10.1.7). This only illustrates that the steady state is reached, as the transient dynamics of the correlation function for the first time argument has, to the knowledge of the author, no straightforwards interpretation.

In Fig. 10.4.1 also the evolution computed via the MPS evolution is shown, which coincides well for photon number and second order correlation function.

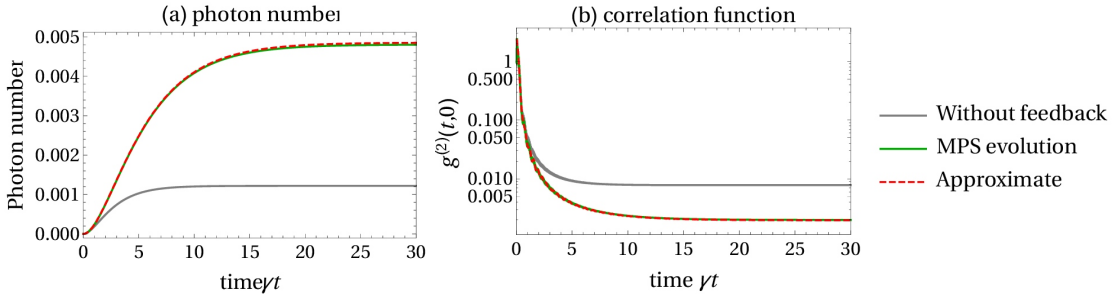

Figure 10.4.1.: The time dynamics of (a) the photon number and (b) the second order correlation function is shown for the case when the system without feedback shows antibunching. For comparison the solution obtained from the MPS evolution method (solid) and the approximate solution (dashed) are shown. For the parameters chosen here, the photon number is increased when antibunching is increased at the same time (green/red). For reference the case without feedback is shown, where the dynamics coincide in the time interval until τ. The parameters used for this plot are $\Delta = \delta = \sqrt{2}g$, $\tau = 0.01/\gamma$, $G_0 = \sqrt{2c\gamma/\pi}$, $\gamma_L = \gamma_R = 0.5\gamma$, $g = 40\gamma$, $\Omega_{\text{cav}} = 0.035\gamma$, and $\omega_0 = 350 \times 100\gamma\pi$. For the MPS evolution method the discretization $\tau/\Delta t = 10$ is used. In case of the approximate solution 1500 momentum values are used with the discretization $\Delta k/g = \frac{1}{80\pi c_0}$.

To gain further insight into this, the behavior of the steady state values as a function of the delay time is shown in the case of short delay times. Fig. 10.4.2 shows a periodicity of $\omega_0\tau$. This corresponds to the change of the phase with which the field is coupled back

into the system. This shows, that antibunching is enhanced when feedback is tuned to constructive interference, i.e. $\omega_0\tau = n2\pi$, $n = 1, 2, ...$ For the case of destructive interference, when $\omega_0\tau = n2\pi + \pi$, $n = 0, 1, 2, ...,$ antibunching is decreased. In Fig. 10.4.2(c) the entanglement between the two emitters is shown as well. Together with the photon number also the entanglement reaches a maximum in the case of constructive interference. As this entanglement is very small due to the low pump rate and the, in comparison to the pump rate, high losses it cannot be exploited for quantum computing. However, it serves as an indicator for the non-classical state. For applications of entanglement other schemes exist to produce higher entanglement [Hor+09; Cla+03]. Antibunched light may serve for other purposes as discussed in Part II.

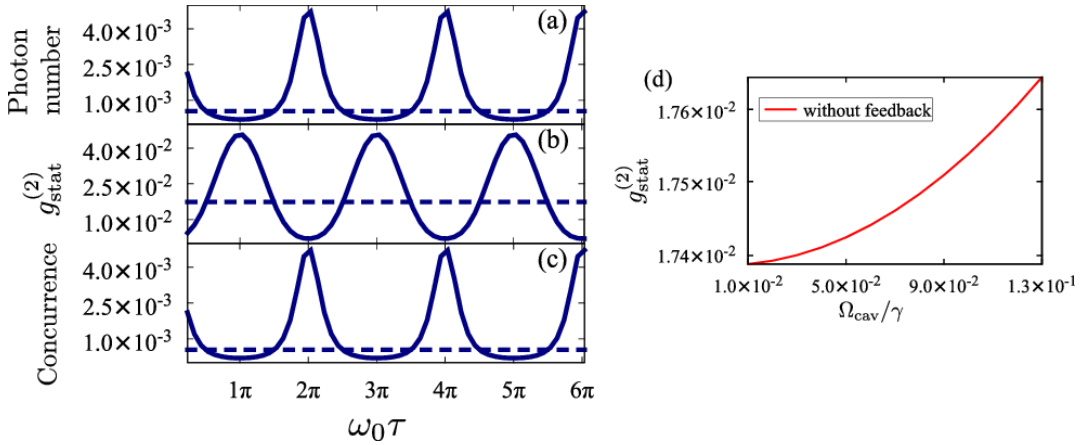

Figure 10.4.2.: The behavior of (a) the photon number, (b) the second order correlation function, and (c) the concurrence as a function of the delay time. The solid line corresponds to the case with feedback. For reference the case without feedback is shown as a dashed line. For feedback the values oscillate with the feedback time. (d) With increasing pump strength, the second order correlation function in the steady state stays nearly constant. By applying feedback, this changes drastically so that the photon number increases while antibunching is also increased. The parameters for these plot are $\omega_0 = 1.1 \times 10^5\gamma$, $g = 40\gamma$, $\epsilon = 0.035\gamma$, and $G_0 = \sqrt{2c\gamma/\pi}$. These figures are adapted from Ref. [Lu+17].

In Fig. 10.4.2(d) the behavior of the stationary second order correlation function for increasing pump strength in the case without feedback is shown. The value of the second order correlation increases slightly with increasing pump strength, i.e., with increasing photon number. With feedback it is possible to increase antibunching while simultaneously increasing the intensity.

10.4.2. Enhancement of bunching

Having considered the case without feedback in which the light is antibunched, now the case with bunching, i.e. $\Delta = \sqrt{1.5}g$, is studied. Here, the state with two excitations $2_+\rangle$ is addressed by pumping at the resonance of the two photon process depicted in Fig. 10.2.1. In Fig. 10.4.3 the convergence of the second order correlation function to the

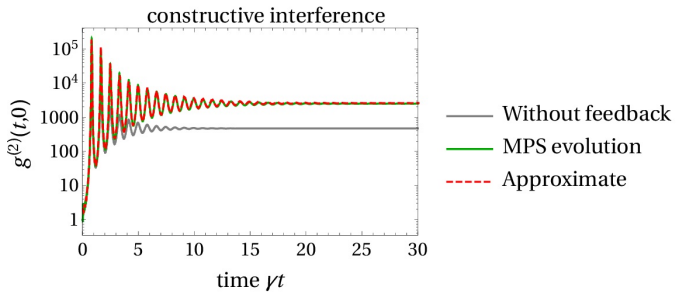

Figure 10.4.3.: The second order correlation function Eq. (10.1.7) converges to a stationary value that is increased with respect to the case without feedback (gray) when feedback is applied (green, red). The dynamcis of the approximate method (dashed) coincides well with the solution from the MPS evolution. The parameters used for this plot are $\Delta = \delta = \sqrt{3/2}g$, $\tau = 0.01/\gamma$, $G_0 = \sqrt{2c\gamma/\pi}$, $\gamma_L = \gamma_R = 0.5\gamma$, $g = 40\gamma$, $\Omega_{\text{cav}} = 0.035\gamma$, and $\omega_0 = 350 \times 100\gamma\pi$.

steady state is shown for the case of constructive interference. Then, the field exhibits a much higher bunching. In this case, the approximation is also in good agreement with the MPS evolution.

Fig. 10.4.4(b), shows that bunching may be controlled in the same fashion as antibunching. For the case of constructive interference, $\omega_0\tau = n2\pi$, now the maximum in the bunching is observed, when the photon number maximal, cf. Fig. 10.4.4(a). In this case the entanglement is controlled as well by the feedback time and reaches the maximum for the case of constructive interference. Thus, bunching, observed, e.g., in systems exhibiting superradiance [Jah+16], can be strongly increased when feedback is present. The bunching can be increased while at the same time the photon output is increased.

10.5. Entanglement and photon statistics

As mentioned before, the entanglement between the two emitters inside the cavity is controlled by the feedback time and in particular the feedback phase. A relationship between the entanglement and the photon statistics is established in Ref. [ZZC16]. Depending on the transition that is pumped, either the single- or two-excitation state is addressed, cf. Fig. 10.2.1. For the detuning $\Delta = \sqrt{2}g$ the $|1_+\rangle$-state is pumped. Due to the strong energy splitting induced by the electron-photon interaction, this transition gives the main contribution after the ground state. Thus, it is very unlikely that more than one photon is present, which manifests itself as antibunching. The single photon state is given in App. D.2. the system state contains the Bell state

$$\psi_+ = \frac{1}{\sqrt{2}} \left(|g, e\rangle_e + |e, g\rangle_e \right), \tag{10.5.1}$$

where the emitters are in an entangled state as indicated by the concurrence. This established the connection between entanglement and antibunching in the case of $\Delta = \sqrt{2}g$. Applying feedback to the system enhances this entanglement between the two emitters and does not only act on the photon field.

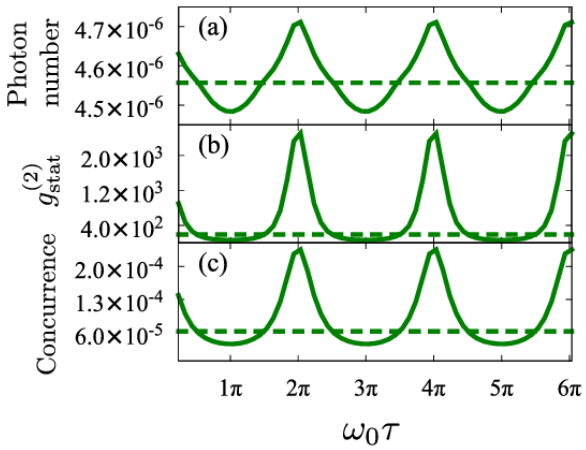

Figure 10.4.4.: Impact of short feedback (solid) on the system in the case of bunching (detuning $\Delta = \sqrt{1.5}g$). We consider (a) the photon number, (b) the second order correlation function and (c) the concurrence. All values oscillate due to the alternating constructive and destructive interference of the cavity field with its former output. As reference, the case without feedback is shown as dashed line. The parameters are taken as $\omega_0 = 1.1 \times 10^5\gamma$, $g = 40\gamma$, $\epsilon = 0.035\gamma$, and $G_0 = \sqrt{\frac{2c\gamma}{\pi}}$. This figure is adapted from Ref. [Lu+17].

For the case of bunching, i.e. $\Delta = \sqrt{1.5}g$, this is analogously true for the $|2_+\rangle$-state, in which two excitations are present. However, the entanglement present in this state is more complex, cf. App. D.2. There, entanglement and bunching are increased simultaneously.

10.6. Conclusion

To summarize, this chapter showed an example of how photon statistics may be manipulated using self-feedback. An approximative model in the Schrödinger picture was introduced, which coincides well with the numerical solution obtained by the MPS evolution presented in Chapter 8 for low pump rates. Using feedback on the cavity mode coupled to two emitters, an additional degree of freedom which can be used to control the cavity photon statistics is introduced. This allows to decrease or increase the non-classical signatures in the second order correlation function while at the same time increasing the photon number. This cannot be achieved by simply increasing the input power as this does not alter the antibunching or bunching signatures significantly. The connection between the entanglement and the second order correlation function established by other authors is still valid if self-feedback is applied to the system.

After investigating the impact of feedback on the intracavity field in a stationary setup, in the following chapter feedback will be considered when acting on a pulsed two level system. Of particular interest is the photon distribution in the emitted field which may be controlled using feedback.

11. Control of photon emission from a two level emitter

In the last chapter the impact of feedback on the photon statistics of the two emitter Tavis-Cummings model was considered. There the non-classical light features of the cavity mode could be controlled by adjusting the feedback time. In this chapter once more the impact of feedback on the photon statistics of a specific system is investigated. In contrast to the previous chapter, however, the interest lies on manipulating the emission statistics of a single two level emitter. In the introduction of Part II several sources of quantum light were discussed. A two level emitter is an ideal single photon emitter as it can only emit a single quantum of light when in the excited state. Once a two level emitter is realize experimentally, e.g. by considering certain energy of an atom [Dar+05] or by a semiconductor nanostructure [Sch+15], a deterministic preparation of the excited state is achieved. Often this is realized by pumping the emitter with a π-pulse, which induces half a period of a Rabi-oscillation in the emitter bringing it from the ground state to the excited state. When decaying afterwards a single photon is emitted.

In experiment, however, the exciting pulse has a finite length. Then, even though the lifetime of the emitter is much longer than the pulse width, there is a nonzero probability that the emitter emits a photon during its excitation by the pulse and is excited again so it may emit a second photon. Then in total two photons are emitted. In a recent proposal this effect was used to generate two-photon emission from a single two level emitter using excitations via a 2π-pulse [Fis+17].

11.1. Modeling the emission of pulsed systems with feedback

The two level system pumped with a pulse, cf. Fig. 11.1.1, is modeled via the Hamiltonian Eq. (8.3.1) but instead of a constant driving amplitude it becomes time dependent

$$H_{\text{sys,pulse}} = \hbar\omega_{\text{TLS}}\sigma_+\sigma_- + \hbar\Omega_{\text{TLS}}(t)\left(e^{-i\omega_{\text{L}}t}\sigma_+ + e^{i\omega_{\text{L}}t}\sigma_-\right). \tag{11.1.1}$$

As before, σ_+ and σ_- are the flip operators inducing a transition from ground to excited state and vice versa. In the following a Gaussian shaped pulse will be assumed in the form

$$\Omega_{\text{TLS}}(t) = \Omega_{\text{TLS},0}e^{-\frac{(t-t_{\text{m}})^2}{2t_{\text{w}}^2}}, \tag{11.1.2}$$

where t_{m} is the time at which the pulse is at its maximum and t_{w} is related to the pulse width. The pulse area is defined as

$$A_{\text{pulse}} = \int_{-\infty}^{\infty} dt\Omega_{\text{TLS}}(t) = \Omega_{\text{TLS},0}t_{\text{w}}\sqrt{2\pi}. \tag{11.1.3}$$

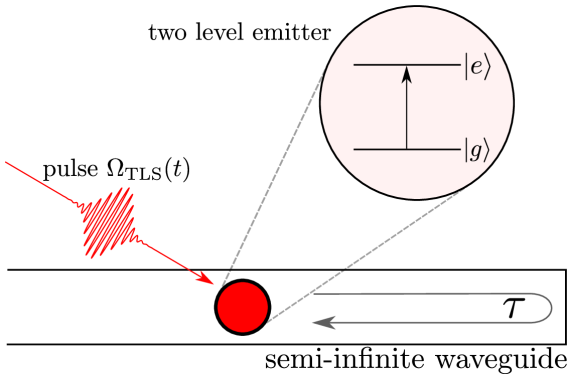

Figure 11.1.1.: A two level system subject to excitation by a Gaussian laser pulse with envelope $\Omega_{\mathrm{TLS}}(t)$ is studied. The emitter is placed inside a semi-infinite waveguide, which induces a feedback with delay time τ.

For a π-pulse this integral has to be $\pi/2$ and for a 2π pulse this integral needs to equal π in the notation used here. This also determines the relation between $\Omega_{\mathrm{cav},0}$ and t_{w}. The time t_{m} is chosen such that the driving amplitude at the beginning is negligible.

The emitter in the system Hamiltonian Eq. (11.1.1) is assumed to be subject to feedback. The procedure is in principle the same as for the Jaynes-Cummings-Hamiltonian in Chapter 8. In Sec. 8.2.3 the MPS evolution method was introduced for time-dependent Hamiltonians with second order evolution operators. There are two different time-scales in the pulsed setup. On the one hand the excitation by the pulse, which is fast, and on the other hand the lifetime of the ensemble of two level emitters, which is long. Thus time needs to be discretized sufficiently fine to resolve the pulse but also enough time-steps need to be made in order to reach the state where the emitter is decayed. This is only solved efficiently by the second order evolution method. With this the time evolution of the pumped emitter may be performed as discussed before.

However, the observable of interest is the probability for the number of photons that are emitted. In Chapter 2 the proportionality between the internal and the emitted field used throughout most of this thesis was discussed. In the case at hand this proportionality will fail in the following. This may be seen when considering the direct mapping of the two level states to a single external mode. By just assuming that $|g\rangle$ corresponds to no emitted photons and $|e\rangle$ corresponds to a single emitted photon, which is assumed in some cases, cf. Ref. [Sch+15], the case that two photons are emitted does not occur.

In Ref. [Fis+17] the probabilities were determined from a trajectory approach. As here the MPS evolution is considered, no trajectories are immediately available. However, the full bath dynamics are taken into account so that the emission probabilities are evaluated from the bath modes. As the overall probability is of interest, all bath modes need to be taken into account. The starting point to evaluate the probabilities are the correlation functions. Note, that while the first order correlation function, which corresponds to the intensity, includes all photon events, the second order correlation function includes only events with at least two photon, and the third order correlation includes only events with at least three photons etc. Thus, the integral over all correlation events needs to be computed. The output field from the two level system is $b(t)$,as introduced in Eq. (8.2.11).

The integrated first order correlation function corresponds to the output intensity and includes all photon events

$$I_1 = \int_{-\infty}^{\infty} dt \langle b^\dagger(t) b(t) \rangle \approx \frac{1}{\Delta t} \sum_{k=-l}^{M} \langle \Delta B^\dagger(t_k) \Delta B(t_k) \rangle. \tag{11.1.4}$$

Here, the continuous field is approximated by the field given by the photon bin operators. For the discretized time the sum corresponds to the integral. As the initial state of the environment is assumed to be a vacuum state there is no output before $t_0 - \tau$. Here, τ is the feedback time and $l = \tau/\Delta t$. The maximal value M has to be chosen large enough that $\langle \Delta B^\dagger(t_k) \Delta B(t_k) \rangle \approx 0$ for $k > M$. To compute I_1 at first the time evolution of the system is computed the way described in Sec. 8.2.4 until all excitation is decayed to the environment and afterwards the correlation, computed as described in Sec. 8.2.6, are summed up. The cumulative second order correlation reads

$$\begin{aligned} I_2 &= \int_{-\infty}^{\infty} \int_{-\infty}^{\infty} dt_1 d_2 \langle b^\dagger(t_1) b^\dagger(t_2) b^\dagger(t_2) b^\dagger(t_1) \rangle \\ &\approx \frac{1}{\Delta t^2} \sum_{k=-l}^{M} \sum_{j=-l}^{M} \langle \Delta B^\dagger(t_k) \Delta B^\dagger(t_j) \Delta B(t_j) \Delta B(t_k) \rangle. \end{aligned} \tag{11.1.5}$$

For the third order correlation this is

$$\begin{aligned} I_3 &= \int_{-\infty}^{\infty} \int_{-\infty}^{\infty} \int_{-\infty}^{\infty} dt_1 dt_2 dt_3 \langle b^\dagger(t_1) b^\dagger(t_2) b^\dagger(t_3) b(t_3) b(t_2) b(t_1) \rangle \\ &\approx \frac{1}{\Delta t^3} \sum_{k=-l}^{M} \sum_{j=-l}^{M} \sum_{p=-l}^{M} \langle \Delta B^\dagger(t_k) \Delta B^\dagger(t_j) \Delta B^\dagger(t_p) \Delta B(t_p) \Delta B(t_j) \Delta B(t_k) \rangle. \end{aligned} \tag{11.1.6}$$

The second order correlation can be measured by a Hanbury Brown-Twiss setup as discussed in Chapter 2. In the experimental setup, however, the intensity of the second order correlation is smaller than the one of the first order correlation by a factor of four. To measure the first order correlation all clicks at a single photon detector are measured. When assuming an ideal photon detector all events are taken into account. However, for the second order correlation it becomes clear form Fig. 2.0.1 that the intensity is divided into two channels. Furthermore, only the two photon events contribute, in which the photon arrives first at detector 1. In total this gives a factor of four. When considering a similar experimental setup for the third order correlation [Isk+11], analogous considerations need to be taken into account. For the theoretical evaluation, however, the correlations emitted from the two level system are evaluated directly.

In order to assign a probability distribution to the values of the correlation functions, the cumulative correlations are attributed to the correlations of a single collective mode. For a single photon mode the correlations are related to the photon probabilities via

$$\langle (c^\dagger c)^m \rangle = \sum_{n=0}^{\infty} \frac{n!}{(n-m)!} p(n). \tag{11.1.7}$$

In the following it will be assumed that the probabilities for single and two photon emission will be most significant. This is checked by also including the third order correlation,

which will be small in the cases considered here. The photon probability distribution is then obtained from

$$p_1 = I_1 - I_2 + \frac{1}{2} I_3 \tag{11.1.8a}$$

$$p_2 = \frac{I_2 - I_3}{2} \tag{11.1.8b}$$

$$p_3 = \frac{1}{6} I_3. \tag{11.1.8c}$$

The zero photon probability is obtained from the relation $p_0 = 1 - \sum_{i=1}^{\infty} p_i$

11.1.1. Numerical evaluation

As the second and third order correlations include two and three time integrals, respectively, their evaluation is numerically intensive. In order to keep the numerical evaluation tractable additional considerations are necessary. First, the symmetry of the correlation functions under exchange of the time arguments is used. Since $\left[\Delta B(t_k), \Delta B^\dagger(t_j)\right] = 0, k \neq j$, only about half of the values need to be computed for the second order correlation. For the third order correlation the effort is even reduced by roughly a factor of six. For the second order correlation terms with $k \neq j$ contribute once and terms with $k = j$ contribute twice. For the third order correlation terms with k, j, and p all different occur six times, terms with twice the same time occur three times and terms with $k = j = p$ occur once.

The deviation of the norm of the state Eq. (8.2.48) needs to be kept small in order to keep the errors in the expectation values small. To do this the time step Δt needs to be sufficiently small. This is tested by making the time step smaller until the results are converged. The integrals approximated by the sums in Eqs. (11.1.4), (11.1.4), and (11.1.4) are also computed by a discretization of the time. However, the discretization in the integrals may be chosen coarser than the discretization of the time evolution for convergence of the integral. Then, in each integration a factor $\Delta t_i / \Delta t$ needs to be introduced, where Δt_i is the time discretization in t_i.

In the next section this approach will be checked for plausibility in the case without feedback.

11.2. Behavior in the non-feedback case

Before investigating the impact of feedback on the photon emission the non-feedback case as studied in Ref. [Fis+17] is discussed and reproduced to give an introduction and to check the approach presented in the last section. The non-feedback case can be simulated by the same method as the feedback case when setting $\gamma_L = 2\gamma$ and $\gamma_R = 0$, cf. Eq. (8.2.11). Then, no coupling back into the emitter after the delay time τ is possible. First, the case where the two level system is pumped by a π-pulse is considered. Without any losses the π-pulse performs half a period of a Rabi oscillation so that the emitter is in the excited state. When a finite decay time is taken into account the shorter the decay time in comparison to the pulse length, the better the approximation. In Fig. 11.2.1(a) the time dynamics of the excited state density and the pulse are shown. The probability that the system is excited comes close to unity and decays afterwards slowly towards zero. The

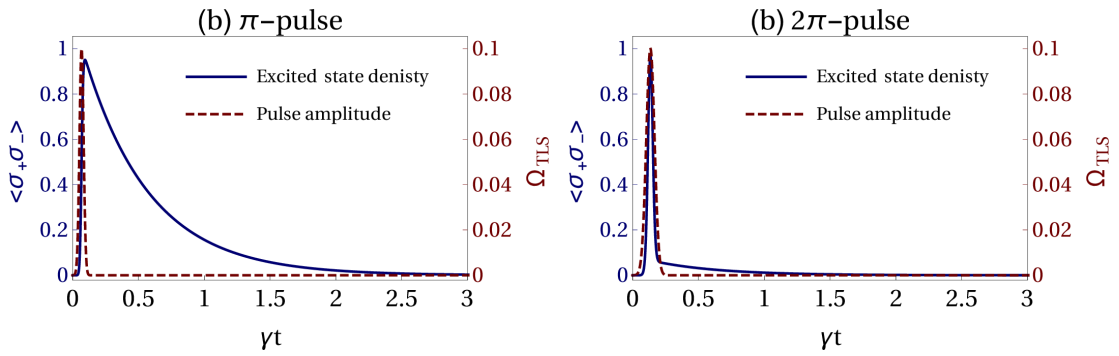

Figure 11.2.1.: Time evolution of the excited state density $\langle\sigma_+\sigma_-\rangle$ and the pump strength Ω_{TLS} for the case of (a) pumping by a π-pulse and (b) pumping by a 2π-pulse. For this figure, the parameters $\gamma_L = 2\gamma$, $\gamma_R = 0$, and $\Omega_{\mathrm{TLS}}/\gamma = 400$ are used. The pulse width t_{w} is chosen according to Eq. (11.1.3) so that a π- or a 2π-pulse is achieved.

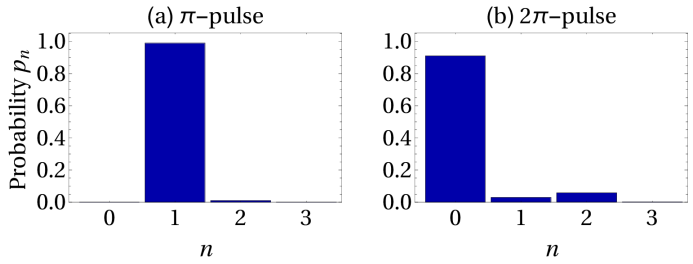

Figure 11.2.2.: Photon probability distributions for the cases of (a) π-pulse and (b) 2π-pulse shown in Fig. 11.2.1.

time integration is performed over a much longer time than shown in Fig. 11.2.1(a), until the excited state density is zero. In Fig. 11.2.2(a) the photon probability distribution is shown. As expected the main contribution is a single photon state, while only a very small but nonzero two photon probability is observed. The two photon contribution corresponds to the process discussed in the introduction.

When a 2π-pulse is applied to the system, cf. Fig. 11.2.1(b), the emitter is most likely in the ground state after the pulse. This is also expected as the 2π-pulse performs a full Rabi oscillation. Only a small excitation probability remains after the pulse, which slowly decays. The probability distribution of the emitted photons is shown in Fig. 11.2.2(b). Most likely no photon is emitted at all, which corresponds to a full cycle in the Rabi oscillation. However, the two photon probability is larger than the single photon probability. Thus, more often two photons are emitted from this setup than a single photon.

In the following the photon probabilities when the emitter is subject to feedback will be considered.

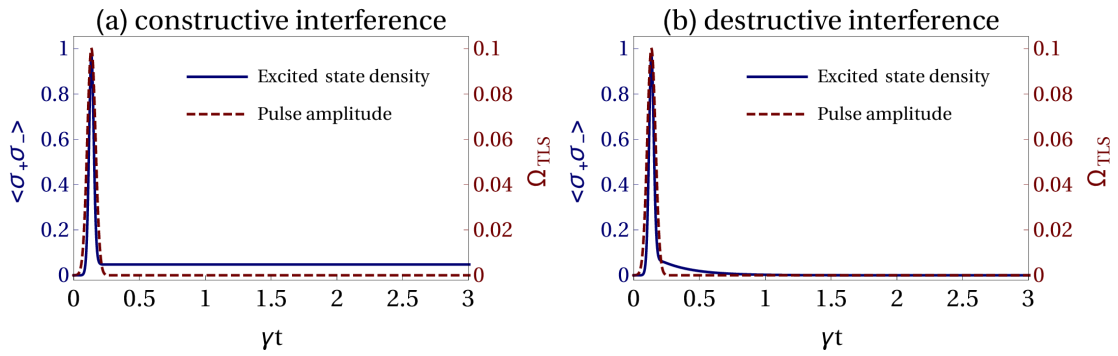

Figure 11.3.1.: Time evolution of the excited state density $\langle\sigma_+\sigma_-\rangle$ and the pump strength Ω_{TLS} for the case of (a) constructive and (b) destructive interference. In the case of constructive interference the main output consists of single photon state, while for destructive interference the mainly two photons are emitted. For this figure, the parameters $\gamma_L = \gamma_R = \gamma$, $\Omega_{\mathrm{TLS}}/\gamma = 400$, and $\gamma\tau = 0.05$ are used. For constructive feedback $\phi = 0$ and for destructive $\phi = 1$.

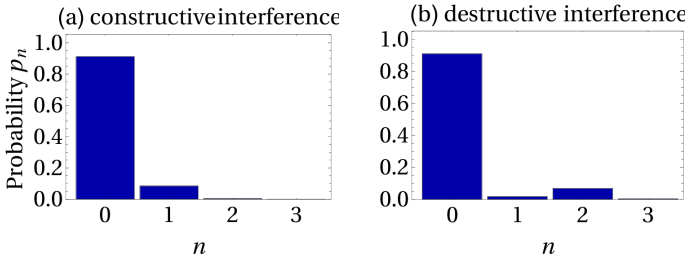

Figure 11.3.2.: Photon probability distributions for the cases of (a)constructive and (b) deconstructive interference shown in Fig. 11.3.1.

11.3. Enhanced two photon emission with feedback

Now the impact of feedback on the case with the 2π-pulse is investigated as this will turn out to increase the two photon probability. As in Chapter 10, also the cases of constructive and destructive interference are of major interest. For constructive interference $\phi = \omega_{\mathrm{L}}\tau = 2\pi n$ with an integer n and for destructive interference $\phi = \omega_{\mathrm{L}}\tau = 2\pi n + \pi$ with an integer n. The value of ω_{L} enters the equations only via the factor $e^{i\phi}$ when the rotating wave approximation is employed. Thus, only the interval $\phi \in [0, 2\pi)$ is considered. The feedback time enters not only through this factor. In Fig. 11.3.1(a) constructive feedback is applied. Here, the Rabi oscillation is performed in most cases but a finite excitation probability is left due to constructive interference. Then, there in most cases no photon is emitted but there is also a significant single photon probability of about 10%. When deconstructive feedback is applied the excited state density decays fully, cf. Fig. 11.3.1(b). In this case, the probability distribution resembles the one for the case without feedback, cf. Fig. 11.2.2(b), however the ratio $r = p_2/p_1$ is increased from $r_{\mathrm{nofb}} \approx 1.94$ to $r_{\mathrm{fb}} \approx 3.86$. As discussed in Ref. [Fis+17] this ratio can also be increased

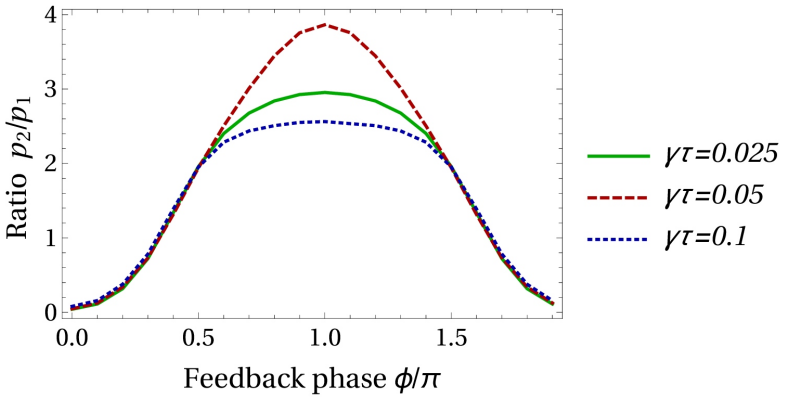

Figure 11.3.3.: Behavior of the ratio p_2/p_1 as a function of the feedback phase and for different feedback times. There is a maximum for this ratio near $\gamma\tau = 0.05$ as for shorter and longer feedback times this ratio decreases. The parameters $\gamma_L = \gamma_R = \gamma$ and $\Omega_{\mathrm{TLS}}/\gamma = 400$ are not changed.

by choosing a higher value for $t_{\mathrm{w}}\gamma$. In Fig. 11.2.2(b) and Fig. 11.3.2(b) the value is $t_{\mathrm{w}}\gamma = 0.0125$. Increasing this value for the case without feedback to $t_{\mathrm{w}}\gamma = 0.025$ increases the two photon probability to $r = 2.27$. However, the three photon probability for the case without feedback is 2.1 times as high as in the case with feedback. Thus, feedback enables a higher two photon probability while increasing the three photon probability not as strongly.

In Fig. 11.3.3 the enhancement of the two photon probability p_2 is shown as a function of the feedback phase. The achievable maximum depends on the feedback time. Interestingly the maximum ratio is achieved for a small but nonzero time τ.

11.4. Conclusion

In this chapter the impact of feedback on the probability distribution of emitted photons was studied. The case without feedback shows a finite two photon probability for a 2π-pulse in certain parameter regimes due to the finite decay time. By applying feedback the ratio between the two and single photon probability is increased while increasing the three photon probability only marginally. The maximal ratio between two and single photon probability is achieved for a short but nonzero delay time.

12. Conclusion and outlook

In this thesis the optical control of nanoscale systems is considered. The thesis is divided into three parts according to three different control methods. In the first part, mechanical modes in optomechanical or semiconductor systems are steered to exhibit certain dynamics by a coherent optical laser. This is used to investigate the analogous behavior of the mechanical mode for optomechanical coupling and the coupling of light field and phonon mode via semiconductor quantum dots. There bistabilities, lasing, and enhancement of damping are observed using a semiclassical approach. When considering phonon lasing with semiconductor quantum dots with a fully quantum mechanical theory collective phonon processes can be distinguished from individual processes. Furthermore, higher order processes such as two phonon generation are explained using this approach. Future investigations might include the regime of an intermediate number of emitters using theoretical schemes that exploit symmetries in the systems. Another interesting direction for future studies is the investigation of different regimes than the lasing regime with fully quantum mechanical models to study enhanced damping and bistable behavior from a quantum mechanical perspective.

Instead of a coherent light source the second part deals with non-classical light, where the possibilities of manipulating the output statistics of a quantum optical system by driving with non-classical light are studied. Here, a quantum optical system is driven via a dissipative channel with antibunched light. Due to the dissipative nature of the coupling channel the non-classical signatures are destroyed for lower order correlations, while higher order correlations still show the sub-Poissonian photon correlations. This shows that driving with non-classical light does not always just imprint the source statistics on the target but introduces more complex light statistics. The investigation performed here includes emitters as simple two level systems. Future investigations could study the behavior of the photon statistics when more realistic models for quantum emitters are employed, e.g., for semiconductor quantum dots.

In the third part, the control of quantum systems via time-delayed coherent feedback is considered. At first the method using the time evolution of matrix product states in the framework of the quantum stochastic Schrödinger equation is presented. This method was initially proposed elsewhere [PZ16] to deal with the complexities of quantum coherent feedback. In this thesis the approach is extended to higher order evolution operators to facilitate the numerical evaluation and is adapted for the simulation of systems with a time-dependent Hamiltonian using sparse matrices. This method allows to investigate the impact of feedback on more complex systems.

Afterwards this method is used in comparison with an approximate model in the Schrödinger picture to simulate the impact of coherent feedback on the steady state behavior of a cavity quantum electrodynamical setup. By applying feedback signatures of single- and two-photon processes in the second order correlation function are increased. Thus, in certain regimes antibunching and bunching of the light field are amplified. As

the observed photon numbers are very small the investigation of the regime of higher excitations can be interesting. As the impact of coherent feedback in the few photon regime is accessible only recently, e.g., three photon processes could be addressed and studied regarding their signatures and their response to feedback.

A two level emitter excited by a laser pulse exhibits single- or two-photon emission depending on the pulse area. By placing the emitter inside a waveguide which introduces a delayed self-feedback the emission properties can be controlled via the delay time. By using destructive feedback two photon emission may be increased. The increase is maximal for a short but finite delay time. A possible direction for future studies is to investigate the possibilities of emitting a certain number of photons with a high probability. Feedback is a promising tool to achieve this.

In summary, this theses presents multiple optical approaches to steer the emission statistics of nanosystems.

Acknowledgments

At this point I would like thank the people who made this thesis possible. First, I would like to thank my supervisor Prof. Dr. Andreas Knorr who offered me the opportunity to work on interesting projects during my PhD, for which he also provided the funding. I thank Priv.-Doz. Dr. Uwe Bandelow for making himself available as second advisor and Prof. Dr. Michael Lehmann for chairing the board of referees.

For their advice and guidance I am grateful to Prof. Dr. Andreas Knorr as well as Dr. Julia Kabuß and Dr. Alexander Carmele. In particular Dr. Julia Kabuß and Dr. Alexander Carmele played a crucial role in the projects that led to this thesis. I thank Prof. Dr. Weng Chow for initiating the project of comparing the optomechanical system with the semiconductor system. Furthermore, my thanks go to my office mate Leon Droenner for the fruitful collaborations and an enjoyable atmosphere. In this context I am also grateful to Yiping Lu and Shahabedin Chatraee Azizabadi. I had the opportunity to work on interesting projects with both of them. Moreover, I thank Julia Kabuss, Alexander Carmele, Sven Hein and Manuel Kraft who were also part of the SFB 910 which entailed many discussions not only about quantum feedback.

For thorough reading of parts of this thesis and valuable comments I thank Leon Droenner, Michael Gegg, Manuel Kraft, Sandra Kuhn, and Judith Specht.

I also thank my former office mates Markus Krecik, Michael Gegg, and Torben Winzer for discussions and a pleasant working place. These thanks expand to all members of the AG Knorr and our lunch group for establishing a good working environment.

This thesis was made possible by the Deutsche Forschungsgemeinschaft in the framework of the SFB 910. Furthermore, the School of Nanophotonics as part of the SFB 787 enabled several conference visits which Prof. Dr. Andreas Knorr kindly supported.

Finally, I would like to thank my parents and my whole family as well as Tine for their constant support.

Part IV.

Appendices

A. Details for the part phonons as an analogue of optomechanics

In this appendix some of the computations regarding the analogy between optomechanics and the electron phonon coupling are shown in greater detail.

A.1. Effective system

For a better understanding of the processes involed in phonon lasing, an effective Hamiltonian for the many emitter case is derived in analogy to the single emitter case is Refs. [Kab+12; KCK13].

By applying the unitary transformation

$$H_{\mathrm{RF}} = UHU^\dagger - i\hbar U\partial_t U^\dagger \tag{A.1.1}$$

with $U = e^{\frac{i}{\hbar}\xi t}$ and $\xi = \hbar\omega_{\mathrm{L}}\hat{\mathbf{p}}^\dagger\hat{\mathbf{p}}$ Hamiltonian is transformed into a rotating frame. This reads

$$H_{\mathrm{RF}} = \underbrace{\hbar\Omega b^\dagger b - \hbar\Delta\hat{\mathbf{p}}^\dagger\hat{\mathbf{p}}}_{=H_0} + \underbrace{\hbar g\hat{\mathbf{p}}^\dagger\hat{\mathbf{p}}\left(b+b^\dagger\right) + i\hbar\mathbf{E}\left(\hat{\mathbf{p}}^\dagger - \hat{\mathbf{p}}\right)}_{=H_{\mathrm{I}}}, \tag{A.1.2}$$

where, $\Delta = \omega_{\mathrm{L}} - \omega$. A second unitary transformation eliminates first order processes by choosing $S = \boldsymbol{\alpha}\hat{\mathbf{p}} + \beta\hat{\mathbf{p}}^\dagger\hat{\mathbf{p}}b + H.c.$. By evaluating this in second order, the transformation reads

$$\begin{aligned} H_{\mathrm{eff}} &= e^{iS}He^{-iS} \approx H_0 + H_{\mathrm{I}} + [iS, H_0 + H_{\mathrm{I}}] + \frac{1}{2}[iS,[iS,H_0]] \\ &= H_0 + \frac{1}{2}[iS, H_{\mathrm{I}}]. \end{aligned} \tag{A.1.3}$$

Taking $\boldsymbol{\alpha} = -\frac{\mathbf{E}}{\Delta}$ and $\beta = i\frac{g}{\Omega}$, the effective Hamiltonian can be evaluated as

$$\begin{aligned} H_{\mathrm{eff}} = \hbar\Omega b^\dagger b - \hbar\Delta\hat{\mathbf{p}}^\dagger\hat{\mathbf{p}} + \frac{\hbar}{\Delta}W - \frac{\hbar g^2}{\Omega}(\hat{\mathbf{p}}^\dagger\hat{\mathbf{p}})^2 + \frac{i\hbar g\mathbf{E}}{2}\left(\frac{1}{\Delta}+\frac{1}{\Omega}\right) \\ \times\left(\hat{\mathbf{p}}^\dagger b^\dagger - \hat{\mathbf{p}}b\right) + i\hbar\frac{g\mathbf{E}}{2}\left(\frac{1}{\Delta}-\frac{1}{\Omega}\right)\left(\hat{\mathbf{p}}^\dagger b - \hat{\mathbf{p}}b^\dagger\right). \end{aligned} \tag{A.1.4}$$

Here, the freedom of choosing the energy scale is used. The first two terms are just the noninteracting parts of the LF and HF component, respectively. These are the same as in the initial Hamiltonian. The third term is a constant energy shift $W_{\mathrm{OM}} = \mathbf{E}^2$ for the OM system and will be neglected. For the SC system this is the self-quenching discussed in Sec. 4.3 and reads $W_{\mathrm{SC}} = -2\sum_{i=1}^{N_{\mathrm{QD}}} E_i^2\hat{p}_i^\dagger\hat{p}_i$. The fourth term is the dispersive shift depending on the number of excitations in the system and the coupling strengths. The fifth term describes the processes relevant for lasing, while the last term describes the ones relevant in the excitation scenario used for increased damping.

A.2. Analytical approximation of the effective damping rate

In Sec. 4.4 analytical formulas for the effective damping rate are presented. The OM one is taken from [Gen+08] and the SC formula is derived in analogy to this. From the linearized equations of motion a susceptibility to some external force F is derived using the Fourier transform. With this Eq. (4.1.3a) reads $\dot{B} = -(i\Omega+\kappa)B - iNgU + iF/\sqrt{2}$. By introducing the reals variables $q = \frac{B+B^*}{\sqrt{2}}$, $p = \frac{B-B^*}{\sqrt{2}i}$, $X = \frac{P+P^*}{\sqrt{2}}$, and $Y = \frac{P-P^*}{\sqrt{2}i}$, the deviation from the steady state q_s is defines as $\delta q(t) = q(t) - q_s$. The Fourier transformation of the linearized equations leads to a set of algebraic equations, which reads

$$-i\bar{\omega}\mathcal{F}_q = \Omega\mathcal{F}_p - \kappa\mathcal{F}_q \tag{A.2.1a}$$
$$-i\bar{\omega}\mathcal{F}_p = -\Omega\mathcal{F}_q - \kappa\mathcal{F}_p - g_X\mathcal{F}_X - g_Y\mathcal{F}_Y + \mathcal{F}_F \tag{A.2.1b}$$
$$-i\bar{\omega}\mathcal{F}_X = \tilde{\Delta}\mathcal{F}_Y - \gamma\mathcal{F}_X + g_Y\mathcal{F}_q \tag{A.2.1c}$$
$$-i\bar{\omega}\mathcal{F}_Y = -\tilde{\Delta}\mathcal{F}_X - \gamma\mathcal{F}_Y - g_X\mathcal{F}_q \tag{A.2.1d}$$

in case of the OM system and

$$-i\bar{\omega}\mathcal{F}_q = \Omega\mathcal{F}_p - \kappa\mathcal{F}_q \tag{A.2.2a}$$
$$-i\bar{\omega}\mathcal{F}_p = -\Omega\mathcal{F}_q - \kappa\mathcal{F}_p - \sqrt{2}Ng\mathcal{F}_U + \mathcal{F}_F \tag{A.2.2b}$$
$$-i\bar{\omega}\mathcal{F}_X = \tilde{\Delta}\mathcal{F}_Y - \tilde{\gamma}\mathcal{F}_X + g_Y\mathcal{F}_q - 2\sqrt{2}E_1\mathcal{F}_U \tag{A.2.2c}$$
$$-i\bar{\omega}\mathcal{F}_Y = -\tilde{\Delta}\mathcal{F}_X - \tilde{\gamma}\mathcal{F}_Y - g_X\mathcal{F}_q \tag{A.2.2d}$$
$$-i\bar{\omega}\mathcal{F}_U = \sqrt{2}E_1\mathcal{F}_X - 2\mathcal{F}_U \tag{A.2.2e}$$

in case of the SC system. Here, $\mathcal{F}$ stands for the Fourier transform, which is a function of $\bar{\omega}$. The shorthand notations used here are $\tilde{\gamma} = (\gamma + \gamma_{\mathrm{PD}})$, $\tilde{\Delta} = \Delta + \sqrt{2}gq_s$, $g_X = \sqrt{2}gX_s$, and $g_Y = \sqrt{2}gY_s$.

By solving this system of equations, a susceptibility describing the linear response to some external force can be derived defined by $\mathcal{F}_q = \chi(\bar{\omega})\mathcal{F}_F$. For the OM system the inverse susceptibility can be evaluated as

$$\chi_{\mathrm{OM}}^{-1}(\bar{\omega}) = -\frac{\bar{\omega}^2 + 2i\bar{\omega}\kappa - \kappa^2 + \Omega^2}{\Omega} - \frac{2g^2P_s^*P_s\tilde{\Delta}}{(\gamma - i\bar{\omega})^2 + \tilde{\Delta}^2}. \tag{A.2.3}$$

While it becomes for the SC system

$$\chi_{\mathrm{SC}}^{-1}(\bar{\omega}) = -\frac{\bar{\omega}^2 + 2i\bar{\omega}\kappa - \kappa^2 + \Omega^2}{\Omega} + \frac{2gE_1N}{i\bar{\omega} - 2\gamma}\frac{g_X\tilde{\Delta} + g_Y(i\bar{\omega} - \tilde{\gamma})}{(-i\omega(1-R) + \tilde{\gamma} + 2R\gamma)(\tilde{\gamma} - i\bar{\omega}) + \tilde{\Delta}^2}. \tag{A.2.4}$$

The additional shorthand notation $R = \frac{4E_1^2}{\bar{\omega}^2+4\gamma^2}$ is introduced. Comparing these equations with Ref. [Gen+08] some differences may be observed, which are due to the different

introduction of the damping. In the limit $\Omega \gg \kappa$, which is considered throughout the thesis, both cases coincide. The effective damping rates Eq. (4.4.1) and Eq. (4.4.2) may be derived from the susceptibilities. For convenience the abbreviations $\mathcal{D} = \frac{1}{2}\frac{R^2\left(1-\frac{2\gamma}{\tilde{\gamma}}\right)^2}{1-\left(1+\frac{2\gamma}{\tilde{\gamma}}\right)R+\frac{2\gamma}{\tilde{\gamma}}R^2}$, $\gamma_r = \tilde{\gamma}\sqrt{1-\frac{2\gamma}{\tilde{\gamma}}R}$, and $\omega_R = \bar{\omega}\sqrt{1+R}$ are introduced.

B. Derivation of cascaded coupling

In this appendix, the master equation for the quantum cascaded setup is derived employing the Born-Markov approximation and assuming a thermal bath [CnL16; GC85; CG84; Gar86]. With this, the bath degrees of freedom may be traced out, reducing the complexity of the computation. As the full density matrix for the systems is considered and no further expansion is employed the numerical evaluation is still quite expensive.

When a non-thermal reservoir needs to be considered, more complex models are needed that reduce the complexity of the problem in a different way [Ric+09; CC14; Kab+11a], especially when the bath needs to be considered explicitly due to non-Markovian effects [Pri+10]. While the model presented in this Chapter only includes thermal reservoirs in Part III a non-Markovian reservoir is considered.

At first the generic master equation for a source with Hamiltonian H_s pumping a target with Hamiltonian H_t via a thermal bath with Hamiltonian H_c will be considered. This setup is depicted schematically in Fig. 6.1.1 Writing the full Hamiltonian as $H = H_0 + H_s + H_c + H_t$, where H_0 contains the free evolution of the subsystems. For now only the coupling Hamiltonian H_c is considered and is transformed into a rotating frame with respect to H_0 by

$$H_{\mathrm{c,rf}} = U_{\mathrm{rf}} H_{\mathrm{tot}} U_{\mathrm{c}}^{\dagger} - i\hbar U_{\mathrm{rf}} \frac{\partial}{\partial t} U_{\mathrm{rf}}^{\dagger} \tag{B.0.1}$$

with $U_{\mathrm{rf}} = \exp\left(iH_0 t/\hbar\right)$. This results in

$$\frac{H_{\mathrm{c}}}{\hbar} = \int d\omega \; b(\omega) \Big[K_{\omega}^{s} J_{s}^{\dagger}(t) + K_{\omega}^{t} J^{\dagger}(t,\tau) \Big] + \mathrm{H.c.}. \tag{B.0.2}$$

Here, J_s is some operator in the source Hilbert space, which couples the source to the bath with coupling strength K_{ω}^{s} and J_t is the operator coupling the target to the bath with strengths K_{ω}^{t}. As, in general, the excitation takes some time to travel from source to target, there is a delay τ between them. Later on this will be neglected. The coupling of source and target to the reservoir is assumed to be frequency independent in accordance with the assumption that the frequencies relevant for the dynamics are in a small bandwidth, where frequency-dependent effects may be neglected [GZ04].

The quantum cascaded coupling is derived from the coupling Hamiltonian Eq. (B.0.2) by employing the second order Born-Markov approximation. This is valid for low coupling strengths between the systems and the bath. This is the standard approach to deal with thermal, Markovian baths, where the bath state is assumed to be independent of the system dynamics and the system and bath density matrices factorize, ie.e. $\chi_{\mathrm{tot}}(t) = \rho(t)\rho_B(0)$. The time dynamics of the system density matrix are then derived from [BP02; Car02]

$$\frac{d\rho}{dt}|_{c} = -\frac{1}{\hbar^2} \int_0^t ds \mathrm{Tr}_B \left\{ [H_{\mathrm{c}}(t), [H_{\mathrm{c}}(s), \rho(t)\rho_B]] \right\}. \tag{B.0.3}$$

The bath degrees of freedom are traced out, so that they do not need to be taken into account explicitly. The most basic model for cascaded coupling is achieved by assuming a bath in the vacuum state. This can be achieved by assuming a thermal state with zero temperature. For the bath modes the commutation relation $[b(\omega), b^\dagger(\omega')] = \delta(\omega - \omega')$ Tracing out the bath will lead to the evaluation of bath correlations. Then, only terms proportional to $\left\langle b(\omega)b^\dagger(\omega)\right\rangle$ will contribute to the coupling between the bath and the system. When evaluating Eq. (B.0.3), it will yield

$$\begin{aligned}\frac{d\rho}{dt}|_c = -2\pi \sum_{i=s,t} (K_0^i)^2 \int_0^t ds\delta(s-t)\Big[J_i^\dagger(t)J_i(s)\rho(s) - J_i(t)\rho(s)J_i^\dagger(s) \\ - J_i(s)\rho(s)J_i^\dagger(s) + \rho(s)J_i^\dagger(s)J_i(t)\Big] \\ - 2\pi K_0^s K_0^t \int_0^t ds\delta(s-(t-\tau))\Big[J_t^\dagger(t)J_s(s)\rho(s) - J_t(t)\rho(s)J_s^\dagger(s) \\ - J_s(s)\rho(s)J_t^\dagger(t) + \rho(s)J_s^\dagger(s)J_t(t)\Big] \\ - 2\pi K_0^s K_0^t \int_0^t ds\delta(s-(t+\tau))\Big[J_s^\dagger(t)J_t(s)\rho(s) - J_s(t)\rho(s)J_t^\dagger(s) \\ - J_t(s)\rho(s)J_s^\dagger(s) + \rho(s)J_t^\dagger(s)J_s(t)\Big].\end{aligned} \tag{B.0.4}$$

When using $\int_0^t ds\delta(t-s)h(s) = h(t)/2$ and noting that $s \leq t$ the last term will not contribute, as the contribution from the δ-distribution lies outside the integration interval. For brevity, the definition $K_0^i = \sqrt{\gamma_i/(2\pi)}$ is introduced. Here, the decay rates of the subsystems γ_i were introduced. From this the master equation follow as

$$\begin{aligned}\frac{d\rho}{dt} = \frac{1}{i\hbar}[H_s + H_t, \rho] + \sum_{i=s,t} \frac{\gamma_i}{2}\left(2J_i(t)\rho(t)J_i^\dagger(t) - \{J_i^\dagger(t)J_i(t), \rho(t)\}\right) \\ - \sqrt{\gamma_s\gamma_t}\left(J_t^\dagger(t)J_s(t_D)\rho(t_D) - J_t(t)\rho(t_D)J_s^\dagger(t_D)\right) \\ - \sqrt{\gamma_s\gamma_t}\left(\rho(t_D)J_s^\dagger(t_D)J_t(t) - J_s(t_D)\rho(t_D)J_t^\dagger(t)\right).\end{aligned} \tag{B.0.5}$$

In this equation the time difference $t_D = t - \tau$ is still present. As delay effects are beyond the scope of the theory applied in this part, as it would introduce even more numerical complexity, the time delay is assumed to be negligible. As noted before, in Part III time delays are considered for more simple systems. To consider the whole Hamiltonian the master equation is transformed back from the rotating frame, so that a master equation for the coupling of a source system H_s to a target system H_t via the intermediate bath that is traced out is given by

$$\begin{aligned}\frac{d\rho}{dt} = \frac{1}{i\hbar}[H_0 + H_s + H_t, \rho] \\ + \sum_{i=s,t} \frac{\gamma_i}{2}\left(2J_i\,\rho J_i^\dagger - \{J_i^\dagger J_i\,, \rho\}\right) - \sqrt{\gamma_s\gamma_t}\left([J_t^\dagger, J_s\rho] + [\rho J_s^\dagger, J_t\,]\right).\end{aligned} \tag{B.0.6}$$

The first term in this equation will give the dynamics of the closed systems. The second term is the loss of the modes coupled to the environment. The third term represents the

coupling of between source and target mediated by the reservoir. To achieve a nonzero coupling between source and target both of them need to allow a dissipation of excitation into the mediating reservoir. While this is obvious for the source as the target cannot be excited if nothing is emitted the need for the target to be subject to losses is less intuitive.

Using this as the starting point for the following study different targets and sources may be considered. In the next section this master equation will be used for the particular system discussed in the introduction, where the source is a Jaynes-Cummings Hamiltonian, while the target is a Tavis-Cummings model.

C. Stroboscopic map and explicit time evolution in first order

To evaluate the dynamics induced by the Hamiltonian numerically, time is discretized and the evolution operator between two adjacent time steps t_k and t_{k+1} is computed with $t_{k+1} - t_k = \Delta t$ in order to solve the iterative Eq. (8.2.13)

$$|\Psi(t_{k+1})\rangle = U(t_{k+1}, t_k)|\Psi(t_k)\rangle, \tag{C.0.1}$$

where $|\Psi\rangle$ is expressed as a matrix product state, which was shown in Sec. 8.2.4. In principle, the time ordering has to be considered, so that

$$U(t_{k+1}, t_k) = \hat{T}\left[\exp\left(-\frac{i}{\hbar}\int_{t_k}^{t_{k+1}} dt' H_{\mathrm{tot,rf}}(t')\right)\right] \tag{C.0.2}$$

has to be evaluated. Here, $\hat{T}$ is the time ordering operator. At first, this is done explicitly in first order of Δt to show the technical aspects involved. In the next step, it is shown how higher order evolution may be implemented. To evaluate the time evolution operator in an Euler-like manner up to first order in Δt, the time evolution operator Eq. (C.0.2) has to be evaluated up to the second order, as will become clear below. This results in

$$\begin{aligned} U(t_{k+1}, t_k) \approx \mathbb{1} + \left(-\frac{i}{\hbar}\right)\Bigg[&\overbrace{\int_{t_k}^{t_{k+1}} dt' H_{\mathrm{sys,rf}}(t')}^{=I_{1,1}} + \overbrace{\int_{t_k}^{t_{k+1}} dt' H_{\mathrm{fb,rf}}(t')}^{=I_{1,2}}\Bigg] \\ &+ \frac{1}{2}\left(-\frac{i}{\hbar}\right)^2 \hat{T}\Bigg[\underbrace{\int_{t_k}^{t_{k+1}} dt'' \int_{t_k}^{t_{k+1}} dt' H_{\mathrm{sys,rf}}(t'') H_{\mathrm{sys,rf}}(t')}_{=I_{2,1}} \\ &\quad + \underbrace{\int_{t_k}^{t_{k+1}} dt'' \int_{t_k}^{t_{k+1}} dt' H_{\mathrm{sys,rf}}(t'') H_{\mathrm{fb,rf}}(t')}_{=I_{2,2}} \\ &+ \underbrace{\int_{t_k}^{t_{k+1}} dt'' \int_{t_k}^{t_{k+1}} dt' H_{\mathrm{fb,rf}}(t'') H_{\mathrm{sys,rf}}(t')}_{=I_{2,3}} + \underbrace{\int_{t_k}^{t_{k+1}} dt'' \int_{t_k}^{t_{k+1}} dt' H_{\mathrm{fb,rf}}(t'') H_{\mathrm{fb,rf}}(t')}_{=I_{2,4}}\Bigg]. \end{aligned} \tag{C.0.3}$$

The integrals from Eq. (C.0.3) are evaluated explicitly (since only one time is involved, the time ordering is correct):

$$\begin{aligned}
I_{1,1} &= \int_{t_k}^{t_{k+1}} dt' H_{\mathrm{sys,rf}} = H_{\mathrm{sys,rf}} \Delta t \\
I_{1,2} &= \int_{t_k}^{t_{k+1}} dt' H_{\mathrm{fb,rf}}(t') \\
&= -i\hbar \int_{t_k}^{t_{k+1}} dt' \Big[\left(\sqrt{\gamma_R} b(t'-\tau) e^{-i\phi} + \sqrt{\gamma_L} b(t') \right) c^\dagger \\
&\qquad - \left(\sqrt{\gamma_R} b^\dagger(t'-\tau) e^{i\phi} + \sqrt{\gamma_L} b^\dagger(t') \right) c \Big] \\
&= -i\hbar \Big[\left(\sqrt{\gamma_R} \Delta B(t_{k-l}) e^{-i\phi} + \sqrt{\gamma_L} \Delta B(t_k) \right) c^\dagger \\
&\qquad - \left(\sqrt{\gamma_R} \Delta B^\dagger(t_{k-l}) e^{i\phi} + \sqrt{\gamma_L} \Delta B^\dagger(t_k) \right) c \Big].
\end{aligned}$$

Here, the time discrete bath operators $\Delta B(t_k) = \int_{t_k}^{t_{k+1}} dt b(t)$ are introduced. In the following also the shorthand notation $\Delta B_k = \Delta B(t_k)$ is used. Furthermore, Δt is chosen such that $l = \tau/\Delta t$ is an integer value, so that

$$\int_{t_k}^{t_{k+1}} dt b(t-\tau) = \int_{t_k-\tau}^{t_{k+1}-\tau} dt b(t) = \int_{t_{k-l}}^{t_{k-l+1}} dt b(t) = \Delta B(t_{k-l}).$$

The second order terms become:

$$I_{2,1} = \hat{T} \int_{t_k}^{t_{k+1}} dt'' \int_{t_k}^{t_{k+1}} dt' H_{\mathrm{sys,rf}} H_{\mathrm{sys,rf}} = H_{\mathrm{sys,rf}}^2 \Delta t^2.$$

As one might expect, this term is in second order of Δt, that is is neglected in the following. The terms, where system and interaction Hamiltonian mix, become

$$\begin{aligned}
I_{2,2} &= \hat{T} \int_{t_k}^{t_{k+1}} dt'' \int_{t_k}^{t_{k+1}} dt' H_{\mathrm{sys,rf}} H_{\mathrm{fb,rf}}(t') \\
&= \int_{t_k}^{t_{k+1}} dt'' H_{\mathrm{sys,rf}} \int_{t_k}^{t_{k+1}} dt' H_{\mathrm{int,rf}}(t') = I_{1,1} I_{1,2} \\
\Rightarrow I_{2,3} &= I_{1,2} I_{1,1}.
\end{aligned}$$

These terms will be considered again in the following. First, the term, which is in second order of the interaction Hamiltonian is evaluated as

$$\begin{aligned}
I_{2,4} &= \hat{T} \int_{t_k}^{t_{k+1}} dt'' \int_{t_k}^{t_{k+1}} dt' H_{\mathrm{fb,rf}}(t'') H_{\mathrm{fb,rf}}(t') \\
&= -\hbar^2 \hat{T} \Bigg\{ \int_{t_k}^{t_{k+1}} dt'' \int_{t_k}^{t_{k+1}} dt' \Big[\left(\sqrt{\gamma_R} b(t''-\tau) e^{-i\phi} + \sqrt{\gamma_L} b(t'') \right) c^\dagger \\
&\qquad - \left(\sqrt{\gamma_R} b^\dagger(t''-\tau) e^{i\phi} + \sqrt{\gamma_L} b^\dagger(t'') \right) c \Big] \\
&\quad \times \left[\left(\sqrt{\gamma_R} b(t'-\tau) e^{-i\phi} + \sqrt{\gamma_L} b(t') \right) c^\dagger - \left(\sqrt{\gamma_R} b^\dagger(t'-\tau) e^{i\phi} + \sqrt{\gamma_L} b^\dagger(t') \right) c \right] \Bigg\}.
\end{aligned}$$

Here, the bath operators have to be ordered correctly. However, by employing the commutation relation Eq. (8.2.12), it becomes apparent that the ordering does not matter after all. For terms involving either only creation- or annihilation operators, they commute for all times. For terms as $\int dt'' \int dt' b^\dagger(t'')b(t')$, only at $t'' = t'$, the operators do not commute, but then, they are simultaneous anyways. The same is true for terms as $\int dt'' \int dt' b^\dagger(t'' - \tau)b(t' - \tau)$. Finally, terms such as $\int dt'' \int dt' b^\dagger(t'')b(t' - \tau)$ do not pose a problem, since the integration time Δt is smaller than τ, such that cases as $t'' = t' - \tau$ do not occur. With this, the time ordering becomes trivial and the second order term becomes

$$
\begin{aligned}
\frac{1}{2}\left(-\frac{i}{\hbar}\right)^2 I_{2,4} &= \frac{1}{2}\left(-\frac{i}{\hbar}\right)^2 I_{1,2}I_{1,2} \\
&= \frac{1}{2}\Big[\left(\sqrt{\gamma_R}\Delta B(t_{k-l})e^{-i\phi} + \sqrt{\gamma_L}\Delta B(t_k)\right)c^\dagger \\
&\qquad - \left(\sqrt{\gamma_R}\Delta B^\dagger(t_{k-l})e^{i\phi} + \sqrt{\gamma_L}\Delta B^\dagger(t_k)\right)c\Big]^2 \\
&= \frac{1}{2}\Big[\gamma_L\Delta B^\dagger(t_k)\Delta B^\dagger(t_k) + \sqrt{\gamma_L\gamma_R}e^{i\phi}\Delta B^\dagger(t_k)\Delta B^\dagger(t_{k-l}) \\
&\qquad + \sqrt{\gamma_R\gamma_L}e^{i\phi}\Delta B^\dagger(t_{k-l})\Delta B^\dagger(t_k) + e^{2i\phi}\gamma_R\Delta B^\dagger(t_{k-l})\Delta B^\dagger(t_{k-l})\Big]cc \\
&- \frac{1}{2}\Big[\gamma_L\Delta B^\dagger(t_k)\Delta B(t_k) + \sqrt{\gamma_L\gamma_R}e^{-i\phi}\Delta B^\dagger(t_k)\Delta B(t_{k-l}) \\
&\qquad + \sqrt{\gamma_R\gamma_L}e^{i\phi}\Delta B^\dagger(t_{k-l})\Delta B(t_k) + \gamma_R\Delta B^\dagger(t_{k-l})\Delta B(t_{k-l})\Big]cc^\dagger \\
&- \frac{1}{2}\Big[\gamma_L\Delta B(t_k)\Delta B^\dagger(t_k) + \sqrt{\gamma_L\gamma_R}e^{i\phi}\Delta B(t_k)\Delta B^\dagger(t_{k-l}) \\
&\qquad + \sqrt{\gamma_R\gamma_L}e^{-i\phi}\Delta B(t_{k-l})\Delta B^\dagger(t_k) + \gamma_R\Delta B(t_{k-l})\Delta B^\dagger(t_{k-l})\Big]c^\dagger c \\
&+ \frac{1}{2}\Big[\gamma_L\Delta B(t_k)\Delta B(t_k) + \sqrt{\gamma_L\gamma_R}e^{-i\phi}\Delta B(t_k)\Delta B(t_{k-l}) \\
&\qquad + \sqrt{\gamma_R\gamma_L}e^{-i\phi}\Delta B(t_{k-l})\Delta B(t_k) + e^{-2i\phi}\gamma_R\Delta B(t_{k-l})\Delta B(t_{k-l})\Big]c^\dagger c^\dagger.
\end{aligned}
$$

In order to see which terms have to be kept in order to get a consistent equation in first order of Δt the commutation relation of the discretized bath operators are computed as

$$
\begin{aligned}
\left[\Delta B(t_k), \Delta B^\dagger(t_j)\right] &= \int_{t_k}^{t_{k+1}} dt \int_{t_j}^{t_{j+1}} dt' \left[b(t), b^\dagger(t')\right] \\
&= \int_{t_k}^{t_{k+1}} dt \int_{t_j}^{t_{j+1}} dt' \delta(t - t') \\
&= \begin{cases} \int_{t_k}^{t_{k+1}} dt = \Delta t, & k = j \\ 0, & k \neq j \end{cases} \\
&= \Delta t \delta_{k,j}.
\end{aligned}
$$

The photon bins are orthogonal, but not normalized. When constructing the basis set for the bath, in order to conserve the normalization of the state, the factor $\sqrt{\Delta t}$ is included (One could also include the normalization factor in the bath operators, however,

to maintain the correspondence to Ito calculus, the operators are chosen $\propto \sqrt{\Delta t}$). These operators may be interpreted as the number of photons destroyed or created in the time interval Δt. The relevant basis set constructed from the vacuum state is

$$|i_p\rangle = \frac{\left(\Delta B^\dagger(t_p)\right)^{i_p}}{\sqrt{i_p!\Delta t^{i_p}}}|\mathrm{vac}\rangle. \tag{C.0.4}$$

Here i_p is the number of photons in the photon bin p. From this relation, it becomes clear, that the operators for the discretized photon bath introduce terms of the order $\sqrt{\Delta t}$. This means that the terms involving ΔB up to second order have to be taken into account, while terms $\propto \Delta t \Delta B$ may be discarded, so that $I_{2,2}$ and $I_{2,3}$ are neglected. Thus, the evolution operator becomes

$$\begin{aligned}
U(t_{k+1},t_k) = \mathbb{1} &- \frac{i}{\hbar}H_{\mathrm{sys,rf}}\Delta t \\
&- \Big[\left(\sqrt{\gamma_R}\Delta B(t_{k-l})e^{-i\phi} + \sqrt{\gamma_L}\Delta B(t_k)\right)c^\dagger \\
&- \left(\sqrt{\gamma_R}\Delta B^\dagger(t_{k-l})e^{i\phi} + \sqrt{\gamma_L}\Delta B^\dagger(t_k)\right)c\Big] \\
&+ \frac{1}{2}\Big[\gamma_L\Delta B^\dagger(t_k)\Delta B^\dagger(t_k) + \sqrt{\gamma_L\gamma_R}e^{i\phi}\Delta B^\dagger(t_k)\Delta B^\dagger(t_{k-l}) \\
&\quad + \sqrt{\gamma_R\gamma_L}e^{i\phi}\Delta B^\dagger(t_{k-l})\Delta B^\dagger(t_k) + e^{2i\phi}\gamma_R\Delta B^\dagger(t_{k-l})\Delta B^\dagger(t_{k-l})\Big]cc \\
&- \frac{1}{2}\Big[\gamma_L\Delta B^\dagger(t_k)\Delta B(t_k) + \sqrt{\gamma_L\gamma_R}e^{-i\phi}\Delta B^\dagger(t_k)\Delta B(t_{k-l}) \\
&\quad + \sqrt{\gamma_R\gamma_L}e^{i\phi}\Delta B^\dagger(t_{k-l})\Delta B(t_k) + \gamma_R\Delta B^\dagger(t_{k-l})\Delta B(t_{k-l})\Big]cc^\dagger \\
&- \frac{1}{2}\Big[\gamma_L\Delta B(t_k)\Delta B^\dagger(t_k) + \sqrt{\gamma_L\gamma_R}e^{i\phi}\Delta B(t_k)\Delta B^\dagger(t_{k-l}) \\
&\quad + \sqrt{\gamma_R\gamma_L}e^{-i\phi}\Delta B(t_{k-l})\Delta B^\dagger(t_k) + \gamma_R\Delta B(t_{k-l})\Delta B^\dagger(t_{k-l})\Big]c^\dagger c \\
&+ \frac{1}{2}\Big[\gamma_L\Delta B(t_k)\Delta B(t_k) + \sqrt{\gamma_L\gamma_R}e^{-i\phi}\Delta B(t_k)\Delta B(t_{k-l}) \\
&\quad + \sqrt{\gamma_R\gamma_L}e^{-i\phi}\Delta B(t_{k-l})\Delta B(t_k) + e^{-2i\phi}\gamma_R\Delta B(t_{k-l})\Delta B(t_{k-l})\Big]c^\dagger c^\dagger.
\end{aligned}$$

With this, the time-evolution is described in an Euler-like manner in first order of the time step Δt. To evaluate this evolution numerically, the operator U and the state are expanded in the basis set spanned by $|i_\mathrm{T}, i_\mathrm{cav}\rangle \bigotimes_{p=-\infty}^{\infty}|i_p\rangle$, cf. Eq. (C.0.4). Here, i_cav is the number of photons in the cavity, $i_\mathrm{T} = e, g$ indicates whether the two level system is in the excited state, and i_p is the number of photons in the pth photon bin. Since U will be diagonal for all indices except for the ones for the system, the current time bin t and the time bin at $t-\tau$, only these will be written down explicitly. The shorthand notation $j_\tau = j_{k-l}$, $i_\tau = i_{k-l}$ for the indices for the bin at the time $t-\tau$ is used. The indices j_k and i_k represent the time bin at time t, j_T and i_T are the indices for the two level system (these may be either g or e) of the Jaynes-Cummings model, and j_cav and i_cav are the

indices for the photonic mode of the JCM. Then, the evolution matrix becomes

$$
\begin{aligned}
U^{i_k,i_\mathrm{T},i_\mathrm{cav},\ldots,i_\tau}_{j_k,j_\mathrm{T},j_\mathrm{cav},\ldots,j_\tau} &= \langle j_k, j_\mathrm{T}, j_\mathrm{cav}, j_\tau | U(t_{k+1},t_k) | i_k, i_\mathrm{T}, i_\mathrm{cav}, i_\tau \rangle \\
&= \delta_{j_k,i_k}\delta_{j_\mathrm{T},i_\mathrm{T}}\delta_{j_\mathrm{cav},i_\mathrm{cav}}\delta_{j_{k-1},i_{k-1}}\ldots\delta_{j_{k+1-l},i_{k+1-l}}\delta_{j_\tau,i_\tau} \\
&- i\Delta t\Big[\Delta_\mathrm{T}\delta_{j_\mathrm{T},e}\delta_{i_\mathrm{T},e}\delta_{j_\mathrm{cav},j_\mathrm{cav}} + i_\mathrm{cav}\Delta_\mathrm{cav}\delta_{j_\mathrm{T},i_\mathrm{T}}\delta_{j_\mathrm{cav},i_\mathrm{cav}} \\
&+ \Omega_\mathrm{T}\delta_{j_\mathrm{T},g}\delta_{ie,e}\delta_{j_\mathrm{cav},i_\mathrm{cav}} + \Omega^*_\mathrm{T}\delta_{j_\mathrm{T},e}\delta_{ie,g}\delta_{j_\mathrm{cav},i_\mathrm{cav}} \\
&+ g\delta_{j_\mathrm{T},g}\delta_{i_\mathrm{T},e}\sqrt{j_\mathrm{cav}}\delta_{j_\mathrm{cav},i_\mathrm{cav}+1} + g\delta_{j_\mathrm{T},e}\delta_{i_\mathrm{T},g}\sqrt{i_\mathrm{cav}}\delta_{j_\mathrm{cav}+1,i_\mathrm{cav}} \\
&+ \delta_{j_\mathrm{T},i_\mathrm{T}}\left(\sqrt{i_\mathrm{cav}}\Omega_\mathrm{cav}\delta_{j_\mathrm{cav}+1,i_\mathrm{cav}} + \sqrt{j_\mathrm{cav}}\Omega^*_\mathrm{cav}\delta_{j_\mathrm{cav},i_\mathrm{cav}+1}\right)\Big] \\
&\qquad \times \delta_{j_k,i_k}\delta_{j_{k-1},i_{k-1}}\ldots\delta_{j_{k+1-l},i_{k+1-l}}\delta_{j_\tau,i_\tau} \\
&+ \Big[\sqrt{\Delta t j_\mathrm{cav}}\delta_{j_\mathrm{cav},i_\mathrm{cav}+1}\left(\sqrt{\gamma_L}\sqrt{i_k}\delta_{j_k+1,i_k}\delta_{j_\tau,i_\tau} + \sqrt{\gamma_R}\sqrt{i_\tau}e^{-i\phi}\delta_{j_k,i_k}\delta_{j_\tau+1,i_\tau}\right) \\
&- \sqrt{\Delta t i_\mathrm{cav}}\delta_{j_\mathrm{cav}+1,i_\mathrm{cav}}\left(\sqrt{\gamma_L}\sqrt{j_k}\delta_{j_k,i_k+1}\delta_{j_\tau,i_\tau} + \sqrt{\gamma_R}\sqrt{j_\tau}e^{i\phi}\delta_{j_k,i_k}\delta_{j_\tau,i_\tau+1}\right) \\
&+ \frac{\Delta t}{2}\sqrt{j_\mathrm{cav}+1}\sqrt{j_\mathrm{cav}+2}\delta_{j_\mathrm{cav}+2,i_\mathrm{cav}} \\
&\times \Big(\gamma_L\sqrt{i_k+1}\sqrt{i_k+2}\delta_{j_k,i_k+2}\delta_{j_\tau,i_\tau} + \sqrt{\gamma_L\gamma_R}e^{i\phi}\sqrt{j_k}\sqrt{j_\tau}\delta_{j_k,i_k+1}\delta_{j_\tau,i_\tau+1} \\
&+ \sqrt{\gamma_R\gamma_L}e^{i\phi}\sqrt{j_k}\sqrt{j_\tau}\delta_{j_k,i_k+1}\delta_{j_\tau,i_\tau+1} + \gamma_R e^{2i\phi}\sqrt{i_\tau+1}\sqrt{i_\tau+2}\delta_{j_k,i_k}\delta_{j_\tau,i_\tau+2}\Big) \\
&- (i_\mathrm{cav}+1)\,\delta_{j_\mathrm{cav},i_\mathrm{cav}}\Big(\gamma_L i_k\delta_{j_k,i_k}\delta_{j_\tau,i_\tau} + \sqrt{\gamma_L\gamma_R}e^{-i\phi}\sqrt{j_\tau}\sqrt{i_k}\delta_{j_k,i_k+1}\delta_{j_\tau+1,i_\tau} \\
&+ \sqrt{\gamma_R\gamma_L}e^{i\phi}\sqrt{i_\tau}\sqrt{j_k}\delta_{j_k,i_k+1}\delta_{j_\tau+1,i_\tau} + \gamma_R i_\tau\delta_{j_k,i_k}\delta_{j_\tau,i_\tau}\Big)\frac{\Delta t}{2} \\
&- (i_\mathrm{cav})\,\delta_{j_\mathrm{cav},i_\mathrm{cav}}\Big(\gamma_L\,(i_k+1)\,\delta_{j_k,i_k}\delta_{j_\tau,i_\tau} + \sqrt{\gamma_L\gamma_R}e^{i\phi}\sqrt{j_\tau}\sqrt{i_k}\delta_{j_k+1,i_k}\delta_{j_\tau,i_\tau+1} \\
&+ \sqrt{\gamma_R\gamma_L}e^{-i\phi}\sqrt{i_\tau}\sqrt{j_k}\delta_{j_k,i_k+1}\delta_{j_\tau+1,i_\tau} + \gamma_R i_\tau\delta_{j_k,i_k}\delta_{j_\tau,i_\tau}\Big)\frac{\Delta t}{2} \\
&+ \frac{\Delta t}{2}\sqrt{i_\mathrm{cav}+1}\sqrt{i_\mathrm{cav}+2}\delta_{j_\mathrm{cav},i_\mathrm{cav}+2} \\
&\times \Big(\gamma_L\sqrt{i_k}\sqrt{i_k-1}\delta_{j_k,i_k-2}\delta_{j_\tau,i_\tau} + \sqrt{\gamma_L\gamma_R}e^{-i\phi}\sqrt{j_k}\sqrt{j_\tau}\delta_{j_k+1,i_k}\delta_{j_\tau+1,i_\tau} \\
&+ \sqrt{\gamma_R\gamma_L}e^{-i\phi}\sqrt{i_k}\sqrt{i_\tau}\delta_{j_k+1,i_k}\delta_{j_\tau+1,i_\tau} + \gamma_R e^{-2i\phi}\sqrt{i_\tau}\sqrt{i_\tau-1}\delta_{j_k,i_k}\delta_{j_\tau,i_\tau-2}\Big) \\
&\Big]\delta_{j_\mathrm{T},i_\mathrm{T}}\delta_{j_{k-1},i_{k-1}}\ldots\delta_{j_{k+1-l},i_{k+1-l}}. \qquad \text{(C.0.5)}
\end{aligned}
$$

This is the excerpt of the total evolution matrix for the system and the photon bins between now (t) and before the delay time ($t-\tau$). The matrix is diagonal with regard to most indices. However, when the ordering of the indices in the state is chosen in a certain way (chronologically), it is important to keep in mind that the matrix is in fact a larger one. This issue will be discussed again in Sec. 8.2.4 when the necessary details of the implementation of the evolution algorithm will be shown.

D. Details on the increased antibunching with feedback

In this appendix the equations of motion and the states for Sec. 10 are shown.

D.1. Equations of motion and correlation function

The equations of motion for the time evolution of the state Eq. (10.1.4) are given by the Schrödinger equation

$$i\hbar\frac{\partial}{\partial t}|\varphi(t)\rangle = H|\varphi(t)\rangle. \tag{D.1.1}$$

The coefficient $|C_{gg00}|$ is approximated as unity since weak driving is considered, so that the equations of motion become

$$\begin{aligned}
\partial_t C_{ge00} &= -i\left(\delta C_{ge00} + g_2 C_{gg10} + \epsilon C_{ge10}\right) - \frac{\gamma}{2}C_{ge00} \\
\partial_t C_{eg00} &= -i\left(\delta C_{eg00} + g_1 C_{gg10} + \epsilon C_{eg10}\right) - \frac{\gamma}{2}C_{eg00} \\
\partial_t C_{ee00} &= -i\left(2\delta C_{ee00} + g_1 C_{ge10} + g_2 C_{eg10}\right) - \gamma C_{ee00} \\
\partial_t C_{gg20} &= -i\left(2\Delta C_{gg20} + \sqrt{2}g_2 C_{ge10} + \sqrt{2}g_1 C_{eg10} + \sqrt{2}\epsilon C_{gg10}\right) \\
&\quad + i\int dk G(k,t)\sqrt{2}C_{gg1k} \\
\partial_t C_{ge10} &= -i\left[\left[\Delta C_{ge10} + \left(\delta - \frac{i\gamma}{2}\right)C_{ge10} + \sqrt{2}g_2 C_{gg20} + g_1 C_{ee00} + \epsilon C_{ge00}\right]\right. \\
&\quad + i\int dk G(k,t) C_{ge0k} \\
\partial_t C_{eg10} &= -i\left[\Delta C_{eg10} + \left(\delta - \frac{i\gamma}{2}\right)C_{eg10} + g_2 C_{ee00} + \sqrt{2}g_1 C_{gg20} + \epsilon C_{eg00}\right] \\
&\quad + i\int dk G(k,t) C_{eg0k} \\
\partial_t C_{ge0k} &= -i\left[\left(\delta - \frac{i\gamma}{2}\right)C_{ge0k} + g_2 C_{gg1k}\right] + iG^*(k,t)C_{ge10} \\
\partial_t C_{eg0k} &= -i\left[\left(\delta - \frac{i\gamma}{2}\right)C_{eg0k} + g_1 C_{gg1k}\right] + iG^*(k,t)C_{eg10} \\
\partial_t C_{gg0k} &= -i\epsilon C_{gg1k} + iG^*(k,t)C_{gg10} \\
\partial_t C_{gg0kk'} &= iG^*(k',t)C_{gg1k} + iG^*(k,t)C_{gg1k'},\ \text{if} k \neq k'
\end{aligned} \tag{D.1.2}$$

$$\partial_t C_{gg0kk'} = iG^*(k',t)\sqrt{2}C_{gg1k},\ \text{if} k = k'.$$

$$\partial_t C_{gg1k} = -i\left[\Delta C_{gg1k} + g_2 C_{ge0k} + g_1 C_{eg0k} + \epsilon C_{gg0k}\right] + i\Big[\int_{-\infty}^{k^-} dpG(p,t)C_{gg0pk} + \int_{k+}^{+\infty} dpG(p,t)C_{ggokp} + dkG(k,t)C_{gg0kk}\sqrt{2} + G^*(k,t)C_{gg20}\sqrt{2}\Big]$$

$$\partial_t C_{gg10} = i\int dkG(k,t)C_{gg0k} - i\left[\Delta C_{gg10} + g_2 C_{ge00} + g_1 C_{eg00} + \epsilon\left(C_{gg00} + \sqrt{2}C_{gg20}\right)\right].$$

The state Eq. (10.1.4) can be used to evaluate the second order correlation function Eq. (10.1.7) explicitly as

$$g^{(2)}(t,0) = \frac{2|C_{gg20}|^2}{(|C_{gg10}|^2 + 2|C_{gg20}|^2 + |C_{ge10}|^2 + |C_{eg10}|^2 + \int dk|C_{gg1k}|^2)^2}. \tag{D.1.3}$$

D.2. States of the system with cavity-emitter coupling

Here, we give the states used in Sec. 10.4 to discuss the qualitative behavior of the system. By diagonalizing the the Hamiltonian without feedback reservoir in the above approximation, we get the states [ZZC16]

$$\begin{aligned}
|1_0\rangle &= \frac{1}{\sqrt{2}}|0,g,e\rangle - \frac{1}{\sqrt{2}}|0,e,g\rangle \\
|1_+\rangle &= \frac{1}{\sqrt{2}}|1,g,g\rangle + \frac{1}{2}|0,g,e\rangle + \frac{1}{2}|0,e,g\rangle \\
|1_-\rangle &= \frac{1}{\sqrt{2}}|1,g,g\rangle - \frac{1}{2}|0,g,e\rangle - \frac{1}{2}|0,e,g\rangle \\
|2_0^1\rangle &= \frac{1}{\sqrt{3}}|2,g,g\rangle - \frac{\sqrt{6}}{3}|0,e,e\rangle \\
|2_0^2\rangle &= \frac{1}{\sqrt{2}}|1,g,e\rangle - \frac{1}{\sqrt{2}}|1,e,g\rangle \\
|2_+\rangle &= \frac{\sqrt{3}}{3}|2,g,g\rangle + \frac{1}{2}|1,g,e\rangle + \frac{1}{2}|1,e,g\rangle + \frac{1}{6}|0,e,e\rangle \\
|2_-\rangle &= \frac{\sqrt{3}}{3}|2,g,g\rangle - \frac{1}{2}|1,g,e\rangle - \frac{1}{2}|1,e,g\rangle + \frac{1}{6}|0,e,e\rangle.
\end{aligned}$$

Bibliography

[AB11] M. Aßmann and M. Bayer: "Nonlinearity sensing via photon-statistics excitation spectroscopy". *Phys. Rev. A* **84** (2011), p. 053806.

[AHK99] V. Axt, M. Herbst, and T. Kuhn: "Coherent control of phonon quantum beats". *Superlattices and Microstructures* **26** (2) (1999), pp. 117–128.

[AKM14] M. Aspelmeyer, T. J. Kippenberg, and F. Marquardt: "Cavity optomechanics". *Rev. Mod. Phys.* **86** (2014), pp. 1391–1452.

[Alb+11a] F. Albert, C. Hopfmann, S. Reitzenstein, C. Schneider, S. Höfling, L. Worschech, M. Kamp, W. Kinzel, A. Forchel, and Ido Kanter: "Observing chaos for quantum-dot microlasers with external feedback". *Nature Communications* **2** (2011), p. 366.

[Alb+11b] F. Albert, C. Hopfmann, S. Reitzenstein, C. Schneider, S. Höfling, L. Worschech, M. Kamp, W. Kinzel, A. Forchel, and I. Kanter: "Observing chaos for quantum-dot microlasers with external feedback". *Nature Communications* **2** (2011), p. 366.

[Ash70] A. Ashkin: "Acceleration and Trapping of Particles by Radiation Pressure". *Phys. Rev. Lett.* **24** (1970), p. 156.

[Azi+17] S. C. Azizabadi, N. L. Naumann, M. Katzer, A. Knorr, and A. Carmele: "Quantum cascade driving: Dissipatively mediated coherences". *Phys. Rev. A* **96** (2017), p. 023816.

[Aßm+09] M. Aßmann, F. Veit, M. Bayer, M. van der Poel, and J. M. Hvam: "Higher-Order Photon Bunching in a Semiconductor Microcavity". *Science* **325** (5938) (2009), pp. 297–300.

[BGL99] D. Bimberg, M. Grundmann, and N. N. Ledentsov: *Quantum Dot Heterostructures*. John Wiley & Sons, 1999.

[BH84] R. Beach and S. R. Hartmann: "Incoherent Photon Echoes". *Phys. Rev. Lett.* **53** (1984), pp. 663–666.

[BP02] H. P. Breuer and F. Petruccione: *The Theory of Open Quantum Systems*. Oxford University Press, Oxford, 2002.

[BRV12] S. Buckley, K. Rivoire, and J. Vučković: "Engineered quantum dot single-photon sources". *Reports on Progress in Physics* **75** (12) (2012), p. 126503.

[BT56] R. H. Brown and R. Q. Twiss: "Correlation between Photons in two Coherent Beams of Light". *Nature* **177** (1956), pp. 27–29.

[Bea+10] R. P. Beardsley, A. V. Akimov, M. Henini, and A. J. Kent: "Coherent Terahertz Sound Amplification and Spectral Line Narrowing in a Stark Ladder Superlattice". *Phys. Rev. Lett.* **104** (2010), p. 085501.

[Bou+17] S. Bounouar, M. Strauß, A. Carmele, P. Schnauber, A. Thoma, M. Gschrey, J.-H. Schulze, A. Strittmatter, S. Rodt, A. Knorr, and S. Reitzenstein: "Path-Controlled Time Reordering of Paired Photons in a Dressed Three-Level Cascade". *Phys. Rev. Lett.* **118** (2017), p. 233601.

[Bra10] T. Brandes: "Feedback Control of Quantum Transport". *Phys. Rev. Lett.* **105** (2010), p. 060602.

[Bre+16] H.-P. Breuer, E.-M. Laine, J. Piilo, and B. Vacchini: "Colloquium". *Rev. Mod. Phys.* **88** (2016), p. 021002.

[CA11] G. D. Cole and M. Aspelmeyer: "Cavity optomechanics: Mechanical memory sees the light". *Nature Nanotechnology* **6** (2011), pp. 690–691.

[CC14] J. Cerrillo and J. Cao: "Non-Markovian Dynamical Maps: Numerical Processing of Open Quantum Trajectories". *Phys. Rev. Lett.* **112** (2014), p. 110401.

[CD10] H. J. Caulfield and S. Dolev: "Why future supercomputing requires optics". *Nature Photonics* **4** (2010), p. 261.

[CG84] M. J. Collett and C. W. Gardiner: "Squeezing of intracavity and traveling-wave light fields produced in parametric amplification". *Phys. Rev. A* **30** (1984), pp. 1386–1391.

[Cam+01] I. Camps, S. S. Makler, H. M. Pastawski, and L. E. F. Foa Torres: "GaAs – $Al_xGa_{1-x}As$". *Phys. Rev. B* **64** (2001), p. 125311.

[Car+13] A. Carmele, J. Kabuss, F. Schulze, S. Reitzenstein, and A. Knorr: "Single Photon Delayed Feedback: A Way to Stabilize Intrinsic Quantum Cavity Electrodynamics". *Phys. Rev. Lett.* **110** (2013), p. 013601.

[Car02] H. Carmichael: *Statistical Methods in Quantum Optics 1. Master Equations and Fokker-Planck Equations*. Theoretical and Mathematical Physics. Springer, 2002.

[Car09] H. Carmichael: *An open systems approach to quantum optics: lectures presented at the Université Libre de Bruxelles, October 28 to November 4, 1991*. Vol. 18. Springer Science & Business Media, 2009.

[Car93] H. J. Carmichael: "Quantum trajectory theory for cascaded open systems". *Phys. Rev. Lett.* **70** (1993), pp. 2273–2276.

[Cav80] C. M. Caves: "Quantum-Mechanical Radiation-Pressure Fluctuations in an Interferometer". *Phys. Rev. Lett.* **45** (1980), pp. 75–79.

[Cla+03] S. Clark, A. Peng, M. Gu, and S. Parkins: "Unconditional Preparation of Entanglement between Atoms in Cascaded Optical Cavities". *Phys. Rev. Lett.* **91** (2003), p. 177901.

[Cn+16] J. C. L. Carreño, C. Sánchez Muñoz, E. del Valle, and F. P. Laussy: "Excitation with quantum light. II. Exciting a two-level system". *Phys. Rev. A* **94** (2016), p. 063826.

[CnL16] J. C. L. Carreño and F. P. Laussy: "Excitation with quantum light. I. Exciting a harmonic oscillator". *Phys. Rev. A* **94** (2016), p. 063825.

[DCM92] J. Dalibard, Y. Castin, and K. Mølmer: "Wave-function approach to dissipative processes in quantum optics". *Phys. Rev. Lett.* **68** (1992), pp. 580–583.

[DSM16] K. E. Dorfman, F. Schlawin, and S. Mukamel: "Nonlinear optical signals and spectroscopy with quantum light". *Rev. Mod. Phys.* **88** (2016), p. 045008.

[DVL10] E Del Valle and F. Laussy: "Mollow triplet under incoherent pumping". *Physical review letters* **105** (23) (2010), p. 233601.

[DZ02] U. Dorner and P. Zoller: "Laser-driven atoms in half-cavities". *Phys. Rev. A* **66** (2002), p. 023816.

[Dar+05] B. Darquié, M. P. A. Jones, J. Dingjan, J. Beugnon, S. Bergamini, Y. Sortais, G. Messin, A. Browaeys, and P. Grangier: "Controlled Single-Photon Emission from a Single Trapped Two-Level Atom". *Science* **309** (5733) (2005), pp. 454–456. eprint: `http://science.sciencemag.org/content/309/5733/454.full.pdf`.

[Dic54] R. H. Dicke: "Coherence in Spontaneous Radiation Processes". *Phys. Rev.* **93** (1954), pp. 99–110.

[Dor+83] A. Dorsel, J. D. McCullen, P. Meystre, E. Vignes, and H. Walther: "Optical Bistability and Mirror Confinement Induced by Radiation Pressure". *Phys. Rev. Lett.* **51** (1983), p. 1550.

[Dra06] G. Drake: *Springer Handbook of Atomic, Molecular, and Optical Physics*. Springer Handbook of Atomic, Molecular, and Optical Physics. Springer, 2006. Chap. 78.

[Dro+17] L. Droenner, N. L. Naumann, J. Kabuss, and A. Carmele: "Collective enhancements in many-emitter phonon lasing". *Phys. Rev. A* **96** (2017), p. 043805.

[Dub+07] F. m. c. Dubin, D. Rotter, M. Mukherjee, C. Russo, J. Eschner, and R. Blatt: "Photon Correlation versus Interference of Single-Atom Fluorescence in a Half-Cavity". *Phys. Rev. Lett.* **98** (2007), p. 183003.

[ECZ97] S. J. van Enk, J. I. Cirac, and P. Zoller: "Purifying Two-Bit Quantum Gates and Joint Measurements in Cavity QED". *Phys. Rev. Lett.* **79** (1997), pp. 5178–5181.

[EE10] H. J. Eichler and J. Eichler: *Laser: Bauformen, Strahlführung, Anwendungen*. Springer-Verlag Berlin Heidelberg, 2010.

[EGK96] T. Erneux, A. Gavrielides, and V. Kovanis: "Semiconductor laser bifurcations". In: *Lasers and Electro-Optics Society Annual Meeting, 1996. LEOS 96., IEEE*. Vol. 2. 1996, 286–287 vol.2.

[EK95] A. Ekert and P. L. Knight: "Entangled quantum systems and the Schmidt decomposition". *American Journal of Physics* **63** (5) (1995), pp. 415–423.

[Eis+11] M. D. Eisaman, J. Fan, A. Migdall, and S. V. Polyakov: "Invited Review Article: Single-photon sources and detectors". *Review of Scientific Instruments* **82** (7) (2011), p. 071101.

[Ema13] C. Emary: "Delayed feedback control in quantum transport". *Philosophical Transactions of the Royal Society of London A: Mathematical, Physical and Engineering Sciences* **371** (1999) (2013). eprint: `http://rsta.royalsocietypublishing.org/content/371/1999/20120468.full.pdf`.

[FKC0] F. M. Faulstich, M. Kraft, and A. Carmele: "Unraveling mirror properties in time-delayed quantum feedback scenarios". *Journal of Modern Optics* **0** (0) (0000), pp. 1–9. eprint: `http://dx.doi.org/10.1080/09500340.2017.1363919`.

[Fai+13] A. Fainstein, N. D. Lanzillotti-Kimura, B. Jusserand, and B. Perrin: "Strong Optical-Mechanical Coupling in a Vertical GaAs/AlAs Microcavity for Subterahertz Phonons and Near-Infrared Light". *Phys. Rev. Lett.* **110** (2013), p. 037403.

[Fis+17] K. A. Fischer, L. Hanschke, J. Wierzbowski, T. Simmet, C. Dory, J. J. Finley, J. Vuckovic, and K. Muller: "Signatures of two-photon pulses from a quantum two-level system". *Nature Physics* **13** (2017), pp. 649–654.

[Fox06] A. Fox: *Quantum Optics: An Introduction*. Oxford Master Series in Physics. OUP Oxford, 2006. Chap. 8.5.

[Fra89] J. D. Franson: "Bell inequality for position and time". *Phys. Rev. Lett.* **62** (1989), pp. 2205–2208.

[GBS11] R. Ghobadi, A. R. Bahrampour, and C. Simon: "Quantum Optomechanics in the Bistable Regime". *Phys. Rev. A* **84** (2011), p. 033846.

[GC85] C. W. Gardiner and M. J. Collett: "Input and output in damped quantum systems: Quantum stochastic differential equations and the master equation". *Phys. Rev. A* **31** (1985), pp. 3761–3774.

[GP94] C. W. Gardiner and A. S. Parkins: "Driving atoms with light of arbitrary statistics". *Phys. Rev. A* **50** (1994), pp. 1792–1806.

[GR16] M. Gegg and M. Richter: "Efficient and exact numerical approach for many multi-level systems in open system CQED". *New Journal of Physics* **18** (4) (2016), p. 043037.

[GR17] M. Gegg and M. Richter: "PsiQuaSP – A library for efficient computation of symmetric open quantum systems". *Scientific Reports* **7** (2017), p. 16304.

[GT+13] A. Gonzalez-Tudela, F. P. Laussy, C. Tejedor, M. J. Hartmann, and E. del Valle: "Two-photon spectra of quantum emitters". *New Journal of Physics* **15** (3) (2013), p. 033036.

[GZ04] C. Gardiner and P. Zoller: *Quantum Noise*. Springer-Verlag Berlin Heidelberg, 2004.

[Gai09] V. A. Gaisler: "Single-photon emitters based on semiconductor nanostructures". *Bulletin of the Russian Academy of Sciences: Physics* **73** (1) (2009), pp. 77–79.

[Gar11] P. Gartner: "Two-level laser: Analytical results and the laser transition". *Phys. Rev. A* **84** (2011), p. 053804.

[Gar86] C. W. Gardiner: "Inhibition of Atomic Phase Decays by Squeezed Light: A Direct Effect of Squeezing". *Phys. Rev. Lett.* **56** (1986), pp. 1917–1920.

[Gar93] C. W. Gardiner: "Driving a quantum system with the output field from another driven quantum system". *Phys. Rev. Lett.* **70** (1993), pp. 2269–2272.

[Gau+94] D. J. Gauthier, D. W. Sukow, H. M. Concannon, and J. E. S. Socolar: "Stabilizing unstable periodic orbits in a fast diode resonator using continuous time-delay autosynchronization". *Phys. Rev. E* **50** (1994), p. 2343.

[Gen+08] C. Genes, D. Vitali, P. Tombesi, S. Gigan, and M. Aspelmeyer: "Ground-state cooling of a micromechanical oscillator: Comparing cold damping and cavity-assisted cooling schemes". *Phys. Rev. A* **77** (2008), p. 033804.

[Gri15] A. L. Grimsmo: "Time-Delayed Quantum Feedback Control". *Phys. Rev. Lett.* **115** (2015), p. 060402.

[Gru+10] I. S. Grudinin, H. Lee, O. Painter, and K. J. Vahala: "Phonon Laser Action in a Tunable Two-Level System". *Phys. Rev. Lett.* **104** (2010), p. 083901.

[HP40] T. Holstein and H. Primakoff: "Field Dependence of the Intrinsic Domain Magnetization of a Ferromagnet". *Phys. Rev.* **58** (1940), pp. 1098–1113.

[HS05] P Hövel and E Schöll: "Control of unstable steady states by time-delayed feedback methods". *Phys. Rev. E* **72** (4) (2005), p. 046203.

[HS75] T. Hänsch and A. Schawlow: "Cooling of gases by laser radiation". *Optics Communications* **13** (12) (1975), pp. 68–69.

[Hab+12] S. J. M. Habraken, K Stannigel, M. D. Lukin, P Zoller, and P Rabl: "Continuous mode cooling and phonon routers for phononic quantum networks". *New Journal of Physics* **14** (11) (2012), p. 115004.

[Hei+14] S. M. Hein, F. Schulze, A. Carmele, and A. Knorr: "Optical Feedback-Enhanced Photon Entanglement from a Biexciton Cascade". *Phys. Rev. Lett.* **113** (2014), p. 027401.

[Hei+17] T. Heindel, A. Thoma, M. von Helversen, M. Schmidt, A. Schlehahn, M. Gschrey, P. Schnauber, J. H. Schulze, A. Strittmatter, J. Beyer, S. Rodt, A. Carmele, A. Knorr, and S. Reitzenstein: "A bright triggered twin-photon source in the solid state". *Nature Communications* **8** (2017), p. 14870.

[Hei16] S. M. Hein: "Dynamics and control of quantum statistics in nano-photonic devices". PhD thesis. Technische Universität Berlin, 2016.

[Hoi+15] I.-C. Hoi, A. F. Kockum, L. Tornberg, A. Pourkabirian, G. Johansson, P. Delsing, and C. M. Wilson: "Probing the quantum vacuum with an artificial atom in front of a mirror". *Nat Phys* **11** (12) (2015), pp. 1045–1049.

[Hop+13] C Hopfmann, F Albert, C Schneider, S Höfling, M Kamp, A Forchel, I Kanter, and S Reitzenstein: "Nonlinear emission characteristics of quantum dot–micropillar lasers in the presence of polarized optical feedback". *New Journal of Physics* **15** (2) (2013), p. 025030.

[Hor+09] R. Horodecki, P. Horodecki, M. Horodecki, and K. Horodecki: "Quantum entanglement". *Rev. Mod. Phys.* **81** (2009), pp. 865–942.

[IDM16] I.Aharonovich, D.Englund, and M.Toth: "Solid-state single-photon emitters". *Nat Photon* **10** (10) (2016), 631–641.

[Isk+11] T. Iskhakov, A. Allevi, D. A. Kalashnikov, V. G. Sala, M. Takeuchi, M. Bondani, and M. Chekhova: "Intensity correlations of thermal light". *The European Physical Journal Special Topics* **199** (1) (2011), pp. 127–138.

[Jah+16] F. Jahnke, C. Gies, M. Aßmann, M. Bayer, H. A. M. Leymann, A. Foerster, J. Wiersig, C. Schneider, M. Kamp, and S. Höfling: "Giant photon bunching, superradiant pulse emission and excitation trapping in quantum-dot nanolasers". *Nature Communications* **7** (2016), p. 11540.

[Jah12] F. Jahnke: *Quantum Optics with Semiconductor Nanostructures*. Woodhead Publishing Series in Electronic and Optical Materials. Elsevier Science, 2012.

[Jam+01] D. F. V. James, P. G. Kwiat, W. J. Munro, and A. G. White: "Measurement of qubits". *Phys. Rev. A* **64** (2001), p. 052312.

[Jay+14] H. Jayakumar, A. Predojević, T. Kauten, T. Huber, G. S. Solomon, and G. Weihs: "Time-bin entangled photons from a quantum dot". *Nature Communications* **5** (2014), p. 4251.

[Jen+00] T. Jennewein, C. Simon, G. Weihs, H. Weinfurter, and A. Zeilinger: "Quantum Cryptography with Entangled Photons". *Phys. Rev. Lett.* **84** (2000), pp. 4729–4732.

[KAK02] B. Krummheuer, V. M. Axt, and T. Kuhn: "Theory of pure dephasing and the resulting absorption line shape in semiconductor quantum dots". *Phys. Rev. B* **65** (2002), p. 195313.

[KC94] P. Kochan and H. J. Carmichael: "Photon-statistics dependence of single-atom absorption". *Phys. Rev. A* **50** (1994), pp. 1700–1709.

[KCK13] J. Kabuss, A. Carmele, and A. Knorr: "Threshold behavior and operating regimes of an optically driven phonon laser: Semiclassical theory". *Phys. Rev. B* **88** (2013), p. 064305.

[KK06a] M. Kira and S. W. Koch: "Quantum-optical spectroscopy of semiconductors". *Phys. Rev. A* **73** (2006), p. 013813.

[KK06b] M. Kira and S. Koch: "Many-body correlations and excitonic effects in semiconductor spectroscopy". *Progress in Quantum Electronics* **30** (5) (2006), pp. 155 –296.

[KV08] T. J. Kippenberg and K. J. Vahala: "Cavity Optomechanics: Back-Action at the Mesoscale". *Science* **321** (2008), p. 1172.

[Kab+11a] J. Kabuss, A. Carmele, M. Richter, W. W. Chow, and A. Knorr: "Inductive equation of motion approach for a semiconductor QD-QED: Coherence induced control of photon statistics". *physica status solidi (b)* **248** (4) (2011), pp. 872–878.

[Kab+11b] J. Kabuss, A. Carmele, M. Richter, and A. Knorr: "Microscopic equation-of-motion approach to the multiphonon assisted quantum emission of a semiconductor quantum dot". *Phys. Rev. B* **84** (2011), p. 125324.

[Kab+12] J. Kabuss, A. Carmele, T. Brandes, and A. Knorr: "Optically Driven Quantum Dots as Source of Coherent Cavity Phonons: A Proposal for a Phonon Laser Scheme". *Phys. Rev. Lett.* **109** (2012), p. 054301.

[Kab+15] J. Kabuss, D. O. Krimer, S. Rotter, K. Stannigel, A. Knorr, and A. Carmele: "Analytical study of quantum-feedback-enhanced Rabi oscillations". *Phys. Rev. A* **92** (2015), p. 053801.

[Kab+16] J. Kabuss, F. Katsch, A. Knorr, and A. Carmele: "Unraveling coherent quantum feedback for Pyragas control [Invited]". *J. Opt. Soc. Am. B* **33** (7) (2016), pp. C10–C16.

[Kaz+15] T. Kazimierczuk, J. Schmutzler, M. Aßmann, C. Schneider, M. Kamp, S. Höfling, and M. Bayer: "Photon-Statistics Excitation Spectroscopy of a Quantum-Dot Micropillar Laser". *Phys. Rev. Lett.* **115** (2015), p. 027401.

[Kep+13] K. V. Kepesidis, S. D. Bennett, S. Portolan, M. D. Lukin, and P. Rabl: "Phonon cooling and lasing with nitrogen-vacancy centers in diamond". *Phys. Rev. B* **88** (2013), p. 064105.

[Khu10] J. B. Khurgin: "Viewpoint: Phonon lasers gain a sound foundation". *Physics* **3** (2010), p. 16.

[Kim08] H. J. Kimble: "The quantum internet". *Nature* **453** (7198) (2008), 1023–1030.

[Kir+11] M. Kira, S. W. Koch, R. P. Smith, A. E. Hunter, and S. T. Cundiff: "Quantum spectroscopy with Schrodinger-cat states". *Nat Phys* **7** (10) (2011), 799–804.

[Kop+15] W. Kopylov, M. Radonjić, T. Brandes, A. Balaž, and A. Pelster: "Dissipative two-mode Tavis-Cummings model with time-delayed feedback control". *Phys. Rev. A* **92** (2015), p. 063832.

[Kra+12] A. G. Krause, M. Winger, T. D. Blasius, Q. Lin, and O. Painter: "A high-resolution microchip optomechanical accelerometer". *Nature Photonics* **6** (2012), p. 768.

[LCn+15] J. C. López Carreño, C. Sánchez Muñoz, D. Sanvitto, E. del Valle, and F. P. Laussy: "Exciting Polaritons with Quantum Light". *Phys. Rev. Lett.* **115** (2015), p. 196402.

[LJS14] L. Lu, J. D. Joannopoulos, and M. Soljačić: "Topological photonics". *Nature Photonics* **8** (2014), pp. 821–829.

[LK+07] N. D. Lanzillotti-Kimura, A. Fainstein, C. A. Balseiro, and B. Jusserand: "Phonon engineering with acoustic nanocavities: Theoretical considerations on phonon molecules, band structures, and acoustic Bloch oscillations". *Phys. Rev. B* **75** (2007), p. 024301.

[LK+11] N. D. Lanzillotti-Kimura, A. Fainstein, B. Perrin, B. Jusserand, L. Largeau, O. Mauguin, and A. Lemaitre: "Enhanced optical generation and detection of acoustic nanowaves in microcavities". *Phys. Rev. B* **83** (2011), p. 201103.

[LK80] R. Lang and K. Kobayashi: "External optical feedback effects on semiconductor injection laser properties". *IEEE J. Quantum Electron.* **16** (1980), p. 347.

[LKFJ15] N. Lanzillotti-Kimura, A. Fainstein, and B. Jusserand: "Towards GHz–THz cavity optomechanics in DBR-based semiconductor resonators". *Ultrasonics* **56** (0) (2015), pp. 80–89.

[LKM08] M. Ludwig, B. Kubala, and F. Marquardt: "The optomechanical instability in the quantum regime". *New Journal of Physics* **10** (9) (2008), p. 095013.

[LLZ15] Y. Lu, H. Liu, and Q. Zhao: "Quantum state tomography and fidelity estimation via Phaselift". *Annals of Physics* **360** (2015), pp. 161 –179.

[LZ16] Y. Lu and Q. Zhao: "Minimum Copies of Schrödinger's Cat State in the Multi-Photon System". *Scientific Reports* **6** (2016), p. 32057.

[Lac+04] P. Lacharmoise, A. Fainstein, B. Jusserand, and V. Thierry-Mieg: "Optical cavity enhancement of light–sound interaction in acoustic phonon cavities". *Applied Physics Letters* **84** (17) (2004), pp. 3274–3276.

[Law95] C. K. Law: "Interaction between a moving mirror and radiation pressure: A Hamiltonian formulation." *Phys. Rev. A* **51** (3) (1995), pp. 2537–2541.

[Ley+15] H. A. M. Leymann, A. Foerster, F. Jahnke, J. Wiersig, and C. Gies: "Sub- and Superradiance in Nanolasers". *Phys. Rev. Applied* **4** (2015), p. 044018.

[Lin+13] B. Lingnau, W. W. Chow, E. Schöll, and K. Lüdge: "Feedback and injection locking instabilities in quantum-dot lasers: a microscopically based bifurcation analysis". *New Journal of Physics* **15** (9) (2013), p. 093031.

[Lod+17] P Lodahl, S. Mahmoodian, S. Stobbe, A Rauschenbeutel, P. Schneeweiss, J. Volz, H. Pichler, and P. Zoller: "Chiral quantum optics". *Nature* **541** (7638) (2017), 473–480.

[Lou00] R. Loudon: *The Quantum Theory of Light*. OUP Oxford, 2000.

[Lu+17] Y. Lu, N. L. Naumann, J. Cerrillo, Q. Zhao, A. Knorr, and A. Carmele: "Intensified antibunching via feedback-induced quantum interference". *Phys. Rev. A* **95** (2017), p. 063840.

[MC15] A. Metelmann and A. A. Clerk: "Nonreciprocal Photon Transmission and Amplification via Reservoir Engineering". *Phys. Rev. X* **5** (2015), p. 021025.

[MC17] A. Metelmann and A. A. Clerk: "Nonreciprocal quantum interactions and devices via autonomous feedforward". *Phys. Rev. A* **95** (2017), p. 013837.

[ME15] I. M. Mirza and S. van Enk: "How nonlinear optical effects degrade Hong-Ou-Mandel like interference". *Optics Communications* **343** (2015), pp. 172 –177.

[MEK13] I. M. Mirza, S. J. van Enk, and H. J. Kimble: "Single-photon time-dependent spectra in coupled cavity arrays". *J. Opt. Soc. Am. B* **30** (10) (2013), pp. 2640–2649.

[MHG06] F. Marquardt, J. G. E. Harris, and S. M. Girvin: "Dynamical Multistability Induced by Radiation Pressure in High-Finesse Micromechanical Optical Cavities". *Phys. Rev. Lett.* **96** (2006), p. 103901.

[MW95] L. Mandel and E. Wolf: *Optical Coherence and Quantum Optics*. Cambridge: Cambridge University Press, 1995.

[MZ07] E. A. Muljarov and R. Zimmermann: "Exciton Dephasing in Quantum Dots due to LO-Phonon Coupling: An Exactly Solvable Model". *Phys. Rev. Lett.* **98** (2007), p. 187401.

[Mac06] P. Machnikowski: "Change of Decoherence Scenario and Appearance of Localization due to Reservoir Anharmonicity". *Phys. Rev. Lett.* **96** (2006), p. 140405.

[Mad13] O. Madelung: *Festkörpertheorie II: Wechselwirkungen*. Heidelberger Taschenbücher. Springer Berlin Heidelberg, 2013.

[Mah+12] I. Mahboob, K Nishiguchi, H. Okamoto, and H. Yamaguchi: "Phonon-cavity electromechanics". *Nature Physics* **8** (2012), pp. 387–392.

[Mah+13] I. Mahboob, K. Nishiguchi, A. Fujiwara, and H. Yamaguchi: "Phonon Lasing in an Electromechanical Resonator". *Phys. Rev. Lett.* **110** (2013), p. 127202.

[Mar+07] F. Marquardt, J. P. Chen, A. A. Clerk, and S. M. Girvin: "Quantum Theory of Cavity-Assisted Sideband Cooling of Mechanical Motion". *Phys. Rev. Lett.* **99** (2007), p. 093902.

[Men+10] J. T. Mendonça, H. Terças, G. Brodin, and M. Marklund: "A phonon laser in ultra-cold matter". *EPL (Europhysics Letters)* **91** (3) (2010), p. 33001.

[Mic03] P. Michler: *Single Quantum Dots: Fundamentals, Applications and New Concepts*. Physics and Astronomy Online Library. Springer, 2003.

[Mil+15] T. J. Milburn, J. Doppler, C. A. Holmes, S. Portolan, S. Rotter, and P. Rabl: "General description of quasiadiabatic dynamical phenomena near exceptional points". *Phys. Rev. A* **92** (2015), p. 052124.

[Mun+14] C. S. Munoz, E. del Valle, A. G. Tudela, MullerK., LichtmanneckerS., KaniberM., TejedorC., FinleyJ. J., and LaussyF. P.: "Emitters of N-photon bundles". *Nat Photon* **8** (7) (2014), pp. 550–555.

[Mun+17] P. Munnelly, B. Lingnau, M. M. Karow, T. Heindel, M. Kamp, S. Höfling, K. Lüdge, C. Schneider, and S. Reitzenstein: "On-chip optoelectronic feedback in a micropillar laser-detector assembly". *Optica* **4** (3) (2017), pp. 303–306.

[Nau+14] N. L. Naumann, S. M. Hein, A. Knorr, and J. Kabuss: "Steady-state control in an unstable optomechanical system". *Phys. Rev. A* **90** (2014), p. 043835.

[Nau+16] N. L. Naumann, L. Droenner, W. W. Chow, J. Kabuss, and A. Carmele: "Solid-state-based analog of optomechanics". *J. Opt. Soc. Am. B* **33** (7) (2016), pp. 1492–1501.

[Nau+17] N. L. Naumann, S. M. Hein, M. Kraft, A. Knorr, and A. Carmele: "Feedback control of photon-statistics". In: *Proc. of SPIE Vol.* Vol. 10098. 2017, 100980N–1.

[Oht06] J. Ohtsubo: "Semiconductor Lasers: Stability, Instability and Chaos" (2006).

[Olv13] P. Olver: *Introduction to Partial Differential Equations*. Undergraduate Texts in Mathematics. Springer International Publishing, 2013.

[Ott+12] C Otto, K Lüdge, A. G. Vladimirov, M Wolfrum, and E Schöll: "Delay-induced dynamics and jitter reduction of passively mode-locked semiconductor lasers subject to optical feedback". *New Journal of Physics* **14** (11) (2012), p. 113033.

[PCZ96] J. F. Poyatos, J. I. Cirac, and P. Zoller: "Quantum Reservoir Engineering with Laser Cooled Trapped Ions". *Phys. Rev. Lett.* **77** (1996), pp. 4728–4731.

[PKM17] M. Peiris, K. Konthasinghe, and A. Muller: "Franson Interference Generated by a Two-Level System". *Phys. Rev. Lett.* **118** (2017), p. 030501.

[PZ16] H. Pichler and P. Zoller: "Photonic Circuits with Time Delays and Quantum Feedback". *Phys. Rev. Lett.* **116** (2016), p. 093601.

[Par96] A. S. Parkins: "Optical pumping with nonclassical light". *Phys. Rev. A* **53** (1996), pp. 2893–2896.

[Pre+07] W. H. Press, S. A. Teukolsky, W. T. Vetterling, and B. P. Flannery: *Numerical recipes in C. The art of scientific computing*. Third. Cambridge: University Press, 2007.

[Pri+10] J. Prior, A. W. Chin, S. F. Huelga, and M. B. Plenio: "Efficient Simulation of Strong System-Environment Interactions". *Phys. Rev. Lett.* **105** (2010), p. 050404.

[Pyr92] K. Pyragas: "Continuous control of chaos by self-controlling feedback". *Physics Letters A* **170** (1992), pp. 421–428.

[RC94] P. R. Rice and H. J. Carmichael: "Photon statistics of a cavity-QED laser: A comment on the laser˘phase-transition analogy". *Phys. Rev. A* **50** (1994), pp. 4318–4329.

[RHP14] Á. Rivas, S. F. Huelga, and M. B. Plenio: "Quantum non-Markovianity: characterization, quantification and detection". *Reports on Progress in Physics* **77** (9) (2014), p. 094001.

[RM10] M. Richter and S. Mukamel: "Ultrafast double-quantum-coherence spectroscopy of excitons with entangled photons". *Phys. Rev. A* **82** (2010), p. 013820.

[Ric+09] M. Richter, A. Carmele, S. Butscher, N. Bücking, F. Milde, P. Kratzer, M. Scheffler, and A. Knorr: "Two-dimensional electron gases: Theory of ultrafast dynamics of electron-phonon interactions in graphene, surfaces, and quantum wells". *Journal of Applied Physics* **105** (12) (2009), p. 122409.

[Rit+10] S. Ritter, P. Gartner, C. Gies, and F. Jahnke: "Emission properties and photon statistics of a single quantum dot laser". *Opt. Express* **18** (10) (2010), pp. 9909–9921.

[Roz+09] G. Rozas, M. F. P. Winter, B. Jusserand, A. Fainstein, B. Perrin, E. Semenova, and A. Lemaître: "Lifetime of THz Acoustic Nanocavity Modes". *Phys. Rev. Lett.* **102** (2009), p. 015502.

[SB15] F. Schlawin and A. Buchleitner: "Enhancement of two-photon transitions with tailored quantum light" (2015). arXiv:1510.06726 [quant-ph].

[SDG99] W. T. Strunz, L. Diósi, and N. Gisin: "Open System Dynamics with Non-Markovian Quantum Trajectories". *Phys. Rev. Lett.* **82** (1999), pp. 1801–1805.

[SH96] C. Simmendinger and O. Hess: "Controlling delay-induced chaotic behavior of a semiconductor laser with optical feedback". *Phys. Lett. A* **216** (1996), p. 97.

[SKH16] E. Schöll, S. H. L. Klapp, and P. Hövel, eds.: *Control of Self-Organizing Nonlinear Systems*. Springer International Publishing, 2016.

[SRT11] Ö. O. Soykal, R. Ruskov, and C. Tahan: "Sound-Based Analougue of Cavity Quantum Electrodynamics in Silicon". *Phys. Rev. Lett.* **107** (2011), p. 235502.

[SS08] E. Schöll and H. G. Schuster: *Handbook of Chaos Control*. Wiley-VCH, 2008.

[ST95] V Savona and F Tassone: "Exact quantum calculation of polariton dispersion in semiconductor microcavities". *Solid State Communications* **95** (10) (1995), pp. 673–678.

[SW13] E. M. Stoudenmire and S. R. White: "Real-space parallel density matrix renormalization group". *Phys. Rev. B* **87** (2013), p. 155137.

[SZ08] M. O. Scully and S. Zubairy: *Quantum Optics*. Cambridge University Press, 2008.

[Sap+15] L. Sapienza, M. Davanço, A. Badolato, and K. Srinivasan: "Nanoscale optical positioning of single quantum dots for bright and pure single-photon emission". *Nature Communications* **6** (2015), p. 7833.

[Say+11] C. Sayrin, I. Dotsenko, X. Zhou, B. Peaudecerf, T. Rybarczyk, S. Gleyzes, P. Rouchon, M. Mirrahimi, H. Amini, M. Brune, J.-M. Raimond, and S. Haroche: "Real-time quantum feedback prepares and stabilizes photon number states". *Nature* **477** (7362) (2011), pp. 73–77.

[Sch+05] C. Schön, E. Solano, F. Verstraete, J. I. Cirac, and M. M. Wolf: "Sequential Generation of Entangled Multiqubit States". *Phys. Rev. Lett.* **95** (2005), p. 110503.

[Sch+07] C. Schön, K. Hammerer, M. M. Wolf, J. I. Cirac, and E. Solano: "Sequential generation of matrix-product states in cavity QED". *Phys. Rev. A* **75** (2007), p. 032311.

[Sch+10] J Schachenmayer, I Lesanovsky, A Micheli, and A. J. Daley: "Dynamical crystal creation with polar molecules or Rydberg atoms in optical lattices". *New Journal of Physics* **12** (10) (2010), p. 103044.

[Sch+12] S. Schumacher, J. Förstner, A. Zrenner, M. Florian, C. Gies, P. Gartner, and F. Jahnke: "Cavity-assisted emission of polarization-entangled photons from biexcitons in quantum dots with fine-structure splitting". *Opt. Express* **20** (5) (2012), pp. 5335–5342.

[Sch+14] F. Schulze, B. Lingnau, S. M. Hein, A. Carmele, E. Schöll, K. Lüdge, and A. Knorr: "Feedback-induced steady-state light bunching above the lasing threshold". *Phys. Rev. A* **89** (2014), 041801(R).

[Sch01] W. P. Schleich: *Quantum Optics in Phase Space*. Berlin: Wiley-VCH, 2001.

[Sch11] U. Schollwöck: "The density-matrix renormalization group in the age of matrix product states". *Annals of Physics* **326** (1) (2011). January 2011 Special Issue, pp. 96–192.

[Sch14] F. Schulze: "Quantized Description of Optical Feedback". PhD thesis. Technische Universität Berlin, 2014.

[Shi07] A. J. Shields: "Semiconductor quantum light sources". *Nat Photon* **1** (4) (2007), 215–223.

[Sho95] P. W. Shor: "Scheme for reducing decoherence in quantum computer memory". *Phys. Rev. A* **52** (1995), R2493–R2496.

[Sim+12] N. Sim, M. F. Cheng, D. Bessarab, C. M. Jones, and L. A. Krivitsky: "Measurement of Photon Statistics with Live Photoreceptor Cells". *Phys. Rev. Lett.* **109** (2012), p. 113601.

[Ste+06] R. M. Stevenson, R. J. Young, P. Atkinson, K. Cooper, D. A. Ritchie, and A. J. Shields: "A semiconductor source of triggered entangled photon pairs". *Nature* **439** (7073) (2006), pp. 179–182.

[Str+16] M. Strauß, M. Placke, S. Kreinberg, C. Schneider, M. Kamp, S. Höfling, J. Wolters, and S. Reitzenstein: "Photon-statistics excitation spectroscopy of a single two-level system". *Phys. Rev. B* **93** (2016), p. 241306.

[Str00] S. H. Strogatz: *Nonlinear Dynamics and Chaos*. Westview Press, 2000.

[TB97] L. Trefethen and D. Bau: *Numerical Linear Algebra*. Society for Industrial and Applied Mathematics, 1997.

[TC68] M. Tavis and F. W. Cummings: "Exact Solution for an N-Molecule-Radiation-Field Hamiltonian". *Phys. Rev.* **170** (1968), pp. 379–384.

[The+02] R. T. Thew, K. Nemoto, A. G. White, and W. J. Munro: "Qudit quantum-state tomography". *Phys. Rev. A* **66** (2002), p. 012303.

[Tri+02] M. Trigo, A. Bruchhausen, A. Fainstein, B. Jusserand, and V. Thierry-Mieg: "Confinement of Acoustical Vibrations in a Semiconductor Planar Phonon Cavity". *Phys. Rev. Lett.* **89** (2002), p. 227402.

[Tro14] F. Troiani: "Entanglement swapping with energy-polarization-entangled photons from quantum dot cascade decay". *Phys. Rev. B* **90** (2014), p. 245419.

[Usa+12] K. Usami, A. Naesby, T. Bagci, B. Melholt Nielsen, J. Liu, S. Stobbe, P. Lodahl, and E. Polzik: "Optical cavity cooling of mechanical modes of a semiconductor nanomembrane". *Nature Physics* **8** (2) (2012), pp. 168–172.

[Vah+07] K. Vahala, M. Herrmann, S. Knunz, V. Batteiger, G. Saathoff, T. W. Hänsch, and T. Udem: "A phonon laser". *Nat Phys* **5** (2007), pp. 682–686.

[Ver+12] E. Verhagen, S. Deléglise, S. Weis, A. Schliesser, and T. J. Kippenberg: "Quantum-coherent coupling of a mechanical oscillator to an optical cavity mode". *Nature* **482** (2012), p. 63.

[Vid03] G. Vidal: "Efficient Classical Simulation of Slightly Entangled Quantum Computations". *Phys. Rev. Lett.* **91** (2003), p. 147902.

[Vid04] G. Vidal: "Efficient Simulation of One-Dimensional Quantum Many-Body Systems". *Phys. Rev. Lett.* **93** (2004), p. 040502.

[Vit+07] D. Vitali, S. Gigan, A. Ferreira, H. R. Böhm, P. Tombesi, A. Guerreiro, V. Vedral, A. Zeilinger, and M. Aspelmeyer: "Optomechanical Entanglement between a Movable Mirror and a Cavity Field". *Phys. Rev. Lett.* **98** (2007), p. 030405.

[WM06] H. Wiseman and G. Milburn: *Quantum Measurement and Control*. Cambridge University Press, Oxford, 2006.

[WM08] D. F. Walls and G. J. Milburn: *Quantum Optics*. SpringerLink: Springer e-Books. Springer, 2008.

[WNB15] S. Walter, A. Nunnenkamp, and C. Bruder: "Quantum synchronization of two Van der Pol oscillators". *Annalen der Physik* **527** (1-2) (2015), pp. 131–138.

[WR+07] I. Wilson-Rae, N. Nooshi, W. Zwerger, and T. J. Kippenberg: "Theory of Ground State Cooling of a Mechanical Oscillator Using Dynamical Backaction". *Phys. Rev. Lett.* **99** (2007), p. 093901.

[Wal15] I. A. Walmsley: "Quantum optics: Science and technology in a new light". *Science* **348** (6234) (2015), pp. 525–530.

[Web+08] C. Weber, M. Richter, S. Ritter, and A. Knorr: "Theory of the Optical Response of Single and Coupled Semiconductor Quantum Dots". In: *Semiconductor Nanostructures*. Ed. by D. Bimberg. Springer Berlin Heidelberg, 2008, pp. 189–210.

[Wei12] U. Weiss: *Quantum Dissipative Systems*. Series in modern condensed matter physics. World Scientific, 2012.

[Woo98] W. K. Wootters: "Entanglement of Formation of an Arbitrary State of Two Qubits". *Phys. Rev. Lett.* **80** (1998), pp. 2245–2248.

[Wu+17] J. Wu, S.-W. Huang, Y. Huang, H. Zhou, J. Yang, J.-M. Liu, M. Yu, G. Lo, D.-L. Kwong, S. Duan, and C. Wei Wong: "Mesoscopic chaos mediated by Drude electron-hole plasma in silicon optomechanical oscillators". *Nature Communications* **8** (2017), p. 15570.

[Yua+02] Z. Yuan, B. E. Kardynal, R. M. Stevenson, A. J. Shields, C. J. Lobo, K. Cooper, N. S. Beattie, D. A. Ritchie, and M. Pepper: "Electrically driven single-photon source". *Science* **295** (5552) (2002), pp. 102–105.

[ZBM14] K. Zhang, F. Bariani, and P. Meystre: "Quantum Optomechanical Heat Engine". *Phys. Rev. Lett.* **112** (2014), p. 150602.

[ZZC16] Y. Zhang, J. Zhang, and Chang-shui Yu: "Photon statistics on the extreme entanglement". *Scientific Reports* **6** (2016), p. 24098.

[Zha+01] X. B. Zhang, T Taliercio, S Kolliakos, and P Lefebvre: "Influence of electron-phonon interaction on the optical properties of III nitride semiconductors". *Journal of Physics: Condensed Matter* **13** (32) (2001), p. 7053.

[Zho+12] X. Zhou, I. Dotsenko, B. Peaudecerf, T. Rybarczyk, C. Sayrin, S. Gleyzes, J. M. Raimond, M. Brune, and S. Haroche: "Field Locked to a Fock State by Quantum Feedback with Single Photon Corrections". *Phys. Rev. Lett.* **108** (2012), p. 243602.

[Sch+15] Schulte Carsten H. H., Hansom Jack, Jones Alex E., Matthiesen Clemens, Le Gall Claire, and Atature Mete: "Quadrature squeezed photons from a two-level system". *Nature* **525** (7568) (2015), pp. 222–225.

[Zol+05] Zoller, P., Beth, Th., Binosi, D., Blatt, R., Briegel, H., Bruss, D., Calarco, T., Cirac, J. I., Deutsch, D., Eisert, J., Ekert, A., Fabre, C., Gisin, N., Grangiere, P., Grassl, M., Haroche, S., Imamoglu, A., Karlson, A., Kempe, J., Kouwenhoven, L., Kröll, S., Leuchs, G., Lewenstein, M., Loss, D., Lütkenhaus, N., Massar, S., Mooij, J. E., Plenio, M. B., Polzik, E., Popescu, S., Rempe, G., Sergienko, A., Suter, D., Twamley, J., Wendin, G., Werner, R., Winter, A., Wrachtrup, J., and Zeilinger, A.: "Quantum information processing and communication - Strategic report on current status, visions and goals for research in Europe". *Eur. Phys. J. D* **36** (2) (2005), pp. 203–228.